Mechanistic Insights into Photochromic Behavior and Photocatalytic Hydrogen Evolution Performed by Ru(II)-polypyridyl Complexes

Takuya Sawaki

February 2016

Mechanistic Insights into Photochromic Behavior and Photocatalytic Hydrogen Evolution Performed by Ru(II)-polypyridyl Complexes

Takuya Sawaki
Doctoral Program in Chemistry

Submitted to the Graduate School of
Pure and Applied Sciences
in Partial Fulfillment of the Requirements
for the Degree of Doctor of Philosophy in
Science

at
the University of Tsukuba

Contents Pages

Chapter 1
General introduction

Ruthenium, which belongs to group 8 in the periodic table, has been extensively investigated in various research fields such as chemistry, biochemistry and industry, because a ruthenium ion exhibits various oxidation states and forms stable complexes.[1, 2] The range of the possible oxidation states for a ruthenium ion is wider than that for an iron ion, belonging to the same group in the periodic table. Particularly, ruthenium(II), ruthenium(III) and ruthenium(IV) complexes, which are relatively stable, have been utilized for various investigations such as magnetism,[3] catalysis,[4] and photochemistry.[5] Ruthenium complexes have been also investigated as structural and functional models of heme-iron and non-heme iron enzymes,[6,7] even though the ruthenium ion is not included in natural proteins.

A ruthenium(II) ion is in a d^6-electron configuration and exhibits similar properties to an iron(II) ion. On the other hand, a ligand field splitting of a ruthenium(II) complex are generally larger than that of an iron(II) complex; thus, a ruthenium(II) complex is strictly in the low-spin state. Since all of the six *d*-electrons of the ruthenium(II) center occupy the three $d\pi$ orbitals, a ruthenium(II) ion forms stable complexes with use of the unoccupied $d\sigma$ orbitals. Furthermore, a ruthenium(II) ion encourages a π-back-bonding to ligands having low-lying π* orbitals, and the π-back-bonding makes the coordination bonds stronger (*vide infra*). Therefore, ruthenium(II) complexes exhibit high durability in electrochemical and photochemical reactions. Particularly, ruthenium(II) complexes having polypyridine ligands have been used for catalytic reactions[4, 6-25] and employed to display unique photochemical functions,[5, 26-42] on the basis of the high durability and accessible triplet excited states by visible-light irradiation.

In contrast, ruthenium(III) and more high-valent ruthenium complexes have been used as oxidants.[2, 43] $Ru^{VIII}O_4$ is an extremely strong oxidant to oxidize most of all organic substrates that are normally resistant to oxidation at ambient temperature; for example, 1-phenyl-3-heptanol acetate has been oxidized by $Ru^{VIII}O_4$ into 4-acetyloxy-octanoic acid.[43b] The oxidation power of $Ru^{VIII}O_4$, however, is too strong to cause many side reactions, and thus, is not appropriate for practical organic syntheses. In contrast, ruthenium(III) and ruthenium(IV) complexes can act as mild oxidants, both catalytically and stoichiometrically, and these complexes have been well investigated as oxidants in various selective oxidation reactions (*vide infra*).

1-1. Properties of ruthenium(II)-polypyridine complexes

Ruthenium(II) complexes having an *N*-containing heteroaromatic ligand such as pyridine are very stable, because strong coordination bonds are formed with use of σ-donation from lone pairs of the ligand to the unoccupied $d\sigma$ orbitals of the ruthenium(II) center as well as π back-donation from the fully occupied $d\pi$ orbitals of the ruthenium(II) center to π* orbitals of the ligand.[44] Ruthenium(II)-polypyridine complexes, which have multi-dentate chelating ligands, are more stable; if one of the coordination bonds of the chelate ligand is cleaved, the ligand is still bound to the metal center with other coordination bonds and thus the dissociated moiety recoordinates to the metal center.[5] In terms of photochemical properties, most of ruthenium(II)-polypyridine complexes show MLCT absorption bands, which are based on charge-transfer

transitions from a $d\pi$ orbital of the ruthenium(II) center to a π^* orbital of the polypyridine ligands.[5, 22] For example, $[Ru^{II}(bpy)_3]^{2+}$ ion (bpy = 2,2'-bipyridine) shows an absorption band around 450 nm, assigned to the MLCT transition, and a phosphorescence centered at 600 nm from the triplet MLCT excited state, which are typical photochemical properties for ruthenium(II)-polypyridine complexes (Figure 1-1). Upon

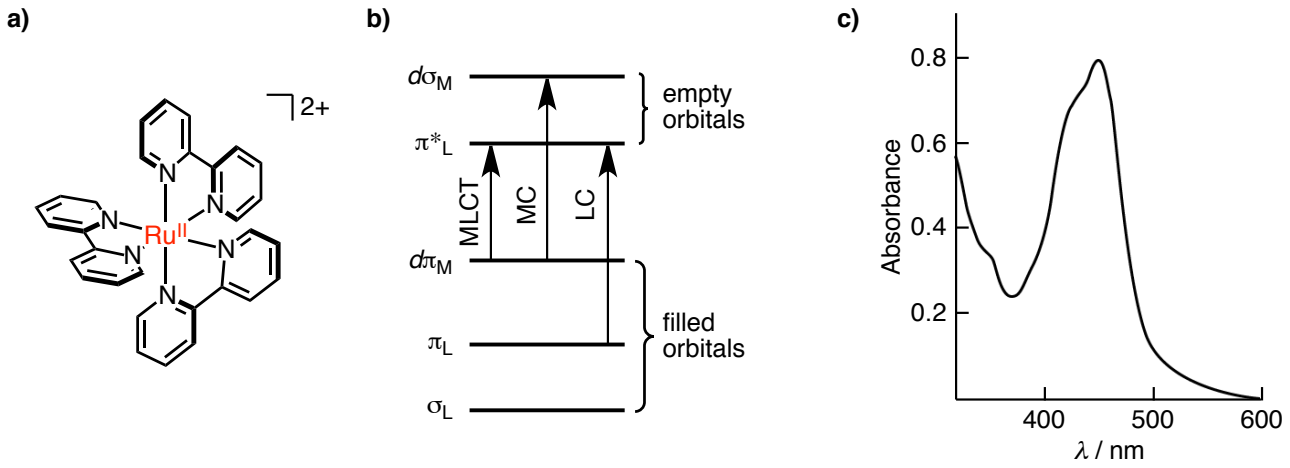

Figure 1-1. (a) The molecular structure of $[Ru^{II}(bpy)_3]^{2+}$. (b) A simplified MO diagram for ruthenium(II)-polypyridine complexes in their O_h symmetry, showing the three types of electronic transitions.[5] (c) UV-vis spectra of $[Ru^{II}(bpy)_3](PF_6)_2$ in CH_2Cl_2.[22]

photoexcitation of $[Ru^{II}(bpy)_3]^{2+}$, the singlet MLCT excited state (^{1}MLCT*), which has a quite short lifetime due to the heavy-atom effect of the ruthenium(II) ion, is formed at first and then the ^{1}MLCT* state immediately transits to the triplet MLCT excited state (^{3}MLCT*).[5, 23] The ^{3}MLCT* state has a relatively long lifetime and decays to the ground state with showing the phosphorescence. In addition, the ^{3}MLCT* state of $[Ru^{II}(bpy)_3]^{2+}$ can play a role as a reductant, and thus, $[Ru^{II}(bpy)_3]^{2+}$ ion is frequently used as a photosensitizer in photocatalytic systems (*vide infra*). On the other hand, a part of the ^{3}MLCT* state transits to the ^{3}MC* (^{3}(*d*-*d*)*) state, which is a triplet *d*-*d* transition state involving an apparent shift of an electron from a $d\pi$ orbital to a $d\sigma$ orbital of the ruthenium(II) center (Figure 1-2).[5, 24]

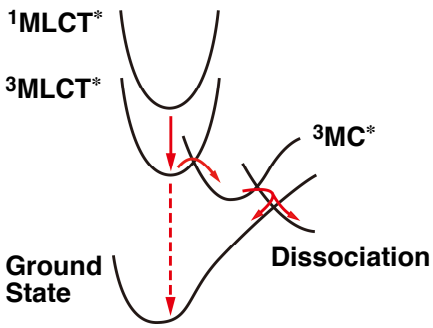

Figrure 1-2. An energy diagram presenting relative positions of ^{3}MC* or ^{3}MLCT* of ruhtneium(II)-polypyridine complexes.[5]

In the ^{3}MC* state of $[Ru(bpy)_3]^{2+}$, the coordination of the bpy ligand to the metal center is weaken, because the excited electron in the $d\sigma$ orbital causes electrostatic repulsion against the bonding electrons donated from the lone pair of the ligand. As a result, one of the bpy ligands partially dissociates from the ruthenium(II) center; however, the partially dissociated ligand mostly recoordinates to the metal center, because the ligand still coordinates to the ruthenium(II) center with a single bond (Scheme 1-1).[5, 22] Continuing photoirradiation of $[Ru(bpy)_3]^{2+}$ in the presence of chloride ions, the bpy ligand is completely dissociated and substituted to two chloride ions.[22] In contrast, in the case of a ruthenium(II) complex having a monodentate pyridine ligand, the monodentate pyridine ligand is readily dissociated through the photoexcited ^{3}MC* (^{3}(*d*-*d*)*) state; this photodissociation reaction has been used for synthesis of ruthenium(II) complexes.[25] Therefore, when there are other coordinating molecules such as another pyridine derivative or a chloride ion in the solution, ligand substitution occurs by photoexcitation. With use of the photoinduced ligand substitution, ruthenium(II)-polypyridine complexes are often used as a building block of a photoswitching molecule.[26-31]

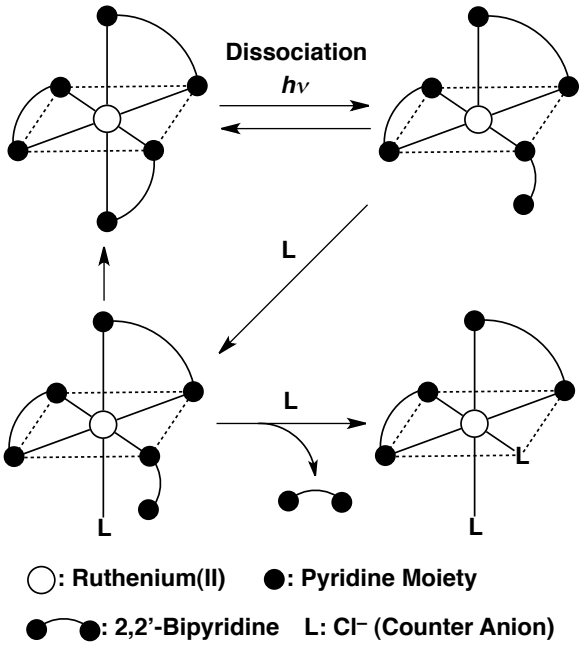

Scheme 1-1. The mechanism of the partial and complete photodissociation and the ligand substitution of $[Ru^{II}(bpy)_3]^{2+}$.[22]

Ruthenium(II)-polypyridine complexes have been known to show reversible redox behaviors both for the oxidation and reduction; the first oxidation wave derived from a Ru(II)/Ru(III) process is observed by cyclic voltammetry (CV). For example, $[Ru^{II}(bpy)_3]^{2+}$ exhibits the redox couple of the Ru^{II}/Ru^{III} process at +1.27 V vs SCE in acetonitrile (Figure 1-3).[5, 24, 45, 46] On the other hand, reduction waves derived from the polypyridine ligands are also observed in the CV; for example, the reduction potentials of $[Ru^{II}(bpy)_3]^{2+}$ are more negative than –1.3 V vs SCE in acetonitrile. Both the redox processes exhibit good reversibility, and $[Ru^{III}(bpy)_3]^{3+}$, an oxidation product of $[Ru^{II}(bpy)_3]^{2+}$, is relatively stable under acidic conditions or in the

solid state.[25, 47] Therefore, ruthenium(III)-diimine complexes have been frequently used as an electron-transfer oxidant for various oxidation reactions.

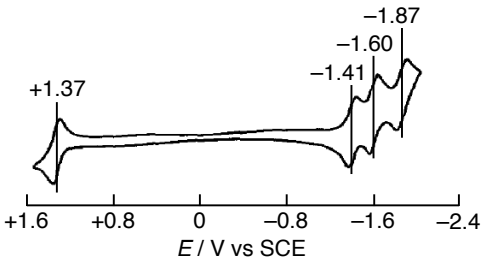

Figure 1-3. A cyclic voltammogram of $[Ru^{II}(bpy)_3]^{2+}$ in acetonitrile.[5]

1-2. Catalytic activity of ruthenium(II) complexes

Ruthenium(II)-polypyridine complexes have been intensively used as an oxidation catalyst, based on the oxidation activities of the corresponding high-valent ruthenium-oxo complexes generated through a proton-coupled electron transfer (PCET) oxidation. In 1978, Moyer and Meyer reported the formation of a ruthenium(IV)-oxo complex, $[Ru^{IV}(O)(bpy)_2(py)]^{2+}$, and the oxidation reaction of PPh_3 by the complex to afford $O{=}PPh_3$ as the oxidation product, which bound to the ruthenium(II) center as a ligand (Scheme 1-2).[7d]

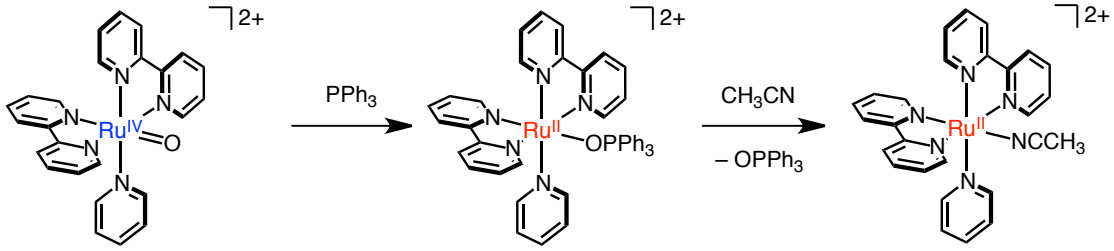

Scheme 1-2. An oxidation reaction of PPh_3 with a ruthenium(IV)-oxo complex through an adduct formation.[7d]

In addition, the same research group also has reported water oxidation with $[(bpy)_2(H_2O)Ru^{III}(\mu\text{-}O)\text{-}Ru^{III}(H_2O)(bpy)_2]^{4+}$ (Scheme 1-3a), so-called "the blue dimer", which has been generated by heating $[Ru^{II}Cl(bpy)_2(H_2O)]^+$ in H_2O at reflux. The blue dimer can be oxidized to form $[(bpy)_2ORu^{V}ORu^{V}O(bpy)_2]^{4+}$ by a cerium(IV) complex as a chemical oxidant *via* proton-coupled electron transfer (PCET); finally, O_2 is evolved from a water oxidation reaction by the dinuclear $Ru^{V}\text{-}O\text{-}Ru^{V}$ complex as an active species (Scheme 1-3b).[7e, 8]

Thereafter, oxidation reactions with use of high-valent ruthenium complexes, such as ruthenium(IV)-oxo and ruthenium(V)-oxo complexes, have been actively investigated; for instance, Huynh and co-workers have reported that a ruthenium(II)-aqua complex having a labile heteroscorpionate ligand, *fac*-$[Ru^{II}(H_2O)(dpp)(tppm)]^{2+}$ (dpp = di(pyrazol-1-yl)propane, tppm = tris(pyrid-2-yl)pentoxymethane), catalyzes an oxidation reaction of methyl-*p*-tolyl-sulfide to afford methyl-*p*-tolyl-sulfoxide under O_2 (11.4

psi) at 25 ºC in *o*-dichlorobenzene.[8, 9] The oxidation reaction presumably proceeds through a mechanism involving *fac*-$[Ru^{IV}(O)(dpp)(tppm)]^{2+}$ as a reactive intermediate, which is generated from a reaction of the ruthenium(II)-aqua complex with O_2.

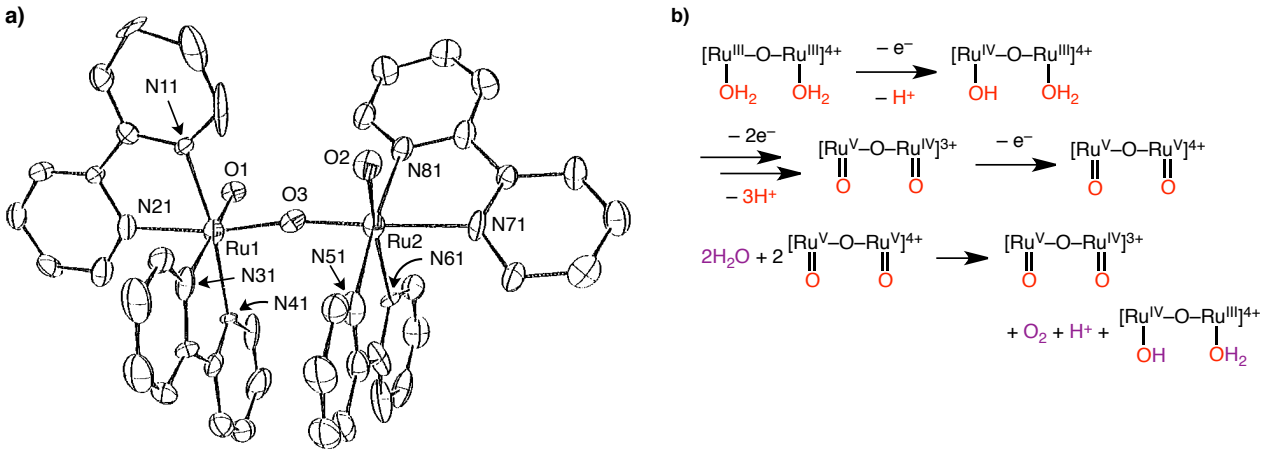

Scheme 1-3. (a) A crystal structure of the cationic part of $[(bpy)_2(H_2O)Ru^{III}ORu^{IV}(OH)(bpy)_2]^{4+}$. (b) Water-oxidation mechanism catalyzed by $[(bpy)_2(H_2O)Ru^{III}ORu^{III}(H_2O)(bpy)_2]^{4+}$.[8]

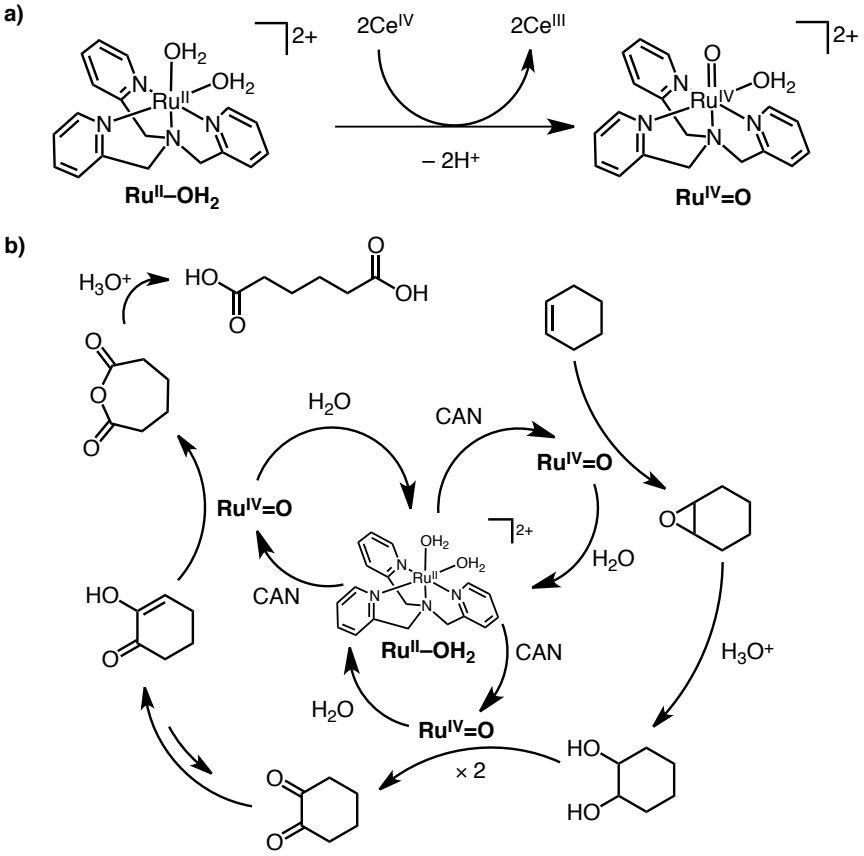

Scheme 1-4. (a) The oxidation of $[Ru^{II}(TPA)(H_2O)_2]^{2+}$ to the corresponding $[Ru^{IV}(O)(TPA)(H_2O)]^{2+}$ by a cerium(IV) complex as an oxidant through a PCET mechanism. (b) A proposed mechanism for the catalytic oxygenation of cyclohexene to produce adipic acid in strongly acidic water.[10a]

Kojima and co-workers have also reported the ruthenium-catalyzed selective and efficient oxygenation of hydrocarbons with water as an oxygen source (Scheme 1-4).[10] In this reaction, $[Ru^{II}(TPA)(H_2O)_2]^{2+}$ (TPA = tris(2-pyridylmethyl)amine) is oxidized to the corresponding ruthenium(IV)-oxo complex through a PCET oxidation using a cerium(IV) complex as an oxidant in an aqueous solution (Scheme 1-4a). The ruthenium complex catalyzes the oxidation of cyclohexene to adipic acid under strongly acidic conditions *via* successive eight-electron oxidation (Scheme 1-4b).[10a] In addition, the catalyst shows a high durability; the turnover number has reached to 2560 for the oxidation of cyclohexene. As described, most of all ruthenium(II)-polypyridine complexes and the corresponding high-valent ruthenium complexes show high durability in oxidation reactions without self-oxidation or dissociation of the ligands.

1-3. Photoinduced structural change of ruthenium(II) complexes

As described above, ruthenium(II)-polypyridine complexes show partial dissociation of a ligand upon photoirradiation. This phenomenon allows us to observe photochromism of ruthenium(II)-polypyridine complexes. In the first report on photochromic behaviors of ruthenium(II) complexes by Meyer and co-workers, $[Ru^{II}(bpy)_2(OH_2)_2]^{2+}$ has been described to exhibit the photoisomerization, in which the complex changes from the *cis*-form to the *trans*-form by visible-light irradiation (Scheme 1-5).[26] $[Ru^{II}(bpy)_2(OH_2)_2]^{2+}$ is initially in the *cis*-form when obtained, and one of the aqua ligands is dissociated upon photoirradiation, and subsequently, the dissociated aqua ligand recoordinates to the ruthenium(II) center at the different

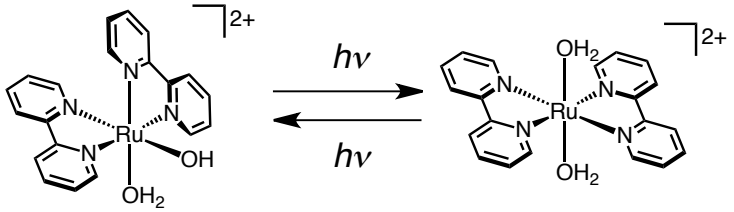

Scheme 1-5. The photoisomerization of *cis*- (left) and *trans*-$[Ru^{II}(bpy)_2(OH_2)_2]^{2+}$ (right).[26]

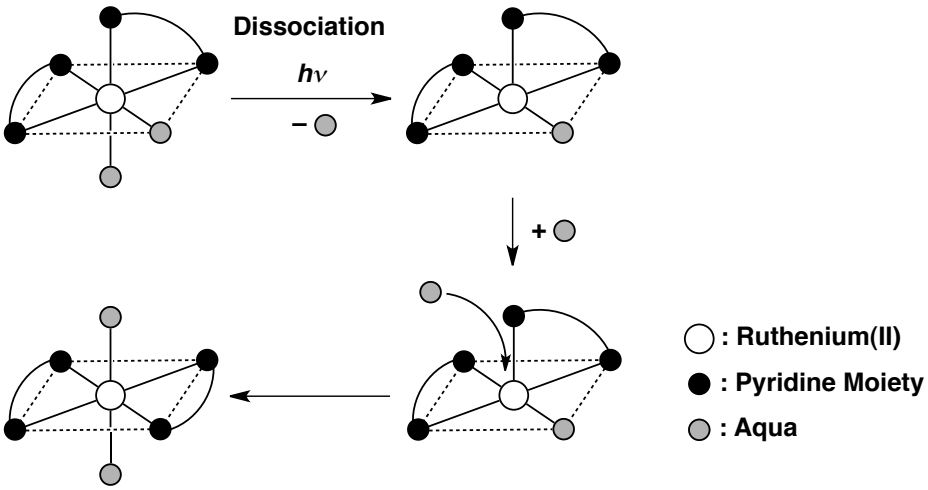

Scheme 1-6. The mechanism of the photoisomerization of $[Ru^{II}(bpy)_2(OH_2)_2]^{2+}$ through dissociation of an aqua ligand.[5, 26]

position from the original position that the aqua ligand used to coordinate. The recoordination of the water molecule results in the formation of the *trans*-isomer complex. The complex in the *trans*-form also changes to the *cis*-form through dissociation of one aqua ligand induced by photoexcitation as in the forward reaction. In this reaction, the wavelength range of the irradiation light required for the photodissociation is comparable for the forward and backward reactions and thus both isomers are inevitably photoexcited. As a result, the photoisomerization falls into a photostationary state, where both isomers exist in the mixture in a certain ratio, and the reaction cannot be controlled by changing the wavelength of the irradiation light.

If the direction of a photochromic reaction of a molecule can be controlled, molecular bistability is achieved to obtain a photoswitching function at a molecular level; from this viewpoint, photochemical and thermal structural change of ruthenium(II) complexes have been investigated so far.[27, 28] For example, a ruthenium(II)-containing [2]catenane complex (Scheme 1-7) has achieved the bistability using the photodissociation of the polypyridine ligand. The [2]catenane complex consists of a 50-membered ring containing two phen (= 1,10-phenanthlorine) units and a 42-membered ring containing the bpy unit.[29] The bpy unit of the 42-membered ring is dissociated from the ruthenium(II) center by photoexcitation, but the dissociated ring does not disengage from the complex, because the dissociated ring is locked by the other 50-membered ring, which has the coordinated phen units. Subsequently, the chloride ions present in the solution coordinates to the metal center at the empty sites. The coordinated chloride ions are dissociated by

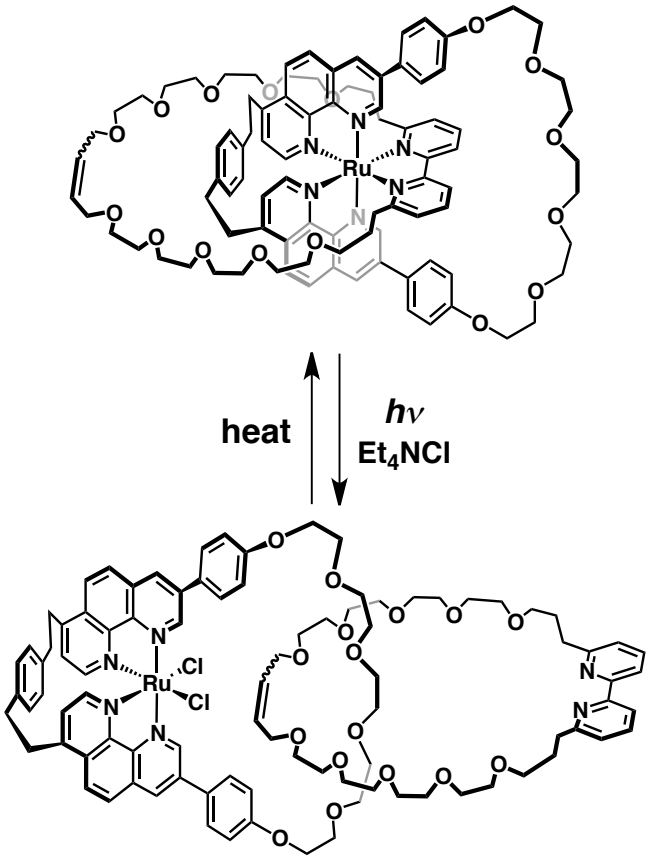

Scheme 1-7. The reversible structural change of the ruthenium(II)-catenane complex by photoirradiation and heating.[29]

heating, and the complex recovers the original structure. Therefore, application of external stimuli such as light and heat can induce the structural change to provide a "molecular switch" based on the bistability.

When TPA is used as a polypyridine ligand together with diimine ligands such as bpy, the ruthenium(II) complex has been demonstrated to exhibit unique photochromism, involving the partial dissociation of the TPA ligand by photoirradiation: The ruthenium(II)-TPA complexes, having a diimine ligand such as bpy, phen or bpm (= 2,2'-bipyrimidine), have been reported to show interconversion between open and closed forms by heating and photoirradiation (Scheme 1-8).[30] In this reaction, the axial pyridine moiety of the tetradentate TPA ligand is partially dissociated by heating in acetonitrile, and an acetonitrile molecule from the solvent is coordinated to the ruthenium(II) center at the resultant vacant site to give the dissociated complex. As the backward reaction, the coordinated acetonitrile is dissociated by photoirradiation, and the dissociated pyridine moiety recoordinates to the metal center to give the fully coordinated original complex. In this photoinduced structural change, the conversion efficiencies were determined to be 40% for the ruthenium(II)-TPA complex with bpy as the diimine ligand (excitation wavelength = 423 nm), 65% for that with phen (423 nm), and 89% for that with bpm (453 nm), respectively. The 89% conversion in the case of the bpm complex is extraordinarily high among photoinduced structural changes of metal complexes.

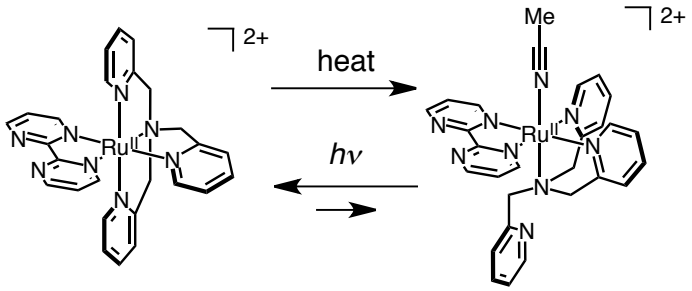

Scheme 1-8. The reversible structural change of the ruthenium(II)-TPA-diimine complex by heating and photoirradiation. In this figure, $[Ru(TPA)(bpm)]^{2+}$ is shown as a representative.[30]

The ruthenium(II)-TPA complex having a deprotonated alloxazine ($Hallo^-$) ligand also indicates the photochromism, involving a 180°-pseudo-rotation of the $Hallo^-$ ligand (Scheme 1-9);[31] however, the process of the structural change is slightly different from those of other diimine complexes described above. The $Hallo^-$ ligand coordinates to the ruthenium(II) center with the 1 and 10 positions, and resultantly forms a unstable four-membered chelate ring, and there is steric hindrance between the $Hallo^-$ ligand and the axial pyridine moiety of the TPA ligand. Based on the unstable coordination structure, N atom at the 10-position of the $Hallo^-$ ligand is partially dissociated by photoirradiation, and an acetonitrile molecule from the solvent coordinates to the metal center at the empty coordination site. Finally, the coordinated acetonitrile is dissociated and the partially dissociated $Hallo^-$ recoordinates to the metal center to complete an apparent 180°-pseudo-rotation of the $Hallo^-$ ligand. The total conversion efficiency of the photoinduced isomerization was determined to be 89%. Additionally, the isomer of the ruthenium(II)-$Hallo^-$ complex, which is photochemically obtained, gradually reverts to the original complex, because the isomer complex is

thermodynamically unstable due to the steric hindrance between the axial pyridine moiety of the TPA ligand and the O atom of the Hallo⁻ ligand.

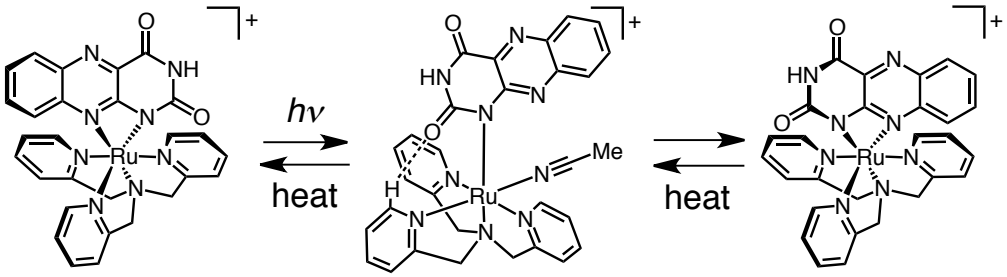

Scheme 1-9. The isomerization with 180°-pseudorotation of the Hallo⁻ ligand by photoirradiation and heating in $[Ru(Hallo)(TPA)]^{2+}$.[31]

As described, the ruthenium(II)-TPA complexes show the photochromic structural changes through partial dissociation of the ligands by photoirradiation or heating. However, the complete conversion had not been achieved until the author started the research, and the improvement of the conversion efficiency is desired due to the interest for the future application to photoswitchable molecular devices.

1-4. $[Ru^{II}(bpy)_3]^{2+}$ as a photosensitizer

The reduction power of ruthenium(II) complexes in the excited $^3[MLCT]^*$ state are quite strong as mentioned above, and the property is often used as a photosensitizer in a photocatalytic system. In a photocatalytic system, electron transfer relatively easily occurs from photoexcited ruthenium(II) complexes generated by photoirradiation to sacrificial electron acceptors; subsequently, ruthenium(II) complexes are oxidized into the corresponding ruthenium(III) complexes, which have an oxidation activity (Chart 1-1).[32–34]

$$[Ru^{II}(bpy)_3]^{2+} \xrightarrow{h\nu} {}^3\{[Ru^{II}(bpy)_3]^{2+}\}^*$$

$${}^3\{[Ru^{II}(bpy)_3]^{2+}\}^* + A \longrightarrow [Ru^{III}(bpy)_3]^{3+} + A^-$$

Chart 1-1. The generation of a ruthenium(III) complex from a ruthenium(II) complex through the triplet MLCT excited state; A = a sacrificial electron acceptor.[32]

As a result, ruthenium(II) complexes catalytically oxidize other compounds through the corresponding ruthenium(III) complexes in the presence of sacrificial electron acceptors upon photoirradiation. $[Ru^{II}(bpy)_3]^{2+}$ has been often used as a photosensitizer in a variety of photocatalytic systems, because it shows a relatively long lifetime (< 1 μs) for the ^{3}MLCT* state and high durability under appropriate conditions.[23, 35, 36] For instance, H. B. Gray and co-workers have reported that the trivalent resting state of the iron-porphyrin cofactor, $[(Por)Fe^{III}–OH]^+$, in horseradish peroxidase isoenzyme *c* is oxidized into the ferryl compound, $[(Por)Fe^{IV}=O]$, through photoinduced electron transfer (Scheme 1-10), where $[Ru^{II}(bpy)_3]^{2+}$ and $[Co^{III}(NH_3)_5Cl]^{2+}$ have been used as a photosensitizer and a sacrificial electron acceptor, respectively.[37]

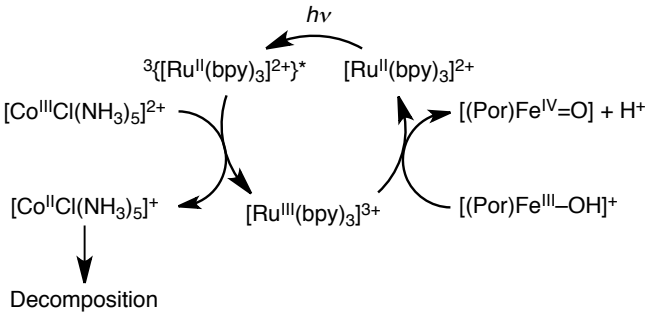

Scheme 1-10. Formation of an Fe^{IV}=O complex by photoinduced electron transfer. Por = porphyrin of horseradish peroxidase isoenzyme *c*.[37b]

Using this photoinduced oxidation system, Fukuzumi and co-workers have reported the oxidation reaction of a manganese(III)-porphyrin-hydroxo complex (Scheme 1-11);[38] in this reaction, the manganese(III)-hydroxo complex is oxidized to the corresponding manganese(IV)-oxo complex by photochemically generated $[Ru^{III}(bpy)_3]^{2+}$, and two molecules of the manganese(IV)-oxo complex disproportionate to form the corresponding manganese(III)-hydroxo complex, the manganese(V)-oxo complex and a proton. The manganese(V)-oxo complex is active for oxidation of organic substrates such as sodium *p*-styrene sulfonate, which is converted to the corresponding epoxide. The quantum yield of the photocatalytic oxidation increases according to the $[Co^{III}(NH_3)_5Cl]^{2+}$ concentration, to reach a constant value approaching 50%, which is the maximum value for the two-electron oxidation.

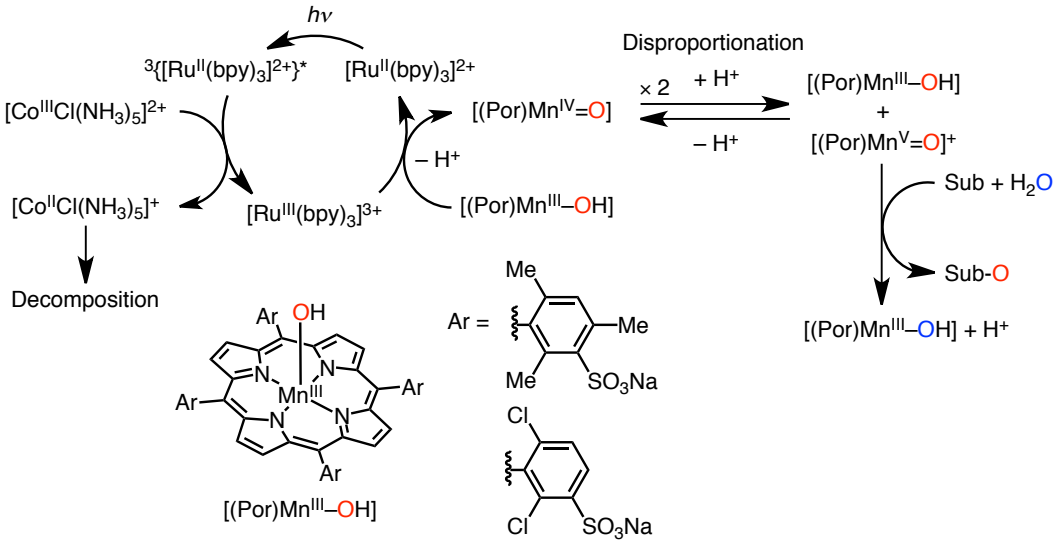

Scheme 1-11. A proposed reaction mechanism of photocatalytic oxygenations using a manganese(III)-porphyrin complex.[38]

Recently, dyads having both a catalyst and a photosensitizer moieties connected by a covalent bond have been also investigated, because through-bond electron transfer is generally more efficient than

through-space electron transfer.[39] For example, Rocha and co-workers have reported a dyad, consisting of a $Ru^{II}(tpy)_2$ moiety (tpy = 2,2':6',2'-terpyridine) as a photosensitizer and a Ru^{II} (tpy)(bpy)(H_2O) moiety as a catalyst. The dyad has been demonstrated to perform photocatalytic oxidation of organic substrates such as alcohols in the presence of $[Co^{III}Cl(NH_3)_5]^{2+}$ as a sacrificial electron acceptor under ambient conditions in a phosphate-buffer solution at pH 6.8 (Scheme 1-12).[40] In this photocatalytic reaction, the $Ru^{II}(H_2O)$ moiety is oxidized to form the corresponding ruthenium(IV)-oxo moiety *via* thermal electron transfer to a $Ru^{III}(tpy)_2$ moiety that is generated by photoinduced electron transfer as depicted in Chart 1-1. The resultant ruthenium(IV)-oxo species oxidizes the substrates.

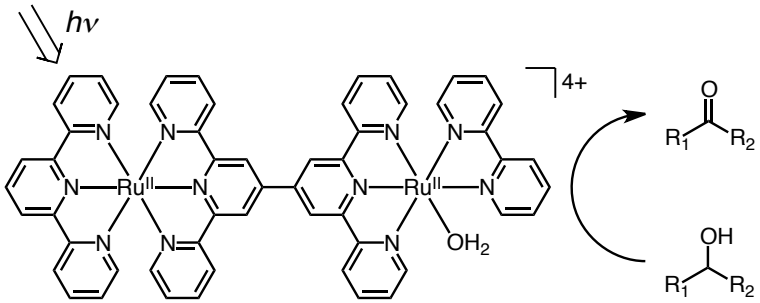

Scheme 1-12. Photocatalytic oxidation of alcohols by a Ru-Ru dyad.[40]

In contrast, ruthenium(II) complexes as photosensitizers have been also used for photocatalytic reduction; for instance, Creutz, Sutin and co-workers have reported the photoreduction of water using a ruthenium(II) complex as a photosensitizer and a cobalt(II) complex as a proton-reducing, *i.e.*, hydrogen-evolving, catalyst (Scheme 1-13).[41] Under photoirradiation, the ruthenium(II) complex at the ^{3}[MLCT]* state reduced $[Co^{II}(bpy)_3]^{2+}$ into $[Co^{I}(bpy)_3]^{+}$, and the ruthenium(II) complex was oxidized into the corresponding ruthenium(III) complex. In the presence of a sacrificial electron donor such as a triethanolamine, the ruthenium(III) complex was reduced back to the ruthenium(II) complex. The generated cobalt(I) complex reduces H_2O into $1/2H_2$ and OH^-.

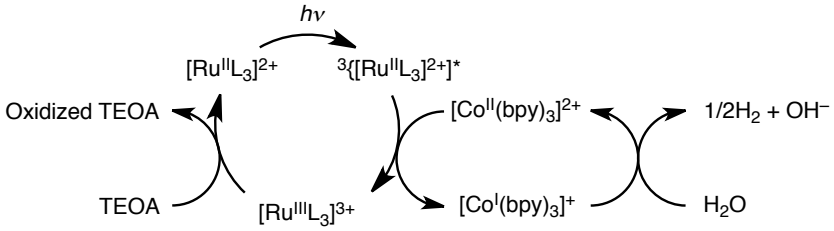

Scheme 1-13. Photocatalytic reduction of water to hydrogen. L is a diimine ligand such as a 4,7-dimethylphenanthlorine.[41b]

Recently, to improve the efficiency of electron transfer between photosensitizer and catalyst units, covalently linked photosensitizer-catalyst dyad complexes have been also frequently investigated for photocatalytic water reduction. Sakai and co-workers have reported a photocatalytic water reduction using a

dyad complex, which has a ruthenium(II) complex moiety as a photosensitizer and a platinum(II) complex moiety as a hydrogen-evolving catalyst.[42] In the presence of EDTA as a sacrificial electron donor, the dyad complex has performed photocatalytic hydrogen evolution by irradiation of visible light. In sharp contrast, a 1:1 mixture containing corresponding mononuclear ruthenium(II) and platinum(II) complexes, having no covalent linkage between the complexes, did not perform hydrogen evolution under photoirradiation in the presence of EDTA.

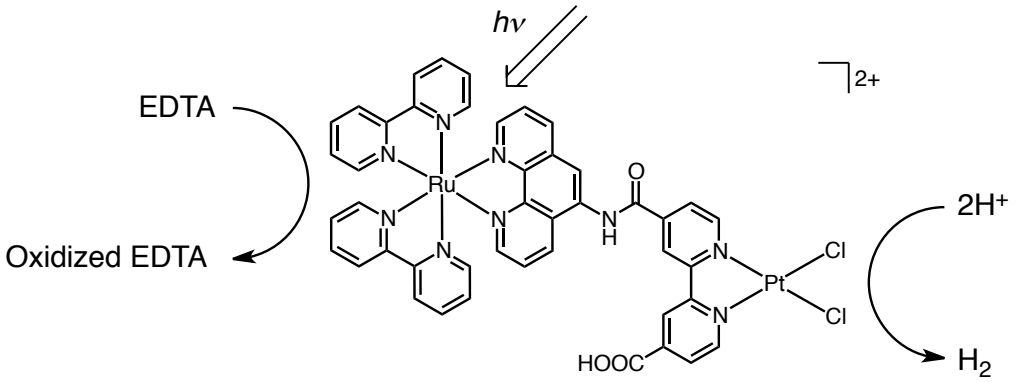

Scheme 1-14. The single-component system consisting of ruthenium(II) complex moiety as a photosensitizer and a platinum(II) complex moiety as a catalyst with EDTA as a sacrificial electron donor.[42]

1-5. Objectives of this thesis

In this thesis, the author describes photochromic structural changes and photocatalytic hydrogen evolution using the unique photochemical properties of ruthenium(II)-polypyridine complexes, such as photodissociation of the ligand *via* metal-centered triplet excited states and photoredox properties. The reversible structural changes of ruthenium(II)-polypyridine complexes around the ruthenium(II) centers containing partial dissociations and recoordinations of ligands are induced by heating and photoirradiation, which indicate complete conversions using two different methods. In one of the methods, isomerization involving a 180º-pseudorotation of a ligand *via* a partial dissociation and recoordination of a ligand is controlled on the basis of difference of characteristics of solvents used in energy barriers of the dissociation and the recoordination (Chapter 2). In the other method, complete structural interconversions of ruthenium(II)-TPA-diimine complexes are achieved by controlling energy levels of the triplet MLCT excited states (Chapter 3). Hydrogen evolution catalyzed by a ruthenium(II) complex is also performed, where a π-extended heteroaromatic diimine ligand of the ruthenium(II) complex has a catalytic activity for hydrogen evolution, while the ruthenium(II) unit only plays a role as a photosensitizer (Chapter 4).

Reference and Notes

[1] P. W. Atkin, D. F. Shriver, *Inorganic Chemistry, 5th Ed*, Oxford University Press, Oxford, **2010**.

[2] W. P. Griffith, *Chem. Soc. Rev.* **1992**, 179-185.

[3] a) J. Larionova, B. Mombelli, J. Sanchis, O. Kahn, *Inorg. Chem.* **1998**, *37*, 679-684; b) R. Andrés, M. Brissard, M. Gruselle, C. Train, J. Vaissermann, B. Malézieux, J.-P. Jamet, M. Verdaguer, *Inorg.*

Chem. **2001**, *40*, 4633-4640; c) T. E. Vos, Y. Liao, W. W. Shum, J.-H. Her, P. W. Stephens, W. W. Reiff, J. S. Miller, *J. Am. Chem. Soc*. **2004**, *126*, 11630-11639; d) W. Kosaka, H. Fukunaga, H. Miyasaka, *Inorg. Chem*. **2015**, *54*, 10001-10006.

[4] J. J. Concepcion, J. W. Jurss, M. K. Brennaman, P. G. Hoertz, A. O. T. Patrocinio, N. Y. M. Iha, J. L. Templeton, T. J. Meyer, *Acc. Chem. Res*. **2009**, *42*, 1954-1965.

[5] A. Juris, V. Balzani, F. Barigelletti, S. Campagna, P. Belser, A. von Zelewsky, *Coord. Chem. Rev*. **1988**, *84*, 85-277.

[6] a) J. T. Groves, R. Quinn, *J. Am. Chem. Soc*. **1985**, *107*, 5790-5792; b) J. T. Groves, J. S. Roman, *J. Am. Chem. Soc*. **1995**, *117*, 5594-5595; c) J.-J. Liang, J.-S. Huang, X.-Q. Yu, N. Zhu, C.-M. Che, *Chem. Eur. J*. **2002**, *8*, 1563-1572; d) S.-M. Au, J.-S. Huang, W.-Y. Yu, W.-H. Fung, C.-M. Che, *J. Am. Chem. Soc*. **1999**, *121*, 9120-9132.

[7] a) S. N. Dhuri, Y.-M. Lee, M. S. Seo, J. Cho, D. D. Narulkar, S. Fukuzumi, W. Nam, *Dalton Trans*. **2015**, *44*, 7634-7642; b) J.-L. Liang, X.-W. Yu, C.-M. Che, *Chem. Commun*. **2002**, 124-125; c) W.-L. Man, W. W. Y. Lam, S.-M. Yiu, T.-C. Lau, S.-M. Peng, *J. Am. Chem. Soc*. **2004**, *126*, 15226-15337; d) B. A. Moyer, T. J. Meyer, *J. Am. Chem. Soc*. **1978**, *100*, 3601-3603; e) S. W. Gersten, G. J. Samuels, T. J. Meyer, *J. Am. Chem. Soc*. **1982**, *104*, 4029-4030.

[8] T. J. Meyer, M. H. V. Huynh, *Inorg. Chem*. **2003**, *42*, 8140-8160.

[9] M. H. V. Huynh, L. M. Witham, J. M. Lasker, M. Wetzler, B. Mort, D. L. Jameson, P. S. White, K. J. Takeuchi, *J. Am. Chem. Soc*. **2003**, *125*, 308-309.

[10] a) Y. Hirai, T. Kojima, Y. Mizutani, Y. Shiota, K. Yoshizawa, S. Fukuzumi, *Angew. Chem. Int. Ed*. **2008**, *47*, 5772-5776; b) T. Kojima, Y. Hirai, T. Ishizuka, Y. Shiota, K. Yoshizawa, K. Ikemura, T. Ogura, S. Fukuzumi, *Angew. Chem. Int. Ed*. **2010**, *49*, 8449-8453; c) S. Ohzu, T. Ishizuka, Y. Hirai, H. Jiang, M. Sakaguchi, T. Ogura, S. Fukuzumi, T. Kojima, *Chem. Sci*. **2012**, *3*, 3421-3431.

[11] W. L. Seok, T. J. Meyer, *Inorg. Chem*. **2005**, *44*, 3931-3941.

[12] F. Li, M. Yu, Y. Jiang, F. Huang, Y. Li, B. Zhang, L. Sun, *Chem. Commun*. **2011**, *47*, 8949-8951.

[13] Y. Xu, T. Åkermark, V. Gyollai, D. Zou, L. Eriksson, L. Duan, R. Zhang, B. Åkermark, L. Sun, *Inorg. Chem*. **2009**, *48*, 2717-2719.

[14] a) L. Duan, Y. Xu, P. Zhang, M. Wang, L. Sun, *Inorg. Chem*. **2010**, *49*, 209-215; b) H. Li, F. Li, B. Zhang, X. Zhou, F. Yu, L. Sun, *J. Am. Chem. Soc*. **2015**, *137*, 4332-4335.

[15] N. Nagoshi, M. Yagi, M. Kaneko, *Bull. Chem. Soc. Jpn*. **2000**, *73*, 2193-2197.

[16] C. Sens, I. Romero, M. Rodríguez, A. Llobet, T. Parella, J. Benet-Buchholz, *J. Am. Chem. Soc*. **2004**, *126*, 7798-7799.

[17] R. Zong, R. P. Thummel, *J. Am. Chem. Soc*. **2005**, *127*, 12802-12803.

[18] V. J. Catalano, R. A. Heck, C. E. Immoos, A. Öhman, M. G. Hill, *Inorg. Chem*. **1998**, *37*, 2150-2157.

[19] J. J. Concepcion, J. W, Jurss, J. L. Templeton, T. J. Meyer, *J. Am. Chem. Soc*. **2008**, *130*, 16462-16463.

[20] O. Hamelin, P. Guillo, F. Loiseau, M.-F. Boissonnet, S. Ménage, *Inorg. Chem*. **2011**, *50*, 7952-7954.

[22] B. Durham, J. V. Casper, J. K. Nagle, T. J. Meyer, *J. Am. Chem. Soc*. **1982**, *104*, 4803-4810.

[23] N. H. Damrauer, G. Cerullo, A. Yeh, T. R. Boussie, C. V. Shank, J. K. McCusker, *Science* **1997**, *275*, 54-57.

[24] D. P. Rillema, C. B. Blanton, R. J. Shaver, D. C. Jackman, M. Boldaji, S. Bundy, L. A. Worl, T. J. Meyer, *Inorg. Chem.* **1992**, *31*, 1600-1606.

[25] a) C. R. Hecker, P. E. Fanwick, D. R. McMillin, *Inorg. Chem.* **1991**, *30*, 659-666; b) S. Bonnet, J.-P. Collin, N. Gruber, J.-P. Sauvage, E. R. Schofield, *Dalton Trans.* **2003**, 4654-4662.

[26] B. Durham, S. R. Wilson, D. J. Hodgson, T. J. Meyer, *J. Am. Chem. Soc.* **1980**, *102*, 600-607.

[27] a) A. A. Rachford, J. L. Petersen, J. J. Rack, *Inorg. Chem.* **2005**, *44*, 8065-8075; b) A. A. Rachford, J. J. Petersen, J. J. Rack, *Inorg. Chem.* **2006**, *45*, 5953-5960.

[28] a) H. Yamazaki, T. Hakamata, M. Komi, M. Yagi, *J. Am. Chem. Soc.* **2011**, *133*, 8846-8849; b) M. Hirahara, M. Z. Ertem, M. Komi, H. Yamazaki, C. J. Cramer, M. Yagi, *Inorg. Chem.* **2013**, *52*, 6354-6364.

[29] P. Mobian, J.-M. Kern, J.-P. Sauvage, *Angew. Chem. Int. Ed.* **2004**, *43*, 2392-2395.

[30] a) T. Kojima, T. Sakamoto, Y. Matsuda, *Inorg. Chem.* **2004**, *43*, 2243-2245; b) T. Kojima, T. Morimoto, T. Sakamoto, S. Miyazaki, S. Fukuzumi, *Chem. Eur. J.* **2008**, *14*, 8904-8915.

[31] S. Miyazaki, T. Kojima, S. Fukuzumi, *J. Am. Chem. Soc.* **2008**, *130*, 1556-1557.

[32] N. Sutin, C. Creutz, *Pure Appl. Chem.* **1980**, *52*, 2717-2738.

[33] T. J. Meyer, *Acc. Chem. Res.* **1989**, *22*, 163-170.

[34] H. D. Gafney, A. W. Adamson, *J. Am. Chem. Soc.* **1972**, *94*, 8238-8239.

[35] G. A. Crosby, *Acc. Chem. Res.* **1975**, *8*, 231-238.

[36] a) J. L. Dempsey, J. R. Winkler, H. B. Gray, *Chem. Rev.* **2010**, *110*, 7024-7039; b) E. L. Tyson, Z. L. Niemeyer, T. P. Yoon, *J. Org. Chem.* **2014**, *79*, 1421436; c) D. A. Nicewicz, D. W. C. Macmillan, *Science* **2008**, *322*, 77-80; d) S. Ohzu, T. Ishizuka, Y. Hirai, S. Fukuzumi, T. Kojima, *Chem. Eur. J.* **2013**, *19*, 1563-1567.

[37] a) D. W. Low, J. R. Winkler, H. B. Gray, *J. Am. Chem. Soc.* **1996**, *118*, 117-120; b) J. Berglund, T. Pascher, J. R. Winkler, H. B. Gray, *J. Am. Chem. Soc.* **1997**, *119*, 2464-2469.

[38] S. Fukuzumi, T. Kishi, H. Kotani, Y.-M. Lee, W. Nam, *Nat. Chem.* **2011**, *3*, 38-41.

[39] O. Hamelin, P. Guillo, F. Loiseau, M.-F. Boissonnet, S. Ménage, *Inorg. Chem.* **2011**, *50*, 7952-7954.

[40] a) W. Chen, F. N. Rein, R. C. Rocha, *Angew. Chem. Int. Ed.* **2009**, *48*, 9672-9675; b) W. Chen, F. N. Rein, B. L. Scott, R. C. Rocha, *Chem. Eur. J.* **2011**, *17*, 5595-5604.

[41] a) C. V. Krishnan, N. Sutin, *J. Am. Chem. Soc.* **1981**. *103*, 2141-2142; b) C. V. Krishnan, B. S. Brunschwig, C. Creutz, N. Sutin *J. Am. Chem. Soc.* **1985**, *107*, 2005-2015.

[42] a) H. Ozawa, M. Haga, K. Sakai, *J. Am. Chem. Soc.* **2006**, *128*, 4926-4927; b) H. Ozawa, K. Sakai, *Chem. Commun.* **2011**, *47*, 2227-2242.

[43] a) L. M. Berkowitz, P. N. Rylander, *J. Am. Chem. Soc.* **1958**, *80*, 6682-6684; b) M. T. Nuñez, V. S. Martín, *J. Org. Chem.* **1990**, *55*, 1928-1932.

[44] a) Y. K. Shin, B. S. Brunschwig, C. Creutz, N. Sutin, *J. Phys. Chem.* **1996**, *100*, 8157-8169; b) Y. K. Shin, B. S. Brunschwig, C. Creutz, N. Sutin, *J. Am. Chem. Soc.* **1995**, *117*, 8668-8669.

[45] a) T. Kakutani, Y. Morihiro, M. Senda, R. Takahashi, K. Matsumoto, *Bull. Chem. Soc. Jpn.* **1978**, *51*, 2847-2854; b) A. Basu, M. A. Weiner, T. C. Strekas, H. D. Gafney, *Inorg. Chem.* **1982**, *21*, 1085-1092; c) R. J. Crutchley, A. B. P. Lever, *Inorg. Chem.* **1982**, *21*, 2276-2282.

[46] D. P. Rillema, G. Allen, T. J. Meyer, D. Conrad, *Inorg. Chem.* **1983**, *22*, 1617-1622.

[47] a) N. G. Connelly, W. E. Geiger, *Chem. Rev.* **1996**, *96*, 877-910; b) K. L. Rollick, J. K. Kochi, *J. Am. Chem. Soc.* **1982**, *104*, 1319-1330.

Chapter 2

Photochromic structural change of a ruthenium(II)-pterin complex

2-1. Introduction

The bistability of molecules controlled by external stimuli including light, heat, and magnetic field has been one of the most important phenomena not only in terms of scientific interest but also in terms of molecular functions such as molecular machines, molecular switches, chemical sensors, and so on.[1] Among phenomena that involve bistability, reversible switching between two states with photoexcitation for at least one direction, accompanied by change of optical absorption, has been known as photochromism, which has attracted considerable attention with regard to its potential applicability to optical memories, optical switches, and so forth.[2] Photochromic molecules developed so far are mainly based on organic dyes including azobenzene,[3] spiropyran, [4] and diarylethene,[5] whereas photochromic behaviors of transition-metal complexes have yet to be explored in depth.[6–11] However, if efficient photochromic systems based on transition-metal complexes were to be developed, they would be superior to traditional organic chromophores because of their structural diversity, with various functional groups of the ligands to control their redox and optical properties.

In the case of photoexcitation of metal complexes, metal-to-ligand charge transfer (MLCT) or ligand-to-metal charge transfer (LMCT) has been utilized to generate, in general, triplet excited states of the species rather than the corresponding singlet excited states due to their very fast internal relaxation.[12] As for Ru(II) complexes that have heteroaromatic compounds with extended π conjugation as ligands, the formation of the triplet excited state of MLCT (^{3}MLCT*) is achieved by visible-light irradiation. The ^{3}MLCT* state can be converted to a metal-centered triplet excited state (^{3}MC*), namely, a *d-d* triplet excited state, in which a $d\sigma$ orbital should be occupied by an electron that facilitates the dissociation of the ligand.[13] Among earlier reports on photochromic behaviors of transition-metal complexes,[6–11] Meyer and co-workers have demonstrated the *cis–trans* photoisomerization of $[Ru(bpy)_2(OH_2)_2]^{2+}$ (bpy = 2,2'-bipyridyl) in an acidic aqueous solution to give a photostationary state in which the *trans*/*cis* ratio under irradiation at 480 nm is 1.5 (See section 1-3).[7] So far, it has been difficult to achieve a complete photochromic conversion of a metal complex between two distinctive states as observed in photochromism of organic molecules. This is due to the similarity in the two switchable states of the chromophores of photochromic metal complexes, which results in the photostationary states.

Bidentate heteroaromatic compounds can be adopted as chromophores of Ru(II) complexes to afford photoexcited states to perform a photochemical structural change of those complexes. In this study, as a bidentate heteroaromatic ligand in a Ru(II) complex, a pterin was adopted, which is a redox-active fused heteroaromatic coenzyme involved in a variety of biological redox reactions.[14] Since pterins can bind to metal ions in a bidentate fashion, many transition-metal complexes with pterin ligands have been intensively explored so far.[15–18] Despite the fact that transition-metal complexes, having pterins as ligands, have been investigated in terms of their structures and redox properties, no example has been reported of their

photochemical reactions.

In this chapter, the author describes a unique photochromic behavior of a Ru(II)–pterin complex, $[Ru(dmdmp)(TPA)]^+$ (**1**) (Hdmdmp = 2-(*N*,*N*-dimethyl)-6,7-dimethylpterin, TPA = tris(2-pyridylmethyl)amine; Scheme 2-1). The complex exhibits a reversible 180° pseudorotation of the pterin ligand with MLCT excitation to afford an isomer with 100% conversion efficiency. Together with the crystal-structure determination of the isomer, the author has elucidated the dynamics of photochemical and thermal transformation of **1** to the isomer and also the backward reaction to recover **1** to clarify the reaction mechanism of this unique photochromic isomerization.

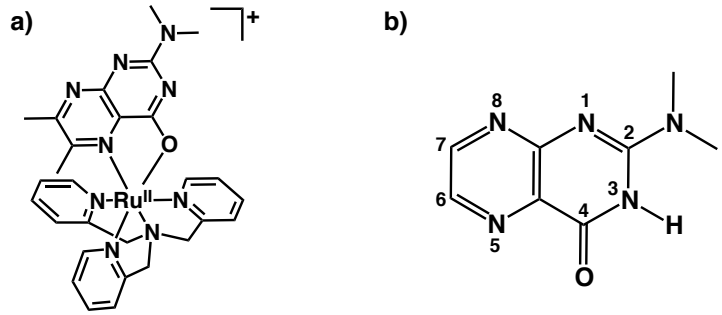

Scheme 2-1. a) Schematic description of structures of a pterin complex, **1**, and b) the numbering scheme of the Hdmdmp skeleton.

2-2. Results and discussion

2-2-1. Photoisomerization

A solution of $[Ru(dmdmp)(TPA)](ClO_4)$ (**1**·ClO_4)[19] in acetone was orange-colored, and its absorption spectrum showed the maxima at 460 and 400 nm at room temperature, which could be assigned to the MLCT transitions from the Ru(II) center to the pterin ligand.[19b] When the solution of **1** was irradiated with incident light centered at λ_{max} = 460 nm under an inert atmosphere, the intensity of the absorption band at

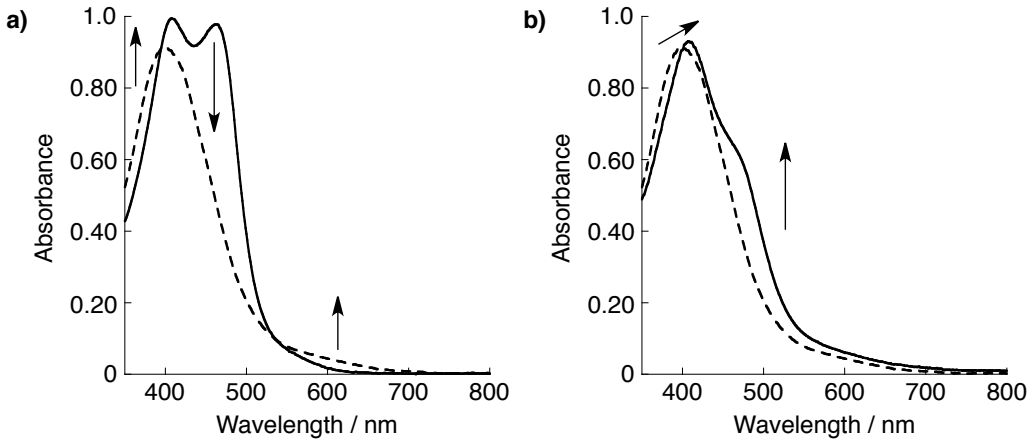

Figure 2-1. UV/Vis spectral change of **1** in acetone a) upon photoirradiation at 460 nm and b) the subsequent thermal reaction at room temperature.

460 nm gradually decreased, and instead the intensity of the band at 400 nm increased and the absorption maxima showed a slight blue-shift (Figure 2-1a). This spectral change shows an isosbestic point at 523 nm. When the solution was kept at room temperature after ceasing the photoirradiation, a further spectral change was observed (Figure 2-1b). At the second stage, the absorption band at 390 nm exhibited a slight red-shift. A shoulder absorption rose at 480 nm, and an isosbestic point was observed at 450 nm. These results clearly indicate that the photochemical reaction is followed by the subsequent thermal reaction to give the final product.

The reaction process was monitored also by ^{1}H NMR spectroscopy. The photoirradiation was conducted to the solution of **1** in acetone-d_6 in an NMR tube for 4 h at room temperature to analyze the product. In the ^{1}H NMR spectra of the photoreaction product measured immediately after photoirradiation for 4 h, two sets of signals derived from two different compounds were observed and both of the signal sets were different from that of the starting complex **1** (Figure 2-2b).[19b] In addition, as time passed after ceasing

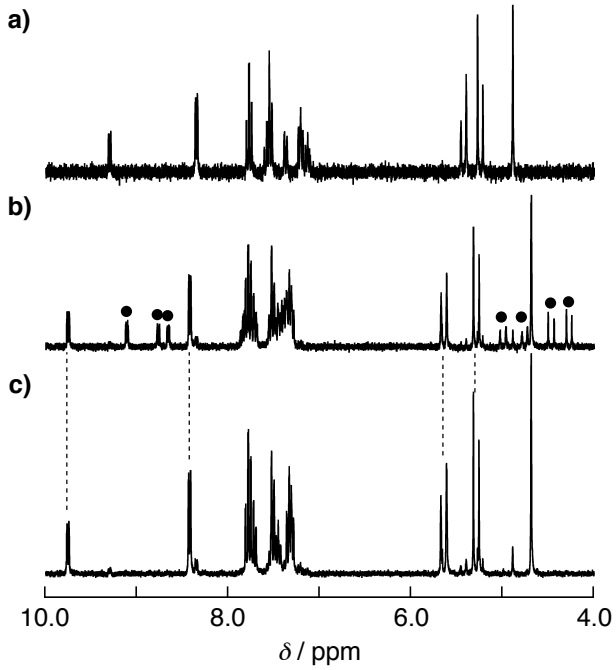

Figure 2-2. ^{1}H NMR spectra of the photoreaction products from a) **1** in acetone-d_6 at room temperature, and b) **1** after photoirradiation for 4 h and c) for 12 h.

photoirradiation, one set of the ^{1}H NMR signals gradually disappeared and instead the intensity of the other signal set increased. The former signal set involves three AB quartet pairs at δ 4.9 and 4.4 ppm, 4.7 and 4.3 ppm, and 3.8 and 3.6 ppm, which can be ascribed to the six methylene protons of the TPA ligand in the intermediate (**I**). The third AB quartet was observed in the relatively up-field region compared to ^{1}H NMR signals of the ordinary methylene protons for Ru(II)-TPA complexes that bear the TPA ligand in the normal tetradentate mode.[19–21] This strongly indicates that one pyridylmethyl arm should be uncoordinated to the Ru(II) center but that the conformational flexibility should be severely restricted.[22] This presumption is supported by the observation for the photoreaction products of Ru(II)-TPA-diimine complexes;[22] the

products also involve one uncoordinated pyridylmethyl group among three of them in the TPA ligand. The resulting vacant coordination site must be occupied by an acetone molecule from the solvent, as evidenced by the ESI-TOF-MS spectrum, which shows a monocationic peak cluster at 668.2 *m*/*z* to be assigned to a [Ru(dmdmp)(TPA)(acetone)]$^+$ ion as depicted in Figure 2-3.

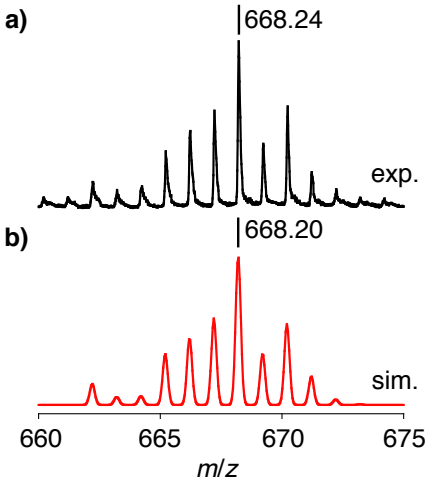

Figure 2-3. ESI-TOF MS spectrum of **I** in acetone (a) and its computer simulation (b).

In order to characterize the second product (the final product) of the photoreaction of **1**, the ^{1}H NMR spectrum of the reaction mixture was analyzed in detail (Figure 2-2c). There are two sets of 2-substituted pyridyl signals in the aromatic region and the integral ratio between the two sets of the pyridyl signals is 1:2, which suggests that all the three pyridyl groups of the TPA ligand that coordinate to the Ru(II) center and the signals of two equatorial pyridines are equivalent.[19] In the aliphatic region of the ^{1}H NMR spectrum, one singlet was observed at δ 4.7 ppm and one pair of AB quartets at δ 5.6 and 5.3 ppm. This signal pattern is typical for Ru(II)-TPA complexes showing a σ_h symmetry.[19–21] Three singlets of the methyl groups of the pterin ligand are also observed at δ 3.3, 2.9, and 2.4 ppm. The differential NOE spectrum of the final product allowed us to clarify the spatial correlation between the 6-Me group of the pterin ligand (observed at δ 2.4

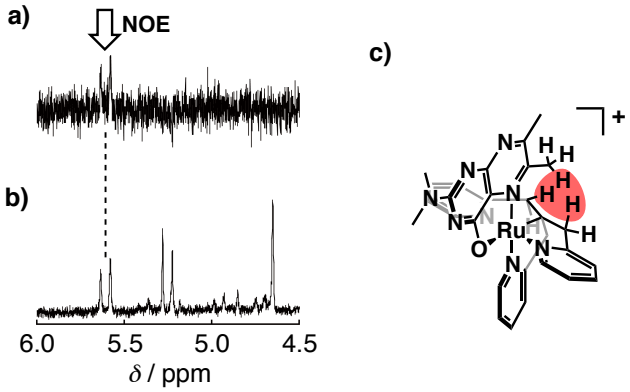

Figure 2-4. (a) Differential NOE and (b) the ambient ^{1}H NMR spectra of complex **2** in acetone-d_6. (c) The structure of **2** and the NOE correlation observed protons (red): irradiated at 2.43 ppm in the NOE measurement.

ppm) and the methylene protons of one equatorial pyridylmethyl moiety of the TPA ligand (observed at δ 5.6 ppm) (Figure 2-4). This NOE observation indicates that, upon the thermal process, the pterin ligand undergoes an apparent 180°-pseudorotation around the axis that passes through the Ru(II) center and the center of the pterin ligand, and consequently the 6-Me group comes close to the equatorial coordination plane. In comparing the spectrum of the second product to that of **1**,[19] the signals of all the 6-pyridyl protons in the final product show downfield shifts relative to the corresponding signals of **1**. Considering the crystal structure of the second product (*vide infra*), the downfield shifts for the 6-pyridyl protons is caused by the hydrogen bonding with the 4-oxygen of the pterin ligand. The ESI-TOF MS spectrum of the final product showed a monocationic signal at 610.2 *m/z* (Figure 2-5), which corresponds to the monocation, $[Ru(dmdmp)(TPA)]^+$. This result also suggests that the final product is an isomer of the starting complex **1**. On the basis of these data, the first product of the photoreaction is the intermediate complex (**I**) with one uncoordinated pyridylmethyl group and a solvent molecule (acetone) as a ligand. The intermediate complex undergoes the subsequent thermal reaction to give an isomer (**2**) of the starting complex **1** as the final product as shown in Scheme 2-2.

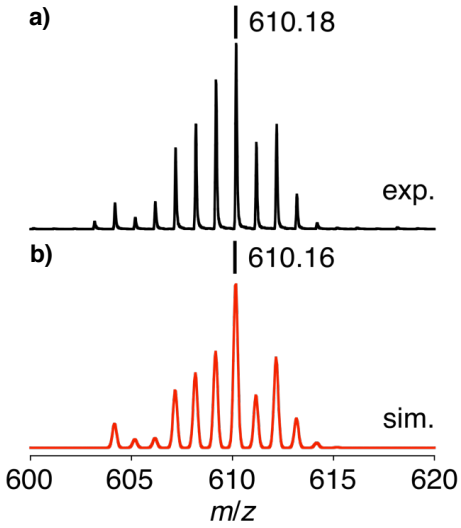

Figure 2-5. ESI-TOF MS spectrum of **2** in acetone (a) and its computer simulation (b).

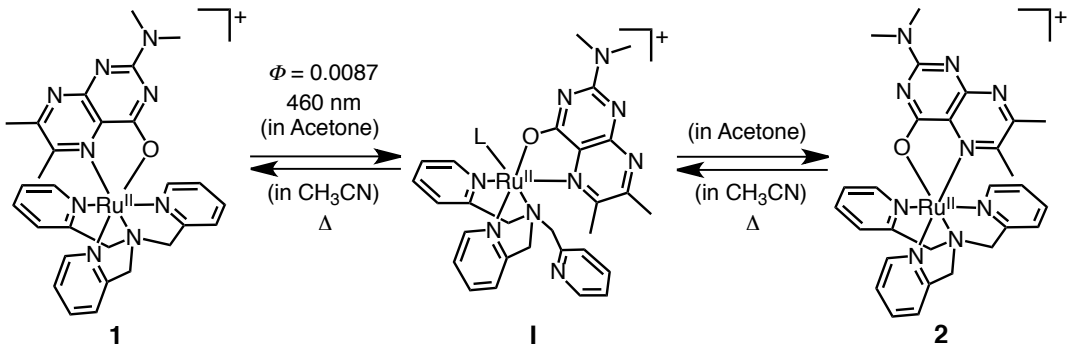

Scheme 2-2. Reversible photoinduced and subsequent thermal isomerization between **1** and **2** including intermediate **I**.

2-2-2. Crystal structure of the isomer 2

The structure of the isomer **2** has been clearly determined by X-ray diffraction analysis using a synchrotron facility. A single crystal of **2** suitable for X-ray crystallography was obtained from recrystallization with vapor diffusion of benzene into its acetone solution. The isomer **2** crystallized in a triclinic space group of $P\ \bar{1}$ and each asymmetric unit included a cationic part of **2**, a perchlorate ion as the counteranion, and two-and-a-half molecules of benzene as solvent molecules of crystallization. The crystal structure of the cationic part of **2** is shown in Figure 2-6 and the selected bond lengths [Å] and angles [°] are summarized in Table 2-1, together with the corresponding values for the crystal structure of **1**.[19a] Similar to complex **1**,[19a] the pterin ligand in **2** coordinates to the Ru(II) center as a monoanion in a bidentate fashion through the N5 and O1 positions to form a five-membered chelate ring. In comparison with **1**, however, the orientation of the pterin ligand relative to the tetradentate TPA ligand in **2** is different from that in **1**. In the structure of **2**, the O1 atom of the pterin ligand is located at the *trans* position to the tertiary amino nitrogen of the TPA ligand and the N5 atom forms the equatorial plane in cooperation with the N1, N2, and N3 atoms

Table 2-1. Selected bond lengths [Å] and angles [°] of complexes **1** and **2**.

	2	**1**[19a]
Ru–O1	2.100(1)	2.083(5)
Ru–N1	2.055(2)	2.082(7)
Ru–N2	2.029(1)	2.086(6)
Ru–N3	2.071(2)	2.050(8)
Ru–N4	2.082(1)	2.041(7)
Ru–N5	2.142(1)	2.107(6)
O1–C23	1.284(2)	1.27(1)
N8–C23	1.332(2)	1.32(1)
N9–C22	1.364(2)	1.369(9)
N7–C22	1.344(2)	1.32(1)
N8–C22	1.366(2)	1.37(1)
O1-Ru-N5	78.88(5)	80.3(2)
N1-Ru-N4	82.87(6)	81.2(3)
N2-Ru-N4	80.80(6)	80.8(3)
N3-Ru-N4	80.06(6)	83.4(3)
N1-Ru-N2	84.56(6)	100.7(3)
O1-Ru-N2 for **1** and -N4 for **2**	169.05(6)	166.1(3)
N1-Ru-N3	162.63(6)	164.4(3)
N5-Ru-N4 for **1** and -N2 for **2**	169.84(6)	169.4(2)

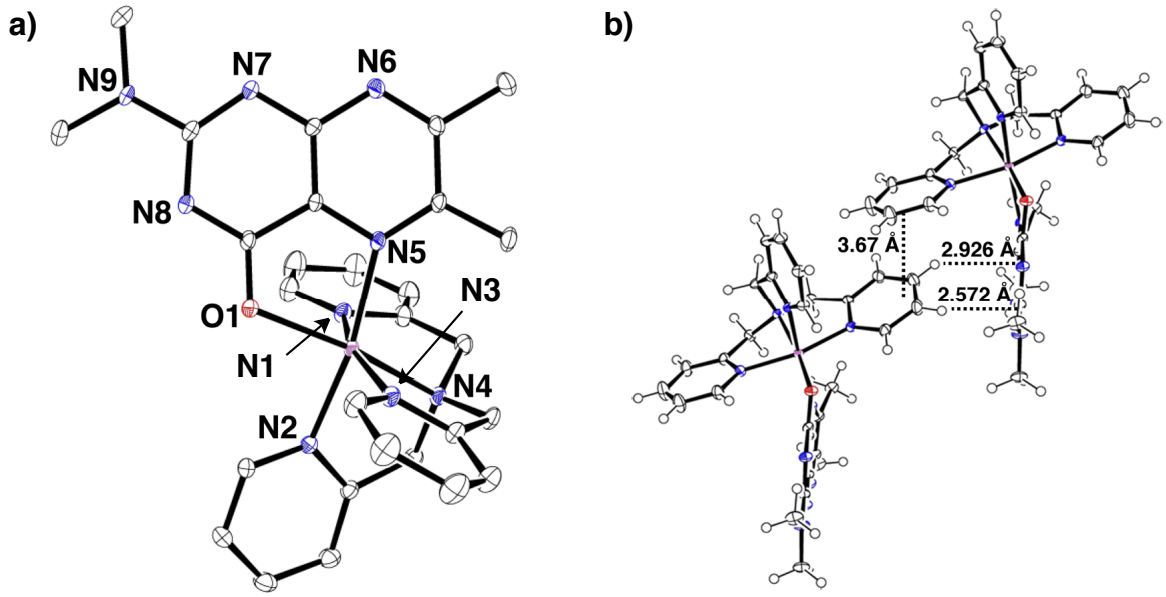

Figure 2-6. Crystal structure of a) the cationic part of complex **2** and b) the dimeric structure with π–π and CH–π interactions.

of the TPA ligand. In complex **1**, the *trans* position of the σ-donating amino nitrogen (N4) of the TPA ligand[23, 24] is occupied by the π-accepting pyrazine nitrogen (N5) of the pterin ligand, and that of the π-accepting pyridine nitrogen (N2) of TPA[23] is coordinated by a strongly π-donating oxygen (O1) of the pterin. In consequence, the coordination environment around the Ru(II) center in **1** is electronically favorable.[24, 25] On the other hand, in complex **2**, the σ-donating N4 and the π-donating O1 atoms are *trans*-positioned to each other, and the π-accepting pyridine nitrogen (N2) and pyrazine nitrogen (N5) atoms are also *trans* to each other. This is the main reason for the thermal instability of complex **2**[24] compared with complex **1** evidenced by the fact that the bond lengths of the pterin ligand to the Ru(II) center in complex **2** (Ru–O1: 2.100(1) Å, Ru–N5: 2.142(1) Å) are longer than those in **1** (Ru–O1: 2.083(5) Å, Ru–N5: 2.107(6) Å). In addition, severe steric repulsion operates between the 6-methyl group of the pterin ligand and the methylene linkage of the equatorial pyridylmethyl groups of the TPA ligand in **2**. This repulsion makes the pterin plane tilt to the equatorial plane of the Ru(II) center, and as a result, the pyrazine ring comes close to the pyridine ring that contains N3. The dihedral angle between the pterin mean plane and the equatorial plane made of O1, N1, N3, and N4 is estimated to be 72.8°. The coordinated oxygen (O1) and the 6-H of the axial pyridine with N2 forms a nonclassical hydrogen bond[26] with a distance of 3.018 Å to cause the downfield shift of its proton signal relative to that of **1** (*vide supra*).

In the crystal packing, the cationic part of **2** forms a supramolecular one-dimensional array (Figure 2-6b) with the force of π–π stacking between the N1- and the N3-pyridine rings of another molecule and the interplane distance is 3.67 Å, which is within the range of π–π stacking distances.[27] Edge-to-face π–π interaction[28] is also observed between the *meta*- and *para*-CH hydrogen atoms of the N1-pyridine ring and the π-conjugated system of the pterin ligand in the adjacent molecule, and the distances from the C–H hydrogen atoms to the pterin plane are 2.57 and 2.93 Å for the *meta*- and *para*-hydrogen atoms, respectively.

2-2-3. Quantum yield of the photodissociation reaction and kinetic analysis of the subsequent thermal process

The quantum yield of the initial photoinduced process (**1** → **I**) in acetone with irradiation at 460 nm was determined to be 0.87% by means of a standard actinometer method (see the Experimental Section).[29] The quantum yield is comparable to that of the photoreaction of diimine-Ru(II)-TPA complexes (diimine = bpy, 2,2'-bipyrimidine (bpm), 1,10-phenanthroline (phen)),[22] which exhibited a characteristic photochromic behavior in which one coordination bond of a pyridine nitrogen of the TPA ligand to the Ru(II) center was cleaved by photoirradiation and the resulting vacant site at the Ru(II) center was filled with a solvent molecule such as acetonitrile. On the other hand, photoisomerization of alloxazine–Ru(II)–TPA complex, $[Ru(Hallo)(TPA)]^+$ (**3**), in which the $Hallo^-$ ligand coordinates to the Ru(II) center through the 1-N and 10-N atoms to form a four-membered chelate ring, gave a larger quantum yield than that of **1**.[21] This reflects the fact that the first process in the photoreaction of **1** is the bond dissociation of the nitrogen in the axial pyridyl group of the TPA ligand to form a fairly stable and five-membered chelate ring from the Ru(II) center, in sharp contrast to the reaction of **3** in which the alloxazine ligand with a less stable and four-membered chelate ring undergoes partial dissociation (*vide infra*).

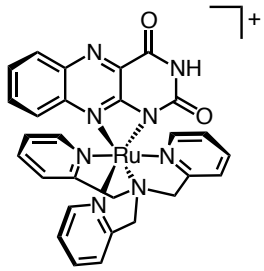

3

The first-order rate constants of the subsequent thermal process (**I** → **2**) in acetone at various temperatures were determined from the absorption change at λ_{max} = 460 nm, and the rate constants thus determined were plotted against the inverse of temperature (Figure 2-7).[30] On the basis of the Eyring plot, the activation parameters of the thermal reaction were determined to be $\Delta H^{\ddagger}$ = 81.8 kJ mol^{-1} and $\Delta S^{\ddagger}$ = –49.8 J mol^{-1} K^{-1}. The negative activation entropy indicates that this process involves the recoordination of the photodissociated pyridylmethyl group of the TPA ligand to the Ru(II) center, but the value is relatively small compared to a typical activation entropy for the reaction that contains the process of one molecule captured by the other molecule in a bimolecular reaction;[21, 22b, 31] this is because it is an intramolecular process, in

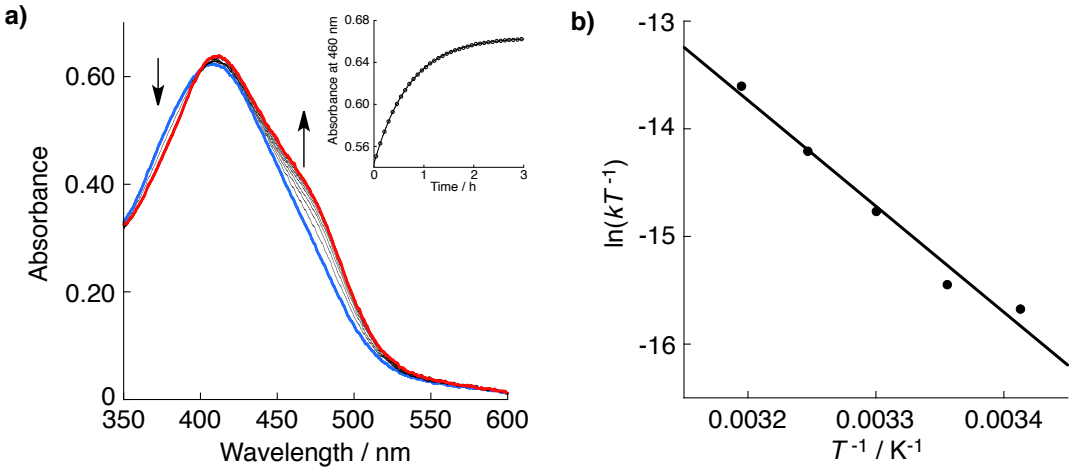

Figure 2-7. a) Absorption spectral change and inset: plot of the absorption change at 460 nm against the time. b) Eyring plot for the thermal process from **I** into **2**.

which the coordinated pyridylmethyl group is anchored by the coordination of the tertiary amino group to the Ru(II) center and loses a degree of its freedom.[31b] The positive activation enthalpy ($\Delta H^{\ddagger}$) indicates that the seven coordination at the Ru(II) center is too energetically unstable to overcome the energetic benefit by the coordination-bond formation in the process.[32]

2-2-4. Thermal back reaction to complex 1

When complex **2** was dissolved in acetone and kept for a long time, it remained intact and never showed reverse isomerization to recover complex **1**, even at reflux. In sharp contrast, upon heating to reflux the solution of **2** in CH_3CN, the absorption spectrum gradually turned into that of **1**. ^{1}H NMR spectroscopic analysis confirmed that the product was complex **1**. Thus, the isomerization reaction of **1** is reversible and the direction of the reaction can be controlled by external stimuli such as light, heat, and solvent.

The back reaction of **2** to afford **1** was monitored by the absorption spectral change at various temperatures and the rate constant at each temperature was determined by first-order kinetic analysis (Figure 2-8a). These data were plotted against the inverse of temperature to provide an Eyring plot,[30] and the activation parameters of the reaction were determined by linear analysis (Figure 2-8b). The activation

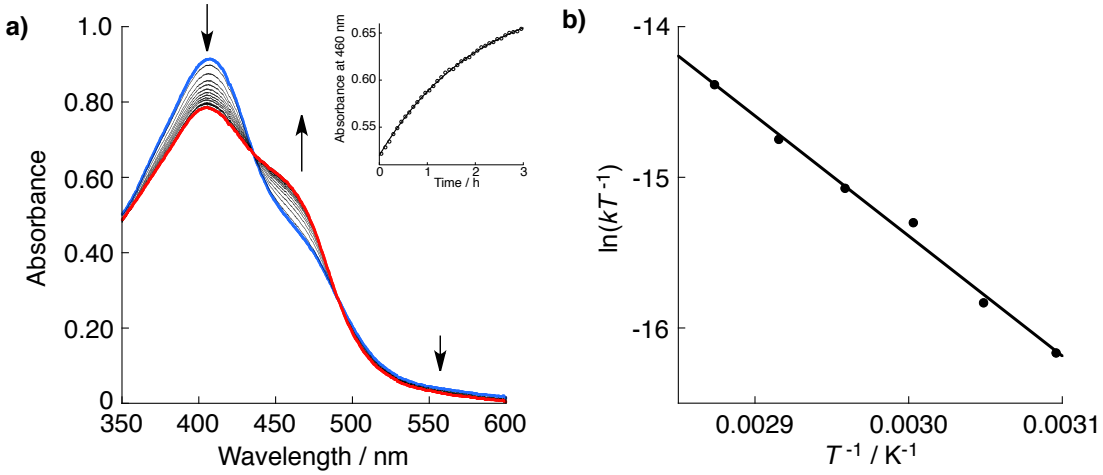

Figure 2-8. a) Absorption spectral change and inset: plot of the absorption change at 460 nm against the time. b) Eyring plot for the thermal process from **2** into **1**.

enthalpy ($\Delta H^{\ddagger}$) and entropy ($\Delta S^{\ddagger}$) were determined to be 59.2 kJmol^{-1} and –147.4 J mol^{-1} K^{-1}, respectively. The large negative activation entropy indicates that the transition state involves strong solvent coordination to the Ru(II) center (*vide infra*) through an interchange associative (I_a) mechanism.[31] The positive activation enthalpy $\Delta H^{\ddagger}$ also indicates that the seven-coordinated Ru(II) complex as a transition state is thermally unstable, but the positive value is smaller than that for the reaction from **I** to **2**, which reflects that the coordination of acetonitrile is stronger than that of acetone or the difference in the free energy between the starting complex **1** and the isomer **2**.

2-2-5. Reaction mechanism

The reaction pathway of the reversible isomerization between complexes **1** and **2** (Scheme 2-3) has been fully elucidated on the basis of the data mentioned above. The first step is the photodissociation of the axial pyridine moiety in the TPA ligand of **1** due to the sterically unfavorable situation as found in the photochromic Ru(II)–TPA–diimine complexes.[22] For the photodissociation reaction, it was concluded that the dissociated pyridine was not the equatorial one but the axial one based on the experiments with use of 5-Me-tpa as a ligand for the photochromic structural change of the Ru(II)-TPA-diimine complexes.[22] In contrast, the first step in the photoreaction of **3**, which also exhibits a photochromic behavior induced by photoirradiation, has been reported to be the bond dissociation between the N10 atom of the Hallo$^-$ ligand and the Ru(II) center.[21] This difference in the reaction pathways between **1** and **3**, both of which involve a redox-active fused heteroaromatic coenzyme[14, 33] as the monoanionic bidentate ligand, may be caused by the difference in the bidentate coordination mode of the heteroaromatic coenzyme ligands. The Hallo$^-$ ligand in **3** forms a unique four-membered chelate ring, which consists of the Ru(II) center, N1, N10 and a carbon atom of the Hallo$^-$ ligand. Thus, the coordination is relatively weak due to the highly strained chelate-ring structure.[34–36] In contrast, the dmdmp$^-$ ligand coordinates to the Ru(II) center to constitute a stable

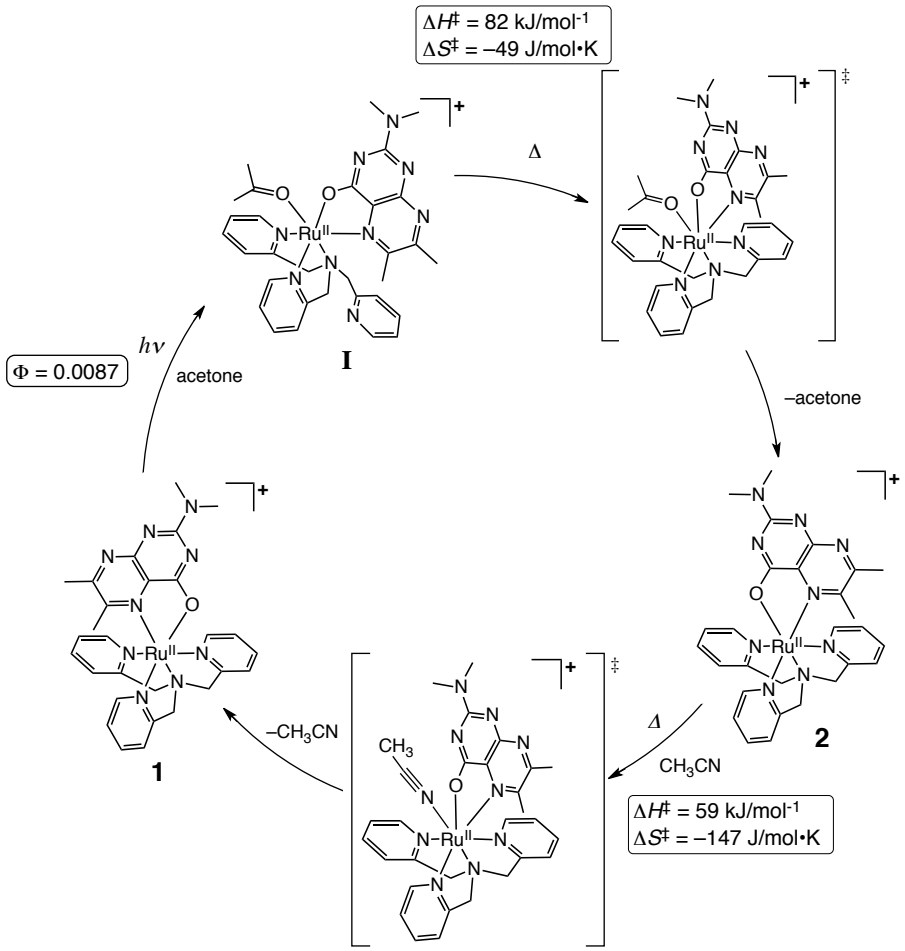

Scheme 2-3. Reaction mechanism of the reversible photoinduced isomerization of **1** including the plausible transition states for the two thermal processes.

five-membered chelate ring with the N5 and O1 of the dmdmp⁻ ligand.[15–19, 37] Consequently, photoexcitation of complex **1** in acetone results in the dissociation of the relatively labile axial pyridine rather than partial dissociation of the dmdmp⁻ ligand.[38]

The subsequent thermal process after the photodissociation of the pyridylmethyl arm in complex **1** gives only isomer **2** without going back to starting complex **1**. In this reaction, the recoordination of the free pyridylmethyl group to the Ru(II) center can be the rate-determining step to give a seven-coordinate transition state and the recoordination may occur only from the relatively less-hindered N5 side of the dmdmp⁻ ligand, resulting in the complete conversion to **2** (*vide infra*, Figure 2-9). The photodissociation and the recoordination of the pyridine ring in these two steps are the factors to accomplish this unique one-way isomerization induced by photoirradiation.

In the thermal back reaction from **2** to **1**, the solvent plays the most important role to control the reactivity. In acetone, complex **2** is quasi-stable not to perform the thermal back reaction even at the boiling point of acetone. On the other hand, when complex **2** is dissolved in acetonitrile and stirred at 70 ºC, it undergoes the back isomerization into **1** with a relatively large rate constant (*vide supra*). This reactivity dependence on the solvent can be caused by the difference in the coordination strength between the two solvents to the Ru(II) center.[39] The coordination of the acetonitrile molecule to the Ru(II) center is generally stronger than that of the acetone molecule due to the softness of Ru(II) ion in the hard and soft (Lewis) acids and bases (HSAB) theory,[40] as represented by the strong π backbonding from the Ru(II) center to the π* orbital of the coordinating acetonitrile.[41] As mentioned above, the presumed transition state of the reaction from **2** to **1** is a seven-coordinated complex, in which the strongly coordinating solvent molecules (*i.e.*, acetonitrile) assists the stabilization of the transition state, and therefore the back reaction can occur only in acetonitrile (see Figure 2-9).

The energy optimization for **1** and **2** was conducted with DFT calculations at the CAM-B3LYP/LANL2DZ level of theory.[42, 43] Comparison was also made for the reaction coordinates in acetone to clarify the influence of solvent on the energies of solvation. Relative energy levels of **1** and the photoisomer **2** are depicted in Figure 2-9a, in which the energy levels of **1** (reactant complex) and **2** (isomer complex) were calculated by including one solvent molecule with a distance of 2–3 Å to adjust the number of atoms for the calculations. In both cases, the free energy of **2** is higher relative to that of **1** by 2.5 kcal mol^{-1} (without acetone) and 4.5 kcal mol^{-1} (with acetone), respectively. The optimization of possible structures of the intermediate (**I**) in the forward reaction reveals that int3 is the most stable species among three as shown in Figure 2-9b. This is consistent with the experimental observations of the differential NOE spectrum of intermediate **I**. In the NOE spectrum, the correlation was observed between the methylene signal of the uncoordinated pyridine moiety and the methyl signal at the 6-position of the pterin ligand (Figure 2-10). The correlation in NOE experiments is generally observed between the protons with spatial distances of less than 5 Å. The calculated distances between the topical protons in the optimized structures are 6.5, 3.7, and 4.5 Å for int1, int2, and int3, respectively. In addition, the isolated products of the photoreaction of Ru(TPA)-diimine complexes are also in the same conformation as int3,[22] which also supports the assignment of the photoreaction product of **1** as int3.

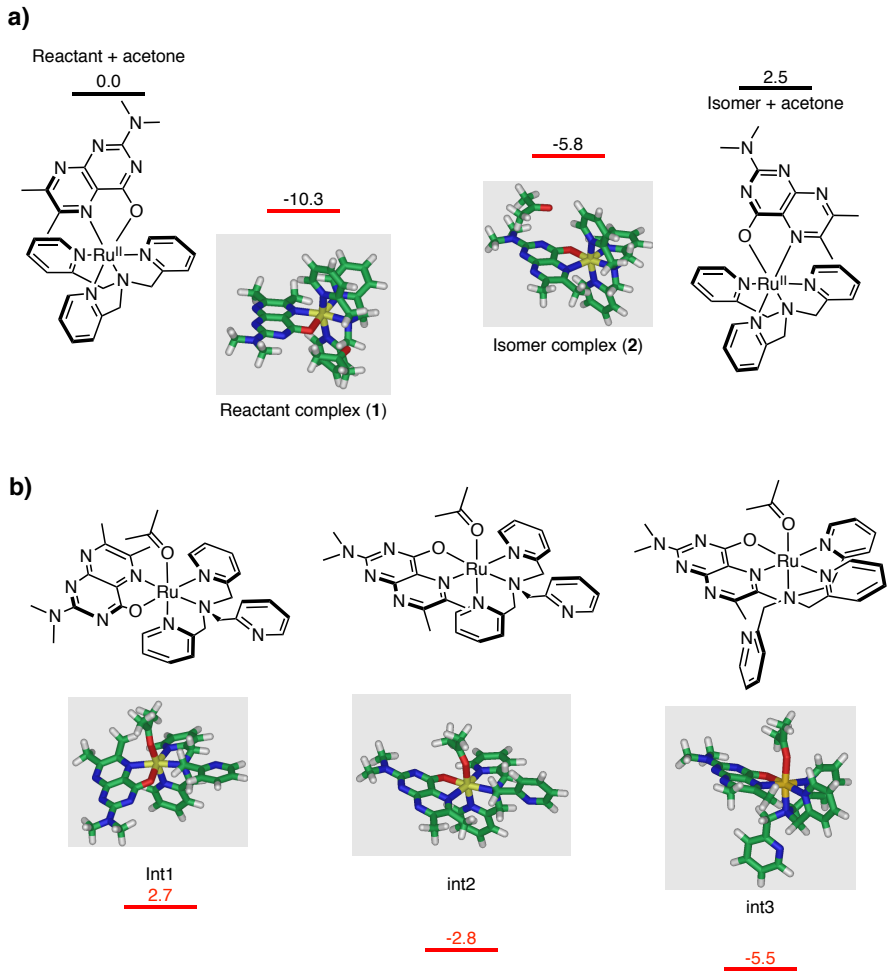

Figure 2-9. a) A diagram for the energy levels [kcal mol^{-1}] of the reactant (**1** solvated with acetone) and the isomer (**2** solvated with acetone) obtained by DFT calculations at the CAM-B3LYP/LANL2DZ level of theory. b) Energetic comparison among three possible structures of the intermediates with a coordinated acetone based on DFT calculations.

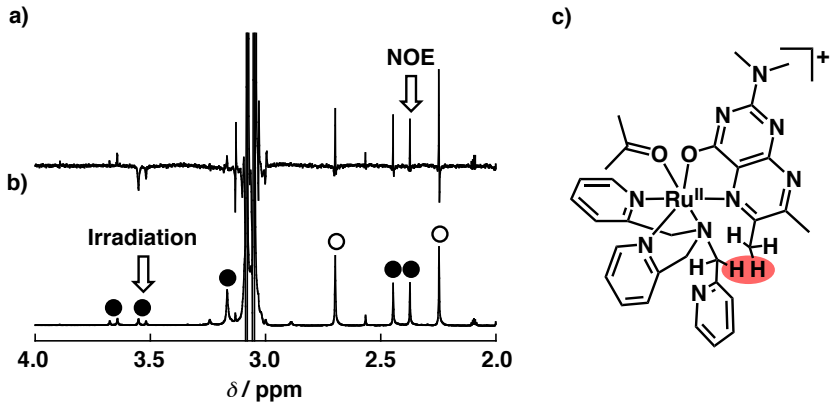

Figure 2-10. (a) Differential NOE and (b) the ambient ^{1}H NMR spectra of intermediate **I** in acetone-d_6. ●: The signals assigned to **I**, ○: The signals assigned to **2**. (c) The plausible structure of **I** (int3 in Figure 2-9) and the NOE correlation observed protons (red).

These unique controls of the reaction pathways by light, steric bulkiness, and solvents have enabled us to accomplish the photochromic isomerization reaction induced by photoirradiation to exhibit 100% conversion efficiency in the forward reaction without forming a photostationary mixture of isomers. On the other hand, the isomerization of alloxazine complex **3** can exhibit 87% conversion at most because the reaction proceeds through the transition state with a monodentate $Hallo^-$ ligand to the Ru(II) center and the $Hallo^-$ rotates around the bond axis to the Ru(II) center to give the isomer.[21] Thus, the reaction direction of **3** is hard to control completely and a photostationary mixture is obtained from the reaction. The 100% conversion efficiency in the photoisomerization and the stability of isomer **2** in acetone allow us not only to fully characterize the structure of **2** by ^{1}H NMR spectroscopy and X-ray diffraction analysis but also to investigate the kinetics of both the forward and backward pathways in this completely reversible isomerization reaction.

2-3. Conclusion

A new photochromic isomerization reaction of a Ru(II)-pterin complex, $[Ru^{II}(dmdmp)(TPA)]^+$ (**1**), has been found and the isomeric complex (**2**) has been fully characterized by ^{1}H NMR spectroscopy, ESI-TOF MS spectrometry, and single-crystal X-ray diffraction analysis. The reaction mechanisms for both the forward and backward thermal reaction pathways of this isomerization have been clarified by kinetic analysis to reveal the transition states and the rate-determining steps as follows. The forward reaction in acetone passes through intermediate **I**, which is the product of the initial photoinduced step that involves the dissociation of the axial pyridylmethyl group of the TPA ligand and the coordination of the solvent acetone molecule. The subsequent thermal process gives only the isomeric complex **2** without going back to the starting **1**, because steric factors in the seven-coordinated transition state control the direction of the recoordination of the photodissociated pyridylmethyl group to afford the product with 100% conversion. The back reaction of **2** to **1** occurs in acetonitrile at high temperature, and the transition state may also be a seven-coordinated complex. Thus, the isomerization reaction of **1** is reversible, and the reaction direction is fully controlled by light, steric hindrance, and solvents. Furthermore, the conversion efficiency of the reaction in both directions is 100%. To the best of the author's knowledge, this is the first example to demonstrate a clear bistability that involves complete switching of the two distinct structures in the photochromism of a transition-metal complex.[6–11] The complete determination of the driving force for each direction is essential to establish two different situations of a compound independently without perturbation from thermodynamic equilibrium or a photostationary state.[44] The molecular bistability observed in the photochromic Ru(II)-pterin complex **1** has presented a new kind of metal complexes that can be excited by visible light and might aid in the development of molecular devices that switch between two different structural motifs[45] to enable complete on/off regulation and the sophisticated control of molecular functionality.

2-4. Experimental section

General. All commercially available chemicals were purchased from appropriate sources and used as

received unless otherwise mentioned. $[RuCl(TPA)]_2(ClO_4)_2$[20] and $[Ru(dmdmp)(TPA)](ClO_4)$ (**1**)[19b] were prepared according to the literature. All NMR spectroscopic measurements were performed using JEOL EX270 and Bruker AVANCE400 spectrometers. UV/Vis absorption spectra were measured in CH_3CN using a Shimadzu UV-3600 spectrophotometer at room temperature. ESI-TOF-MS spectra were measured using an Applied Biosystems QSTAR Pulsar I mass spectrometer.

$[Ru(dmdmp)(TPA)(acetone)](ClO_4)$ (intermediate I): Solid $[Ru(dmdmp)(TPA)](ClO_4)$ (**1**) (1.1 mg, 1.6 μmol) was dissolved in acetone-d_6 (1.0 mL) and irradiated with light centered at 460 nm at room temperature for 4 h. The reaction was monitored with ^{1}H NMR spectroscopy and the product ratio was **I** : **2** = 9 : 10. ^{1}H NMR (acetone-d_6): δ 9.12 (d, J = 6.2 Hz, 1H), 8.77 (d, J = 5.4 Hz, 1H), 8.66 (d, J = 4.9 Hz, 1H), 7.84–7.69 (m, 3H), 7.35–7.29 (m, 6 H), 5.00 and 4.72 (ABq, J_{AB} = 17.8 Hz, 2H), 4.76 and 4.27 (ABq, J_{AB} = 15.5 Hz, 2H), 3.87 and 3.70 (ABq, J_{AB} = 13.4 Hz, 2 H), 3.25 (s, 6 H), 2.62 (s, 3H), 2.53 ppm (s, 3H). MS (ESI): calcd for $[M - ClO_4]^+$: m/z = 668.20, found: m/z = 668.24.

$[Ru(dmdmp)(TPA)](ClO_4)$ (isomer 2): Solid $[Ru(dmdmp)(TPA)](ClO_4)$ (**1**) (1.6 mg, 2.3 μmol) was dissolved in acetone (4 mL) and irradiated with light centered at 460 nm at room temperature for 4 h. The resulting solution was stirred for 12 h at room temperature in the dark. Then the solution was passed through celite, the solvent was removed under vacuum, and the solid was recrystallized from acetone/benzene. A red crystal of **2**: 1.0 mg (63%). ^{1}H NMR (acetone-d_6): δ 9.76 (d, J = 5.7 Hz, 1H), 8.43 (d, J = 5.5 Hz, 2H), 7.82–7.69 (m, 3 H), 7.53–7.29 (m, 6H), 5.65 and 5.29 (ABq, J_{AB} = 16.7 Hz, 4H), 4.89 (s, 2H), 3.30 (s, 6H), 2.89 (s, 3 H), 2.43 ppm (s, 3 H). MS (ESI): calcd for $[M - ClO_4]^+$: m/z = 610.16, found: m/z = 610.18.

Photochemical reactions. Photoirradiation of complex **1** was performed by using an ASAHI SPECTRA MAX-301 xenon light source (300 W), equipped with a bandpath filter of the bandwidth at half-maxima of 20 nm centered at 460 nm. Complex **1** was dissolved in freshly distilled acetone at 8.1×10^{-5} M for the UV/Vis absorption spectroscopic measurements and in acetone-d_6 at 1.4 mM for the ^{1}H NMR spectroscopic experiments, and the solution was degassed by argon bubbling. The degassed solution was irradiated as mentioned above for 12 h and the progress of the reaction was monitored by the absorbance change at 460 nm.

Quantum yield determination. The quantum yield of the photodissociation of **1** was determined by a standard method using an actinometer (potassium ferrioxalate)[29] in water with photoirradiation at 460 nm. The photodissociation reaction was monitored at 460 nm to determine the time course of the decrease in the absorption, and the data in the initial stage, during which the time course exhibited linear change was used to determine the quantum yield.

Kinetic analysis of the two thermal processes. The thermal reaction following the photodissociation of **1** was monitored by the absorption change at 460 nm, and the change was fit to the following first-order kinetic equation [Eq. (1)]:

$$\mathrm{Abs} = \mathrm{Abs}_{\infty} + (\mathrm{Abs}_0 - \mathrm{Abs}_{\infty})e^{-kt} \qquad (1)$$

Similar experiments were conducted at variable temperatures and the rate constants thus determined were plotted according to the following Eyring equation to determine the activation parameters [Eq. (2)]:

$$\ln(kT^{-1}) = \Delta H^{\ddagger}R^{-1}T^{-1} + \Delta S^{\ddagger}R^{-1} + \ln(k_B/h) \qquad (2)$$

X-ray crystallographic analysis of 2. The diffraction data were measured using a Rigaku Mercury CCD system at the Photon Factory Advanced Ring for pulse X-rays (PF-AR NW2A) of the High Energy Accelerator Research Organization (KEK, Tsukuba, Japan). The data were integrated, scaled, and corrected for absorption with the HKL2000 program. Crystallographic data: $C_{28}H_{30}N_9ORu{\cdot}ClO_4{\cdot}2.5C_6H_6$; *MW* = 904.40; red-orange; triclinic; space group $P\ \bar{1}$; a = 9.6594(2), b = 11.3490(1), c = 19.9191(2) Å; α = 85.6650(7), β = 85.3227(7), γ = 70.931(1)°; V = 2054.14(6) Å^3; T = 100(1) K; Z = 2; ρ_{calcd} = 1.462 g cm^{-3}; λ(synchrotron) = 0.6890 Å; 42263 reflections measured; 13725 unique (R_{int} = 0.0675), which were used in all calculations. All calculations were performed using the Bruker APEX2 crystallographic software package. The structure was solved by direct methods (SHELXL-97) and refined by full-matrix least-squares methods on F^2 with 537 parameters. $R1$ = 0.0501 ($I > 2\sigma(I)$) and $wR2$ = 0.1328, GOF = 1.039, max/min residual density: 3.112/–3.224 e Å^{-3}. CCDC-792042 contains the supplementary crystallographic data. These data can be obtained free of charge from The Cambridge Crystallographic Data Centre via www.ccdc.cam.ac.uk/data_request/cif.

DFT calculations. Local minima was optimized on the potential energy using the Coulomb-attenuating method B3LYP functional called CAMB3LYP.[42, 43, 46] For Ru atoms, the LANL2DZ basis sets developed by Hay and Wadt were used,[47] and for the H, C, N, and O atoms, the D95** basis set was applied.[48] Vibration frequencies were systematically computed to ensure that on a potential-energy surface each optimized geometry corresponds to a local minimum that has no imaginary frequency. The Gaussian 09[49] program package was used for all DFT calculations.

Reference and notes

[1] a) J. S. Miller, *Angew. Chem. Int. Ed.* **2003**, *42*, 27–29; b) O. Sato, *Acc. Chem. Res.* **2003**, *36*, 692–700; c) A. Hanster, J. Jeftic, H. Romstedt, R. Hinek, H. Siering, *Coord. Chem. Rev.* **1999**, *190–192*, 471–491; d) P. Gütlich, Y. Garcia, H. A. Goodwin, *Chem. Soc. Rev.* **2000**, *29*, 419–427; e) C. P. Collier, G. Mattersteig, E. W. Wang, Y. Luo, K. Beverly, J. Sampaio, F. M. Raymo, J. F. Stoddart, J. R. Heath, *Science* **2000**, *289*, 1172–1175.

[2] a) *Photochromism: Molecules and Systems* (Eds.: H. Dürr, H. Bouas-Laurent,), Elsevier, Amsterdam, **2003**; b) S. Kawata, Y. Kawata, *Chem. Rev.* **2000**, *100*, 1777–1788; c) M. Irie, Bull. *Chem. Soc. Jpn.* **2008**, *81*, 917–926; d) G. Jiang, Y. Song, X. Gup, D. Zhang, D. Zhu, *Adv. Mater.* **2008**, *20*, 2888–2898; e) D. Gust, T. A. Moore, A. L. Moore, *Chem. Commun.* **2006**, 1169–1178; f) M.-S. Wang,

G. Xu, Z.-J. Zhang, G.-C. Guo, *Chem. Commun.* **2010**, *46*, 361–376; g) E. Hadjoudis, I. M. Mavridis, *Chem. Soc. Rev.* **2004**, *33*, 579–588; h) F. M. Raymo, M. Tomasulo, *Chem. Soc. Rev.* **2005**, *34*, 327–336.

[3] a) G. S. Kumar, D. C. Neckers, *Chem. Rev.* **1989**, *89*, 1915–1925; b) Y. Einaga, *Bull. Chem. Soc. Jpn.* **2006**, *79*, 361–372; c) Y. Zhao, *Pure Appl. Chem.* **2004**, *76*, 1499–1508; d) A. Natason, P. Rochon, *Chem. Rev.* **2002**, *102*, 4139–4176; e) T. Muraoka, K. Kinbara, T. Aida, *Nature* **2006**, *440*, 512–515; f) K. Ichimura, S.-K. Oh, M. Nakagawa, *Science* **2000**, *288*, 1624–1626; g) Y. Yu, M. Nakao, T. Ikeda, *Nature* **2003**, *425*, 145.

[4] a) G. Berkovic, V. Krongauz, V. Weiss, *Chem. Rev.* **2000**, *100*, 1741–1754; b) K. Nakatani, P. Yu, *Adv. Mater.* **2001**, *13*, 1411–1413; c) I. Cabrera, V. Krongauz, *Nature* **1987**, *326*, 582–585; d) I. Cabrera, F. Shvartsman, O. Veinberg, V. Krongauz, *Science* **1984**, *226*, 341–343; e) N. Kida, M. Hikita, I. Kashima, M. Okubo, M. Ito, M. Enomoto, K. Kato, M. Takata, N. Kojima, *J. Am. Chem. Soc.* **2009**, *131*, 212–220; f) J. L. Bahr, G. Kodis, L. de La Garza, S. Lin, A. L. Moore, T. A. Moore, D. Gust, *J. Am. Chem. Soc.* **2001**, *123*, 7124–7133.

[5] a) M. Irie, *Chem. Rev.* **2000**, *100*, 1685–1716; b) M. Morimoto, M. Irie, *Chem. Commun.* **2005**, 3895–3905; c) H. Tian, S. Yang, *Chem. Soc. Rev.* **2004**, *33*, 85–97; d) H. Tian, S. Wang, *Chem. Commun.* **2007**, 781–792; e) S.-J. Lim, B.-K. An, S. D. Jung, M.-A. Chung, S. Y. Park, *Angew. Chem. Int. Ed.* **2004**, *43*, 6346–6350; f) K. E. Maly, M. D. Wand, R. P. Lemieux, *J. Am. Chem. Soc.* **2002**, *124*, 7898–7899; g) S. Kobatake, S. Takami, H. Muto, T. Ishikawa, M. Irie, *Nature* **2007**, *446*, 778–781.

[6] J. G. Vos, M. T. Pryce, *Coord. Chem. Rev.* **2010**, *254*, 2519–2532.

[7] B. Durham, S. R. Wilson, D. J. Hodgson, T. J. Meyer, *J. Am. Chem. Soc.* **1980**, *102*, 600–607.

[8] a) B. A. McClure, J. J. Rack, *Angew. Chem. Int. Ed.* **2009**, *48*, 8556–8558; b) J. J. Rack, J. R. Winkler, H. B. Gray, *J. Am. Chem. Soc.* **2001**, *123*, 2432–2433; c) B. A. McClure, E. R. Abrams, J. J. Rack, *J. Am. Chem. Soc.* **2010**, *132*, 5428–5436, and references therein.

[9] a) Y. Kurauchi, K. Ohga, A. Yokoyama, S. Morita, *Bull. Chem. Soc. Jpn.* **1983**, *56*, 357–358; b) K. Ohga, Y. Kurauchi, *Bull. Chem. Soc. Jpn.* **1987**, *60*, 3269–3275.

[10] a) D. P. Schwendiman, J. I. Zink, *J. Am. Chem. Soc.* **1976**, *98*, 1248–1252; b) T. Weisheit, D. Escudero, H. Petzold, H. Görls, L. González, W. Weigand, *Dalton Trans.* **2010**, *39*, 9493–9504; c) D. Escudero, T. Weisheit, W. Weigand, L. González, *Dalton Trans.* **2010,** *39*, 9505–9513.

[11] a) H. Nakai, T. Nonaka, Y. Miyano, M. Mizuno, Y. Ozawa, K. Toriumi, N. Koga, T. Nishioka, M. Irie, K. Isobe, *J. Am. Chem. Soc.* **2008**, *130*, 17836–17845; b) H. Nakai, M. Mizuno, T. Nishioka, N. Koga, K. Shiomi, Y. Miyano, M. Irie, B. K. Breedlove, I. Kinoshita, Y. Hayashi, Y. Ozawa, T. Yonezawa, K. Toriumi, K. Isobe, *Angew. Chem. Int. Ed.* **2006**, *45*, 6473–6476; c) Y.-W. Zhong, N. Vilá, J. C. Henderson, H. D. Abruña, *Inorg. Chem.* **2009**, *48*, 7080–7085.

[12] a) G. A. Crosby, R. J. Watts, D. H. W. Carstens, *Science* **1970**, *170*, 1195–1196; b) C.-T. Liu, B. Bçttcher, M. Chou, C. Creutz, N. Sutin, *J. Am. Chem. Soc.* **1976**, *98*, 6536–6544; c) B. Durham, J. V. Caspar, J. K. Nagle, T. J. Meyer, *J. Am. Chem. Soc.* **1982**, *104*, 4803–4810; d) A. Juris, V. Balzani, F.

Barigelletti, S. Campagna, P. Belser, A. von Zelewsky, *Coord. Chem. Rev.* **1988**, *84*, 85 –277; e) Y. Sun, Y. Liu, C. Turro, *J. Am. Chem. Soc.* **2010**, *132*, 5594–5595.

[13] C. R. Hecker, P. E. Fanwick, D. R. Mcmillin, *Inorg. Chem.* **1991**, *30*, 659–666.

[14] a) J. A. Endrizzi, J. D. Cronk, W. Wang, G. R. Crabtree, T. Alber, *Science* **1995**, *268*, 556–559; b) X.-D. Lei, S. Kaufman, *Proc. Natl. Acad. Sci. USA* **1998**, *95*, 1500–1504; c) T. J. Kappock, J. P. Caradonna, *Chem. Rev.* **1996**, *96*, 2659–2756; d) C. S. Raman, H. Li, P. Martásek, V. Král, B. S. S. Masters, T. L. Poulos, *Cell* **1998**, *95*, 939–950; e) G. Schwarz, R. R. Mendel, M.W. Pibbe, *Nature* **2009**, *460*, 839–847.

[15] W. Kaim, B. Schwederski, O. Heilmann, F. M. Hornung, *Coord. Chem. Rev.* **1999**, *182*, 323–342.

[16] For Mo: a) S. J. N. Burgmayer, E. I. Steifel, *J. Am. Chem. Soc.* **1986**, *108,* 8310–8311; b) B. Fischer, H. Schmalle, E. Dubler, A. Schäfer, M. Viscontini, *Inorg. Chem.* **1995**, *34*, 5726–5734; c) S. J. N. Burgmayer, M. R. Arkin, L. Bostick, S. Dempster, K. M. Everett, H. L. Layton, K. E. Paul, C. Rogge, A. L. Rheingold, *J. Am. Chem. Soc.* **1995**, *117*, 5812–5823; d) H. L. Kaufmann, L. Liable-Sands, A. L. Rheingold, S. J. N. Burgmayer, *Inorg. Chem.* **1999**, *38*, 2592–2599; e) H. L. Kaufmann, P. J. Carroll, S. J. N. Burgmayer, *Inorg. Chem.* **1999**, *38*, 2600–2606; f) S. J. N. Burgmayer, H. L. Kaufmann, G. Fortunato, P. Hug, B. Fischer, *Inorg. Chem.* **1999**, *38*, 2607 –2613.

[17] For Cu: a) T. Kohzuma, A. Odani, Y. Morita, N. Takani, O. Yamauchi, *Inorg. Chem.* **1988**, *27*, 3854–3858; b) T. Kohzuma, H. Masuda, O. Yamauchi, *J. Am. Chem. Soc.* **1989**, *111*, 3431–3433; c) A. Odani, H. Masuda, K. Inukai, O. Yamauchi, *J. Am. Chem. Soc.* **1992**, *114*, 6294–6300; d) M. S. Nasir, K. D. Karlin, Q. Chen, J. Zubieta, *J. Am. Chem. Soc.* **1992**, *114*, 2264–2265; e) J. Perkinson, S. Brodie, K. Yoon, K. Mosny, P. J. Carroll, T. V. Morgan, S. J. N. Burgmayer, *Inorg. Chem.* **1991**, *30*, 719–727; f) M. Mitsumi, J. Toyoda, K. Nakasuji, *Inorg. Chem.* **1995**, *34*, 3367–3370; g) D.-H. Lee, N. N. Murthy, Y. Lin, N. S. Nasir, K. D. Karlin, *Inorg. Chem.* **1997**, *36*, 6328–6334; h) Y. Funahashi, Y. Hara, H. Masuda, O. Yamauchi, *Inorg. Chem.* **1997**, *36*, 3869–3875.

[18] For Ru: a) A. Abelleira, R. D. Galang, M. J. Clarke, *Inorg. Chem.* **1990**, *29*, 633–639; b) E. C. Glazer, Y. H. L. Nguyen, H. B. Gray, D. B. Goodwin, *Angew. Chem. Int. Ed.* **2008**, *47*, 898–901.

[19] a) T. Kojima, T. Sakamoto, Y. Matsuda, K. Ohkubo, S. Fukuzumi, *Angew. Chem. Int. Ed.* **2003**, *42*, 4951–4954; b) S. Miyazaki, T. Kojima, T. Sakamoto, T. Matsumoto, K. Ohkubo, S. Fukuzumi, *Inorg. Chem.* **2008**, *47*, 333–343; c) S. Miyazaki, K. Ohkubo, T. Kojima, S. Fukuzumi, *Angew. Chem. Int. Ed.* **2008**, *47*, 9669–9672; d) S. Miyazaki, T. Kojima, J. M. Mayer, S. Fukuzumi, *J. Am. Chem. Soc.* **2009**, *131*, 11615–11624.

[20] T. Kojima, T. Amano, Y. Ishii, M. Ohba, Y. Okaue, Y. Matsuda, *Inorg. Chem.* **1998**, *37*, 4076–4085.

[21] S. Miyazaki, T. Kojima, S. Fukuzumi, *J. Am. Chem. Soc.* **2008**, *130*, 1556–1557.

[22] a) T. Kojima, T. Morimoto, T. Sakamoto, S. Miyazaki, S. Fukuzumi, *Chem. Eur. J.* **2008**, *14*, 8904–8915; b) T. Kojima, T. Sakamoto, Y. Matsuda, *Inorg. Chem.* **2004**, *43*, 2243–2245.

[23] a) *Comprehensive Coordination Chemistry, Vol. 5* (Ed.: G. Wilkinson), Pergamon Press, New York, **1987**; b) Z. Tyeklar, R. R. Jacobsen, N. Wei, N. N. Murthy, J. Zubieta, K. D. Karlin, *J. Am. Chem. Soc.* **1993**, *115*, 2677–2689; c) M. R. Bukowski, P. Comba, A. Lienke, C. Limberg, C. L. de Larorden, R.

Mas-Bellest, M. Merz, L. Que, Jr., *Angew. Chem. Int. Ed.* **2006**, *45*, 3446–3449.

[24] a) U. Koelle, *Coord. Chem. Rev.* **1994**, *135/136*, 623–650; b) N. Aebischer, E. Sidorenkova, M. Ravera, G. Laurenczy, D. Osella, J. Weber, A. E. Merback, *Inorg. Chem.* **1997**, *36*, 6009–6020.

[25] a) R. Romeo, M. R. Plutino, L. M. Scolaro, S. Stoccoro, G. Minghetti, *Inorg. Chem.* **2000**, *39*, 4749–4755; b) D. Jaganyi, A. Hofmann, R. van Eldik, *Angew. Chem. Int. Ed.* **2001**, *40*, 1680–1683; c) A. Hofmann, L. Dahlenburg, R. van Eldik, *Inorg. Chem.* **2003**, *42*, 6528–6538; d) A. Hofmann, D. Jaganyi, O. Q. Munro, G. Liehr, R. van Eldik, *Inorg. Chem.* **2003**, *42*, 1688–1700; e) M. Bruschi, P. Fantucci, L. De Giocia, *Inorg. Chem.* **2004**, *43*, 3733–3741.

[26] a) R. Taylor, O. Kennard, *J. Am. Chem. Soc.* **1982**, *104*, 5063–5070; b) P. L. Anelli, P. R. Ashton, R. Ballardini, V. Balzani, M. Delgado, M. T. Gandolfi, T. T. Goodnow, A. E. Kaifer, D. Philip, *J. Am. Chem. Soc.* **1992**, *114*, 193–218; c) D. S. Reddy, D. C. Craig, G. R. Desiraju, *J. Am. Chem. Soc.* **1996**, *118*, 4090–4093; d) F. M. Raymo, M. D. Bartberger, K. N. Houk, J. F. Stoddart, *J. Am. Chem. Soc.* **2001**, *123*, 9264–9267; e) M. Ohkita, M. Kawano, T. Suzuki, T. Tsuji, *Chem. Commun.* **2002**, 3054–3055; f) T. Steiner, *Angew. Chem. Int. Ed.* **2002**, *41*, 48–76.

[27] a) G. R. Desiraju, A. Gavezzotti, *J. Chem. Soc., Chem. Commun.* **1989**, 621–623; b) T. Kojima, K.-i. Hayashi, Y. Matsuda, *Chem. Lett.* **2000**, 1008–1009.

[28] C. A. Hunter, J. K. M. Sanders, *J. Am. Chem. Soc.* **1990**, *112*, 5525–5534.

[29] a) L. J. Heidt, G. W. Tregay, F. A. Middleton, Jr., *J. Phys. Chem.* **1970**, *74*, 1876–1882; b) C. H. Langford, C. A. Houlubor, *Inorg. Chim. Acta* **1981**, *53*, L59L60.

[30] H. Eyring, *J. Chem. Phys.* **1935**, *3*, 107–115.

[31] a) T. Kojima, S. Miyazaki, K. Hayashi, Y. Shimazaki, F. Tani, Y. Naruta, Y. Matsuda, *Chem. Eur. J.* **2004**, *10*, 6402–6410; b) O. Johansson, L. O. Johannissen, R. Lomoth, *Chem. Eur. J.* **2009**, *15*, 1195–1204.

[32] N. Herzmann, A.-V. Mudring, G. Meyer, *Inorg. Chem.* **2008**, *47*, 7954–7956.

[33] a) P. F. Heelis, *Chem. Soc. Rev.* **1982**, *11*, 15–39; b) T. C. Bruice, *Acc. Chem. Res.* **1980**, *13*, 256–262; c) C. Walsh, *Acc. Chem. Res.* **1980**, *13*, 148–155; d) P. F. Fitzpatrick, *Acc. Chem. Res.* **2001**, *34*, 299 – 317.

[34] S. Miyazaki, K. Ohkubo, T. Kojima, S. Fukuzumi, *Angew. Chem. Int. Ed.* **2007**, *46*, 905–908.

[35] a) H. Nakajima, H. Nagao, K. Tanaka, *J. Chem. Soc., Dalton Trans.* **1996**, 1405–1409; b) T. Koizumi, T. Tomon, K. Tanaka, *Bull. Chem. Soc. Jpn.* **2003**, *76*, 1969–1975; c) T. Koizumi, T. Tomon, K. Tanaka, *J. Organomet. Chem.* **2005**, *690*, 4272–4279; d) R. J. Staniewicz, R. F. Sympson, D. G. Hendricker, *Inorg. Chem.* **1977**, *16*, 2166–2171; e) R. J. Staniewicz, D. G. Hendricker, *J. Am. Chem. Soc.* **1977**, *99*, 6581–6588; f) B. G. Harvey, A. M. Arif, R. D. Ernst, *Polyhedron* **2004**, *23*, 2725 –2731.

[36] a) T. Suzuki, T. Kuchiyama, S. Kishi, S. Kizaki, M. Kato, *Bull. Chem. Soc. Jpn.* **2002**, *75*, 2433–2439; b) F. Basuli, S.-M. Peng, S. Bhattacharya, *Inorg. Chem.* **2000**, *39*, 1120–1127; c) F. Basuli, S.-M. Peng, S. Bhattacharya, *Inorg. Chem.* **2001**, *40*, 1126–1133; d) S. Dutta, F. Basuli, A. Castineiras, S.-M. Peng, G.-H. Lee, S. Bhattacharya, *Eur. J. Inorg. Chem.* **2008**, 4538–4546.

[37] a) R. Barbucci, L. Fabbrizzi, P. Paoletti, *Coord. Chem. Rev.* **1972**, *8*, 31–37; b) R. Barbucci, P. Paoletti,

A. Vacca, *Inorg. Chem.* **1975**, *14*, 302 – 305.

[38] When the photoirradiation of **1** was conducted in acetonitrile-d_3 instead of acetone-d_6, the ^{1}H NMR spectrum of the reaction mixture was so complicated, thus indicating the formation of a mixture in sharp contrast to the photoreaction in acetone-d_6. However, when the solution of the mixture was heated at 60 ºC for 5 h, almost all the components of the mixture turned back into complex **1**.

[39] a) T. Kojima, K. Hayashi, Y. Shiota, Y. Tachi, Y. Naruta, T. Suzuki, K. Uezu, K. Yoshizawa, *Bull. Chem. Soc. Jpn.* **2005**, *78*, 2152–2158; b) D. A. Freedman, S. Kruger, C. Roosa, C. Wymer, *Inorg. Chem.* **2006**, *45*, 9558–9568.

[40] a) R. G. Pearson, *Chemical Hardness*, Wiley-VCH, Weinheim, **1997**; b) R. G. Pearson, *J. Am. Chem. Soc.* **1963**, *85,* 3533–3539; c) R. G. Parr, R. G. Pearson, *J. Am. Chem. Soc.* **1983**, *105*, 7512–7516; d) C. Becker, I. Kieltsch, D. Broggini, A. Mezzetti, *Inorg. Chem.* **2003**, *42*, 8417–8429; e) P. Crawford, P. Hu, *J. Phys. Chem. B* **2006**, *110*, 4157 – 4161.

[41] Acetones coordinated to Ru(II) centers are frequently employed as an exchangeable ligand to obtain a variety of Ru(II) complexes; a) J. Bolger, A. Gourdon, E. Ishow, J.-P. Launay, *J. Chem. Soc., Chem. Commun.* **1995**, 1799–1800; b) T. Sugaya, M. Sano, *Inorg. Chem.* **1993**, *32*, 5878–5879; c) M. Sørlie, M. Tilset, *Inorg. Chem.* **1995**, *34*, 5199–5204; d) D. W. Powell. P. A. Lay, *Inorg. Chem.* **1992**, *31*, 3542–3550; e) V. Alezra, G. Bernardinelli, C. Corminboeaf, U. Frey, E. P. Kündig, A. E. Merbach, C. M. Saudan, F. Viton, J. Weber, *J. Am. Chem. Soc.* **2004**, *126*, 4843–4853; f) I. Iwakura, A. Yabushita, T. Kobayashi, *Eur. J. Inorg. Chem.* **2008**, 4856–4860; g) R. Castro-Rodrigo, M. A. Esterelas, S. Fuertes, A. M. López, S. Mozo, E. Oñate, *Organometallics* **2009**, *28*, 5941–5951.

[42] a) A. D. Becke, *Phys. Rev. A* **1988**, *38*, 3098; b) A. D. Becke, *J. Chem. Phys.* **1993**, *98*, 5648.

[43] C. Lee, W. Yang, R. G. Parr, *Phys. Rev. B* **1988**, *37*, 785.

[44] L. Gong, Z. Liu, K. Harms, E. Meggers, *Angew. Chem. Int. Ed.* **2010**, *49*, 7955–7957.

[45] a) M. P. O'Neil, M. P. Niemczyk, W. A. Svec, D. Gosztola, G. L. Gaines III, M. R. Wasielewski, *Science* **1992**, *257*, 63–65; b) N. V. Mockus, D. Ravinovich, J. L. Peterson, J. J. Rack, *Angew. Chem. Int. Ed.* **2008**, *47*, 1458–1461.

[46] T. Yanai, D. P. Tew, N. C. Handy, *Chem. Phys. Lett.* **2004**, *393*, 51–57.

[47] P. J. Hay, W. R. Wadt, *J. Chem. Phys.* **1985**, *82*, 299.

[48] T. H. Dunning, P. J. Hay, *Modern Theoretical Chemistry, Vol. 3* (Ed.: H. F. Schaefer III), Plenum Press, New York, **1976**.

[49] Gaussian 09, Revision A1, M. J. Frisch, G. W. Trucks, H. B. Schlegel, G. E. Scuseria, M. A. Robb, J. R. Cheeseman, J. A. Montgomery, Jr., T. Vreven, K. N. Kudin, J. C. Burant, J. M. Millam, S. S. Iyengar, J. Tomasi, V. Barone, B. Mennucci, M. Cossi, G. Scalmani, N. Rega, G. A. Petersson, H. Nakatsuji, M. Hada, M. Ehara, K. Toyota, R. Fukuda, J. Hasegawa, M. Ishida, T. Nakajima, Y. Honda, O. Kitao, H. Nakai, M. Klene, X. Li, J. E. Knox, H. P. Hratchian, J. B. Cross, V. Bakken, C. Adamo, J. Jaramillo, R. Gomperts, R. E. Stratmann, O. Yazyev, A. J. Austin, R. Cammi, C. Pomelli, J. W. Ochterski, P. Y. Ayala, K. Morokuma, G. A. Voth, P. Salvador, J. J. Dannenberg, V. G. Zakrzewski, S. Dapprich, A. D. Daniels, M. C. Strain, O. Farkas, D. K. Malick, A. D. Rabuck, K. Raghavachari, J. B.

Foresman, J. V. Ortiz, Q. Cui, A. G. Baboul, S. Clifford, J. Cioslowski, B. B. Stefanov, G. Liu, A. Liashenko, P. Piskorz, I. Komaromi, R. L. Martin, D. J. Fox, T. Keith, M. A. Al-Laham, C. Y. Peng, A. Nanayakkara, M. Challacombe, P. M. W. Gill, B. Johnson, W. Chen, M. W. Wong, C. Gonzalez, J. A. Pople, Gaussian, Inc., Wallingford CT, **2004**.

Chapter 3

Photochromism of ruthenium(II)-tpphz complexes

3-1. Introduction

Switchable molecular motions,[1] such as shuttling,[2] sliding,[3] rotation,[4–7] and tweezing,[8] have attracted considerable attention, owing to their relevance to natural biomachines, such as myosin in muscular tissues[1, 9] and the F_1 unit of ATP synthase,[1, 10] as well as for future applications in molecular machines.[11] Synthetic molecular machines can function by using, for example, acid/base reactions,[12] electrochemical redox processes,[13, 14] photoinduced structural changes,[15] and chemical oxidation[16] as the driving force of the motion. These machines can function as molecular sensors,[17] elicit mechanical forces,[18] and perform as cooperative molecular catalysts.[19] Among the various molecular motions, capping/uncapping motions in molecules are expected to be useful for controlled molecular recognition and catalytic reaction systems, whose functions can be switched by using an external stimuli (Figure 3-1a).[20]

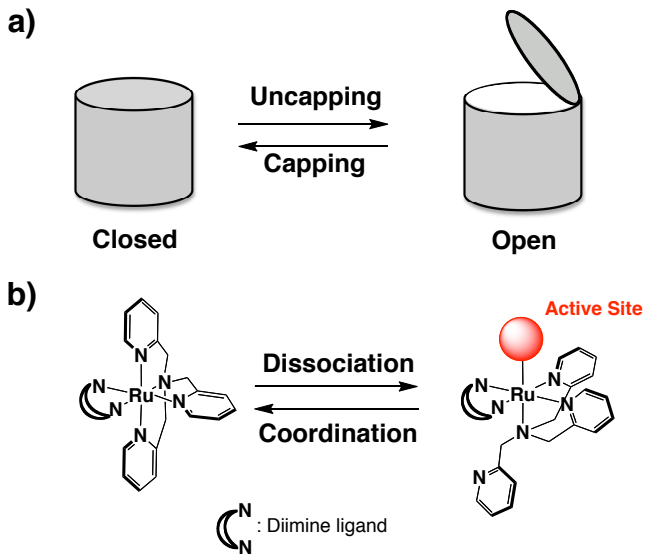

Figure 3-1. (a) Schematic description of the "capping-uncapping" motion and (b) reversible dissociation/coordination reaction of a Ru^{II}(TPA)(diimine) complex.

Reversible structural change in transition-metal complexes at metal centers are also attractive in light of the development of molecular machines and devices to perform various functionalities that are unique to metal complexes, including catalysis and the switching of their physical properties. Transition-metal complexes that respond to external stimuli have been reported to demonstrate reversible structural changes, including reversible ligand-coordination/dissociation owing to changes in pH value[21] and the translocation of metal ions through changes in pH value[22] and redox reactions.[23] As a photochemical response of transition-metal complexes, photochromic reactions, such as reversible structural changes that involve a partial dissociation and the recoordination of a ligand, have also been investigated.[24, 25] In such a structural change, the vacant coordination site that is formed by the partial dissociation of the ligand can be used as a

guest-binding or catalytically active site; thus, the dissociable part of the ligand plays a role as a "cap" for the active site. However, for transition-metal complexes, there have been no examples so far of completely reversible photochromic structural changes for attaining complete interconversion between two states without reaching a photostationary state. Recently, reversible photochromic structural changes in Ru^{II}–tris(2-pyridylmethyl)amine (TPA) complexes that contained a diimine ligand, such as 2,2'-bipyridine (bpy), 2,2'-bipyrimidine (bpm), or 1,10-phenanthlorine (phen, Figure 3-1b) was reported.[26] However, the conversion efficiencies for the photochromic reactions of transition-metal complexes, including previous examples, were not 100% and, in most cases, illumination of the photochromic complexes afforded a photostationary state between two states.[24–27] In this chapter, the first examples of molecular bistability is described, which involve complete photochromic structural changes in new Ru^{II}–TPA complexes that contain tetrapyrido-[3,2-*a*:2',3'-*c*:3'',2''-*h*:2''',3'''-*j*]phenazine (tpphz)[28] as a diimine ligand (Figure 3-2).

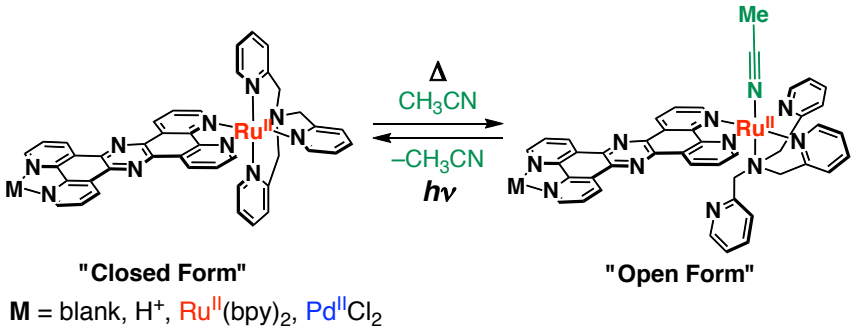

Figure 3-2. Interconversion between the "open" and "closed" forms in Ru^{II}(TPA)(tpphz) complexes.

The tpphz ligand is a highly planar and extensively π-conjugated heteroaromatic molecule. In addition, the tpphz ligand has another coordination site on the opposite side to one that coordinates to the Ru^{II}(TPA) unit and this site is utilized to accept a H^+ ion (proton) or other transition-metal ions, such as Ru^{II} and Pd^{II} ions (Figure 3-2).[29] These kinds of additives can influence both the ground and excited electronic states, owing to their strong interactions with the diimine ligand in different manners. The influence of additives can regulate the dissociation/coordination reactions of the TPA ligand in the Ru^{II}(TPA) moiety to accomplish the complete interconversion between its open form, which contains a facial η^3-TPA ligand, and its closed form, which contains an η^4-TPA ligand, as shown in Figure 3-2.

3-2. Results and discussion

3-2-1. Syntheses and structural characterization

1,10-Phenanthroline-5,6-dione (phendione)[30] was coordinated to a Ru^{II}(TPA) complex to obtain [Ru^{II}(TPA)(phendione)]$(PF_6)_2$. The phendione complex was coupled with 5,6-diamino- 1,10-phenanthroline (phendiamine)[31] to construct the tpphz moiety (Scheme 3-1a). In the previous report of the synthesis of a Ru^{II}(tpphz) complex,[28] the solvent for the coupling reaction between a Ru^{II}(phendione) complex and phendiamine was MeCN. In the case of Ru^{II}(TPA)(diimine) complex, however, MeCN caused the dissociation of a pyridine moiety of the TPA ligand from Ru^{II}(TPA)(diimine) complexes.[26] Thus, the author

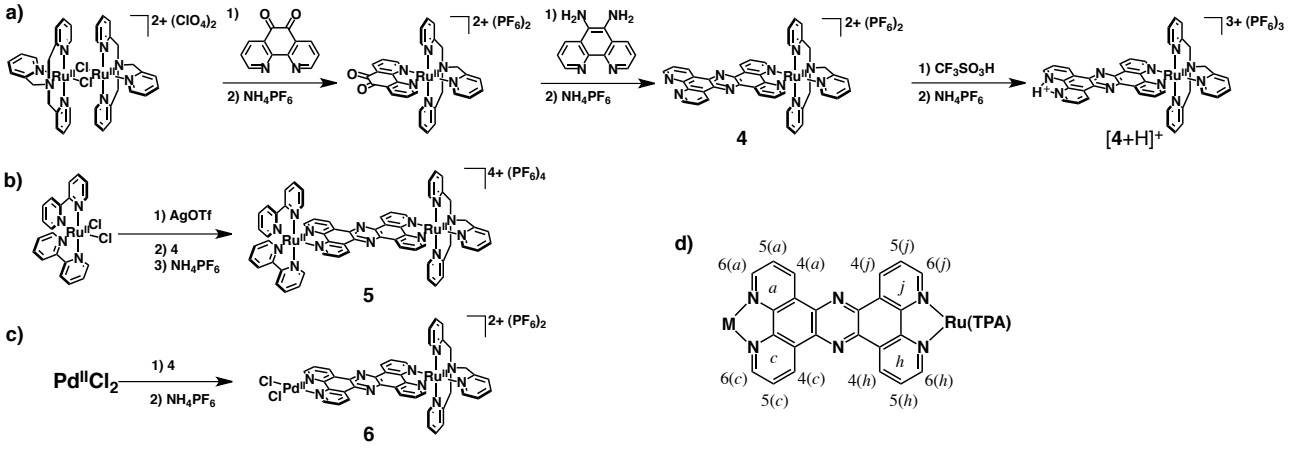

Scheme 3-1. Synthesis of Ru^{II}(TPA)(tpphz) complexes **4**, [**4** + H]$^+$, **5** and **6** (a-c) and the labeling of the tpphz ligand for the ^{1}H NMR assignment (d).

employed MeOH as the reaction solvent and the total yield of target complex, [Ru^{II}(TPA)(tpphz)]$(PF_6)_2$ (**4**), was 74% (over 2 steps). In addition, the protonated complex, [Ru^{II}(TPA)(tpphz-H$^+$)]$(PF_6)_3$ ([**4** + H]$^+$), was isolated by recrystallization from its solution in MeCN in the presence of trifluoromethanesulfonic acid (TfOH), in which EtOAc was used as a poor solvent. The protonation probably occurred at the vacant diimine site of the tpphz ligand (the position of M in Scheme 3-1(d)) and the central pyrazine moiety of the tpphz ligand could not be protonated under these conditions, because the imine nitrogen atom on the pyradine moiety was sterically hindered by the neighboring hydrogen atoms at the 4(*a*), 4(*c*), 4(*h*), and 4(*j*)-positions of the tpphz ligand.[28b]

[$Ru^{II}(bpy)_2(solv)_2$]$(OTf)_2$ (solv = acetone) was prepared according to a literature procedure[32] and was ligated to the vacant coordination site of complex **4** in acetone, which was chosen as the solvent because of the weak coordinating ability without the pyridine-dissociation reaction of the Ru^{II}(TPA) unit (See Chapter 2).[26, 33] After repeated recrystallization, a dinuclear tpphz complex, [$(bpy)_2Ru^{II}(\mu$-tpphz)Ru^{II}(TPA)]$(PF_6)_4$ (**5**), was obtained in 80% yield. A hetero-dinuclear complex, [$Cl_2Pd(\mu$-tpphz)Ru^{II}(TPA)]$(PF_6)_2$ (**6**), was synthesized through the coordination of $PdCl_2$ to the vacant site of complex **4** (Scheme 3-1c). Although the author applied a literature procedure[29, 34] to the synthesis of a $PdCl_2$–μ-tpphz–Ru^{II} complex, at first, the author's attempts were unsuccessful. The coordination reaction at high temperatures in DMF or ethyleneglycol caused the decomposition of the obtained product before completion of the reaction. Finally, the reaction at reflux in EtOH was the best for obtaining the target Pd complex (**6**) and the reaction yield was 43% after isolation by repeated recrystallization. Structural characterization of complexes **4**, [**4** + H]$^+$, **5**, and **6** was performed by using ^{1}H NMR spectroscopy and ESI-TOF-MS spectrometery; complex **4** was also characterized by single-crystal X-ray diffraction (see below). Peak clusters that were ascribed to the mass signals of complexes [**4** – $2PF_6$]$^{2+}$, [**5** – $4PF_6$]$^{4+}$, and [**6** – $2PF_6$]$^{2+}$ were observed at 388.1 *m/z* as a dicationic signal with a 0.5 peak separation, 297.6 *m/z* as a tetracationic signal with a 0.25 peak separation, and 476.5 *m/z* as a dicationic signal with a 0.5 peak separation, respectively (Figure 3-3). The MS (ESI) spectrum of complex [**4** + H]$^+$ gave a peak cluster that was ascribed to deprotonated species, [**4** – $2PF_6$]$^{2+}$, presumably

owing to deprotonation during the ionization process in the MS measurements.

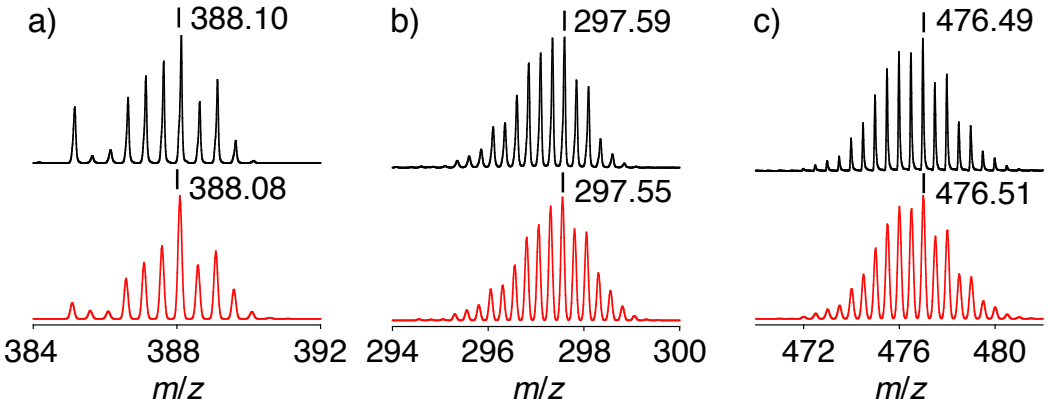

Figure 3-3. ESI-TOF MS spectra of complexes **4** (a), **5** (b) and **6** (c). Above: experimental results, below: simulated spectra.

In the ^{1}H NMR spectra of complexes **4**, [**4** + H]$^+$, **5**, and **6** in MeCN-d_6 (Figure 3-4), the ^{1}H NMR signals of the axial and the two equatorial pyridylmethyl moieties in the TPA ligand were inequivalent and the methylene signals of the equatorial pyridylmethyl moieties were observed at about δ 4.5 ppm as AB quartets with coupling constants of $J \approx 15$ Hz.[26, 33, 35, 36] In all four complexes, the ^{1}H NMR signals of the pyridyl protons at the 6-position of the axial pyridine rings, which was the closest to the tpphz moieties, were downfield-shifted to about δ 10 ppm, owing to the deshielding effect from the ring current of the tpphz

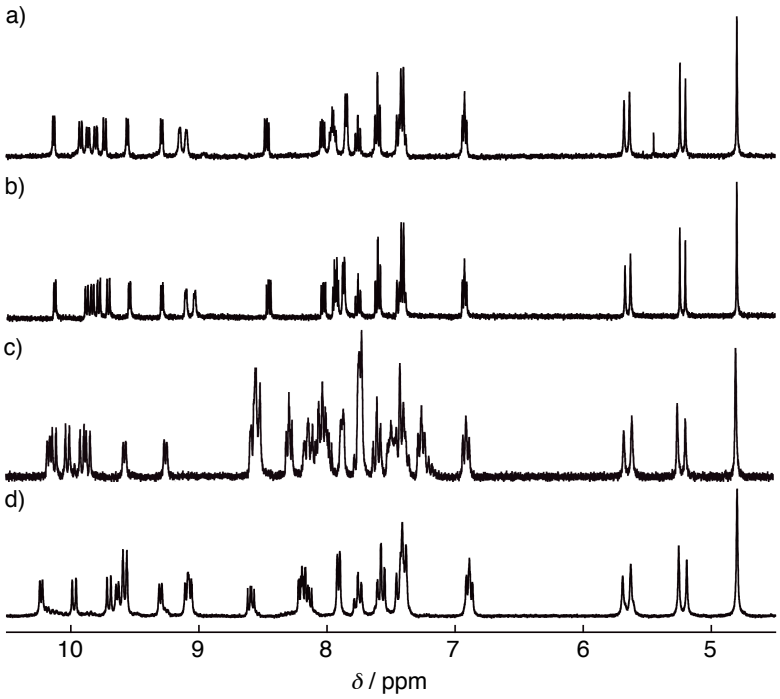

Figure 3-4. ^{1}H NMR spectra of complexes **4** (a), [**4** + H]$^+$ (b), **5** (c) and **6** (d) in MeCN-d_3 ((a) 1.7 mM, (b) 1.6 mM, (c) 1.3 mM, (d) 1.5 mM).

ligand (Figure 3-4). In addition, the ^{1}H NMR signal of the 6-proton on the *h*-pyridine ring in the tpphz ligand was also affected by the ring current of the axial pyridine rings and, hence, was also downfield-shifted. The chemical shift values of the 4(*h*), 4(*j*), 5(*j*), 6(*j*), and py-6(eq) protons in complexes **4**, [**4** + H]$^+$, and **6** were highly dependent on the concentration of the sample solutions (Figure 3-5), whereas the UV/Vis spectra of these three complexes did not exhibit any concentration dependence. These ^{1}H NMR shifts can be ascribed to intermolecular π–π stacking interactions between the tpphz ligands, as previously reported for $[Ru^{II}(bpy)_2(tpphz)]^{2+}$.[28] In contrast, the ^{1}H NMR spectrum of complex **5** did not exhibit any concentration dependence. Two sets of pyridine signals for the bpy ligand in complex **5** were observed, which were assigned to the axial and equatorial pyridine moieties. The independence of the chemical shifts on the concentration of **5** should be derived from the steric congestion of the two bpy and the TPA ligands around the tpphz ligand. The bulkiness of the TPA ligand and the two bpy ligands at the Ru centers may prevent intermolecular π–π stacking of the tpphz ligands and, hence, attempts to crystallize complex **5** were unsuccessful.

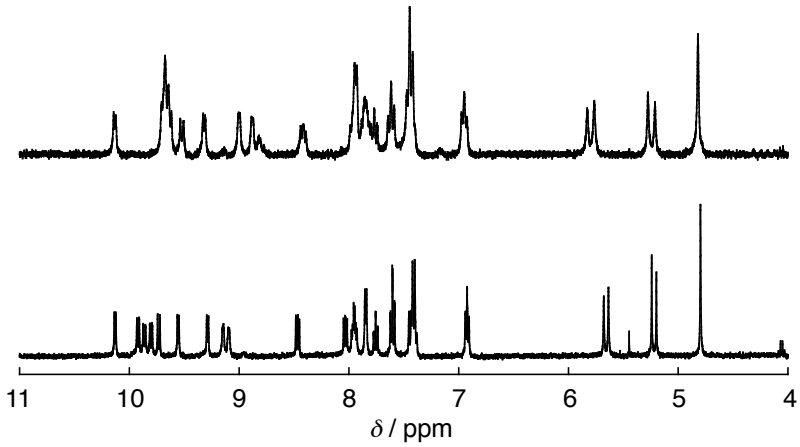

Figure 3-5. ^{1}H NMR spectra of **4** in MeCN-d_3 at room temperature. Above: 6.0 mM, below: 1.7 mM.

The DFT-optimized structure of **5** indicates that the tpphz ligand maintains planarity (mean deviation from the plane of the tphz ligand: 0.021 Å) and causes tilting of one of the pyridine rings of the TPA ligand, owing to steric hindrance, as observed in other related Ru^{II}(TPA)(diimine) complexes (Figure 3-6).[26] The optimized structure of complex **5'** also has a slightly bent tpphz ligand (mean deviation from the plane of the tpphz ligand: 0.165 Å) and a tridentate TPA ligand, with one uncoordinated pyridylmethyl arm. The calculated energy of **5'** is –78.9 kJ mol^{-1} relative to that of complex **5**, with one accompanying free MeCN molecule. Thus, the binding energy of the MeCN ligand was roughly estimated. In addition, the inter-Ru distances were calculated to be 13.02 Å in complex **5** and 12.98 Å in complex **5'**. The LUMO and LUMO+1 resided on the tpphz ligand as π^* orbitals. The HOMO was located on the Ru^{II} center of the Ru^{II}(TPA) unit and the HOMO–1 was located on the Ru^{II} center of the $Ru^{II}(bpy)_2$ unit (Figure 3-7). The order of the energy levels indicates that the Ru^{II} center in the Ru^{II}(TPA) unit is more easily oxidized than that in the $Ru^{II}(bpy)_2$ unit. On the other hand, the relative positions of the HOMO and HOMO–1 were exchanged in complex **5'**.

The HOMO was located on the Ru^{II} center of the $Ru^{III}(bpy)_2$ unit and the HOMO–1 was located on the Ru^{II} center of the MeCN-coordinated Ru^{II}(TPA) unit (Figure 3-8). The relative positions of the LUMO and the LUMO+1 remained unchanged during the isomerization process.

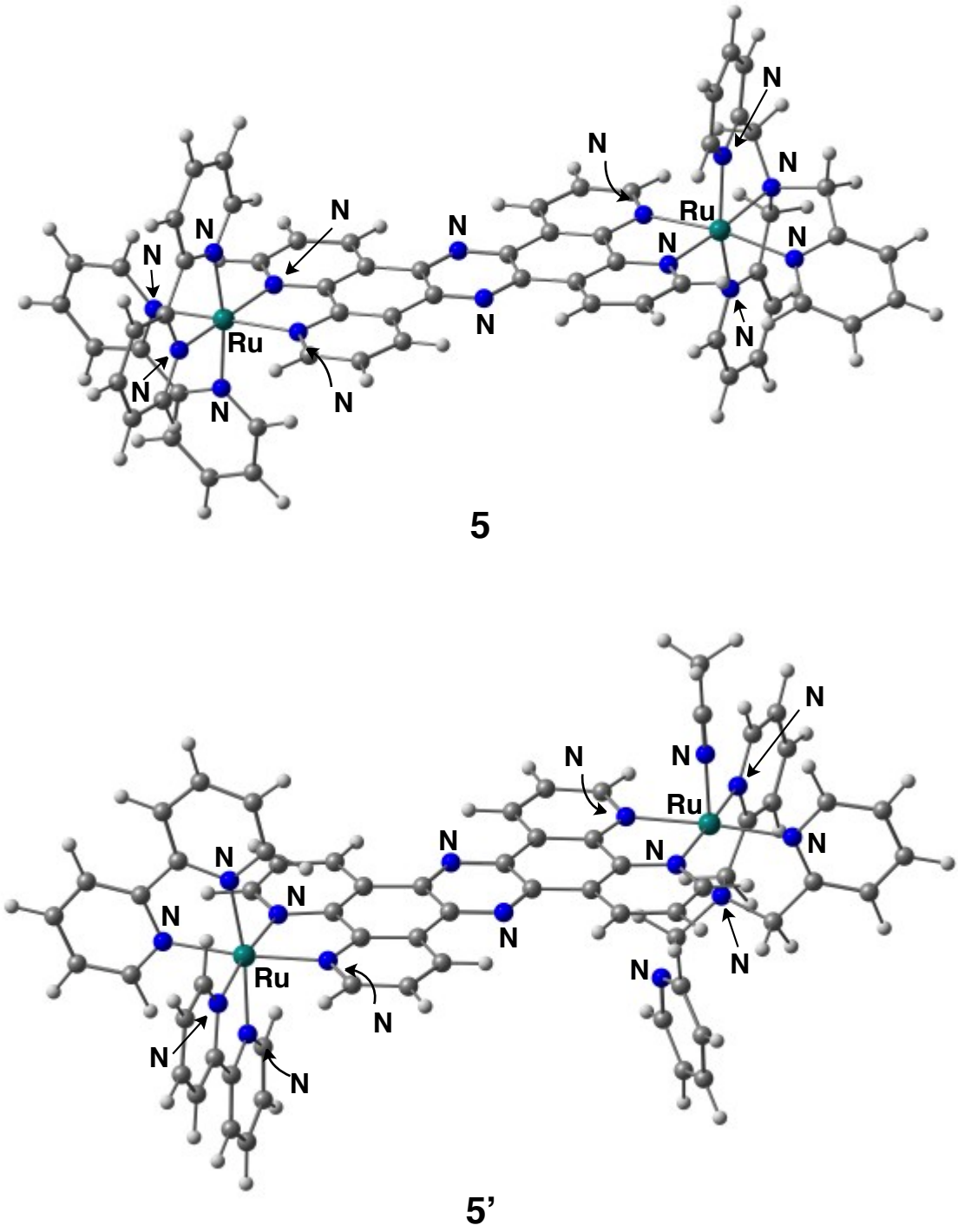

Figure 3-6. DFT-optimized structures of **5** and **5'** at the B3LYP/SDD level of theory.

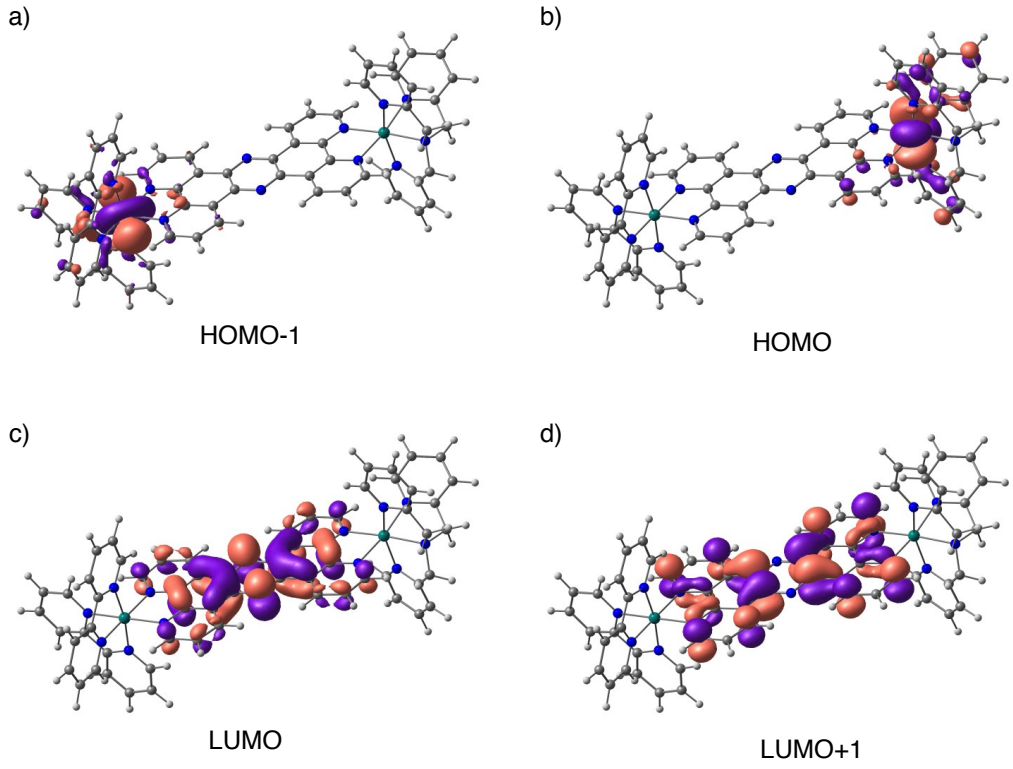

Figure 3-7. Selected MOs of **5**.

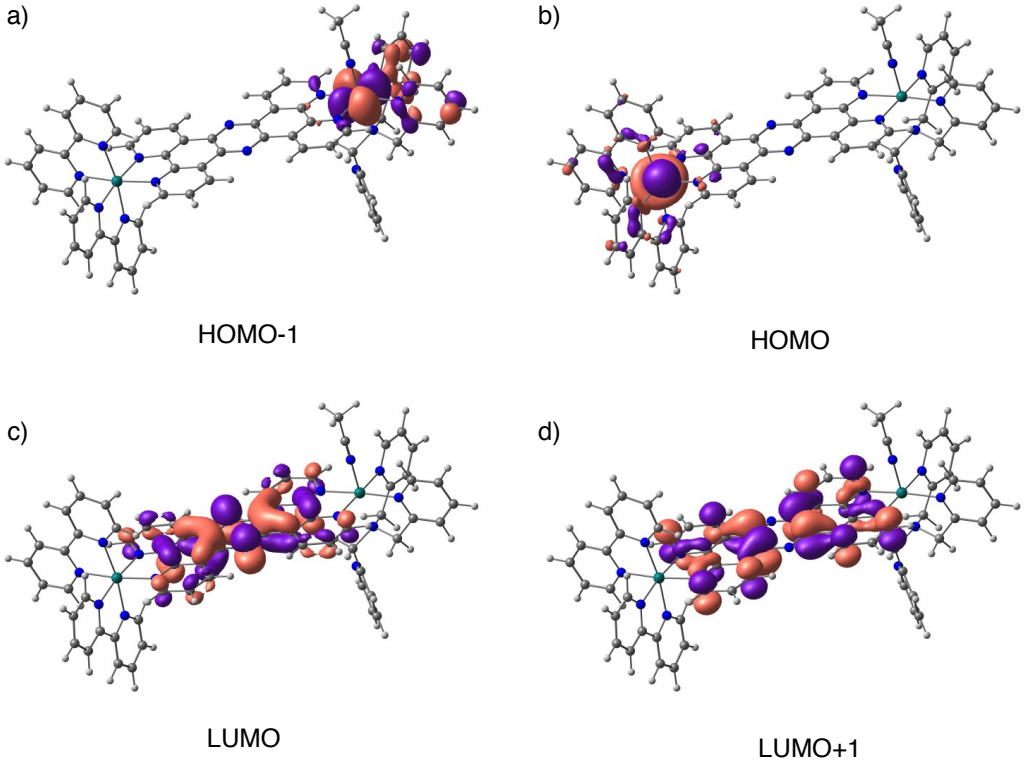

Figure 3-8. Selected MOs of **5'**.

3-2-2. Crystal structure of complex 4

Mononuclear complex **4** was crystallized in the monoclinic space group of $P2_1/n$. The asymmetric unit included one cationic part of **4**, two tetraphenylborate ions as counter anions, and three EtOAc molecules as co-crystallized solvent molecules. Figure 3-9 shows the molecular structure of the cationic moiety of **4**. Compound **4** adopts a similar conformation to those observed in other Ru^{II}(TPA)(diimine) complexes.[26] The tertiary amine nitrogen atom (N1), two pyridyl nitrogen atoms (N3 and N4) of the TPA ligand, and one of the imine nitrogen atoms of the tpphz ligand form the equatorial plane and the tpphz ligand and the axial pyridine ring of the TPA ligand were tilted towards the equatorial plane, owing to steric repulsion between them. The dihedral angles between the equatorial coordination plane and the axial pyridine ring and the tpphz ligand were 119.88 and 153.58, respectively. The interatomic distance between the 6-carbon atom on the axial pyridine ring of the TPA ligand and the C19 carbon atom of the tpphz ligand was 3.33 Å.

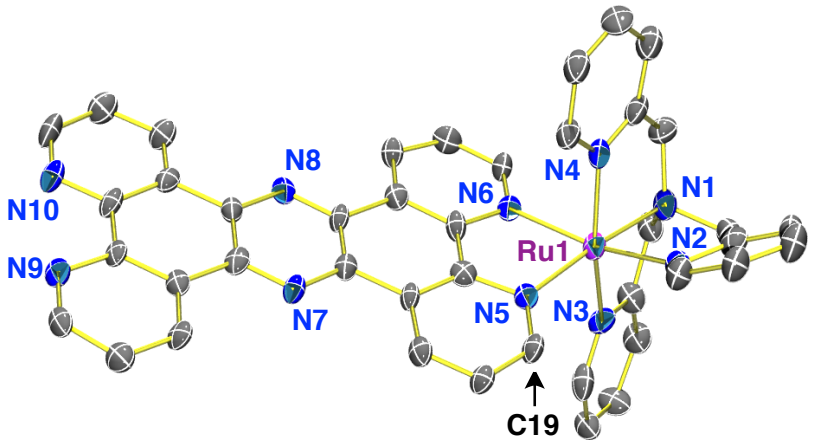

Figure 3-9. Crystal structure of the cationic part of **4**; thermal ellipsoids are set at 50% probability.

Similar distortion, owing to steric repulsion, was also observed in other Ru^{II}(TPA)(diimine) complexes.[26] As a result of the steric repulsion between the tpphz ligand and the axial pyridine ring of the TPA ligand, the Ru–N2 and Ru–N6 bond lengths were elongated compared to those of other Ru–N bonds and the degree of elongation of **4** was larger than that for other Ru^{II}(TPA)(diimine) complexes (Table 3-1).[26] The tpphz ligand was almost planar, even after metal coordination,[28b] and the mean deviation of each atom from the least-square mean plane was 0.031 Å. As a result of the high planarity and the extended π conjugation, the tpphz ligand formed an intermolecular π–π stacked pair (Fgiure 3-10a) and the distance between the two tpphz ligands in the pair was 3.32 Å. The other side of the tpphz ligand formed π–π stacking interactions with two phenyl rings of the tetraphenylborate counter anion, one of which formed a face-to-face π–π interaction whilst the other formed an edge-to-face π–π interaction (Figure 3-10b). The distance between the π–π stacked pair of the tpphz ligands and the phenyl ring of the tetraphenylborate ion was 3.67 Å, whilst that from the edge of the other phenyl ring to the tpphz plane was 3.52 Å.

Table 3-1. Comparison of bond lengths (Å) and angles (°) of Ru^{II}-TPA-diimine complexes.

diimine	bpy[a]	bpm[a]	phen[a]	tpphz (**4**)
Ru1-N1	2.085(3)	2.093(3)	2.084(2)	2.086(7)
Ru1-N2	2.102(3)	2.101(3)	2.115(2)	2.127(7)
Ru1-N3	2.048(3)	2.068(3)	2.042(3)	2.092(7)
Ru1-N4	2.078(3)	2.091(3)	2.079(2)	2.039(7)
Ru1-N5	2.065(3)	2.086(3)	2.074(3)	2.045(7)
Ru1-N6	2.101(2)	2.092(2)	2.096(2)	2.130(7)
N1-Ru1-N2	79.1(1)	79.9(1)	79.0(1)	79.5(3)
N1-Ru1-N3	83.5(1)	82.6(1)	84.5(1)	80.3(3)
N1-Ru1-N4	80.6(1)	79.8(1)	80.0(1)	83.9(3)
N5-Ru1-N6	77.3(1)	77.8(1)	79.1(1)	79.0(3)
N1-Ru1-N5	175.9(1)	171.7(1)	172.8(1)	174.9(3)
N2-Ru1-N6	167.9(1)	168.8(2)	169.5(1)	165.2(2)
N2-Ru1-N5	100.6(1)	100.4(1)	100.9(1)	98.8(3)

[a] Ref [26]

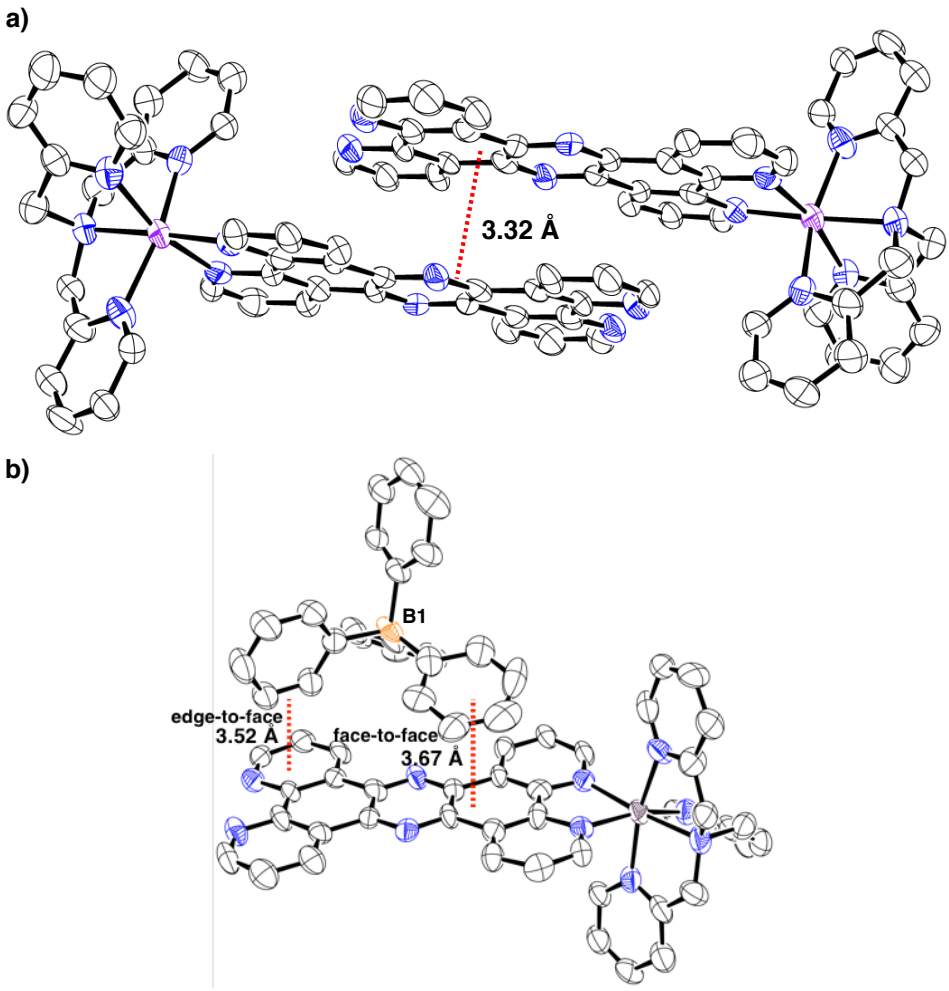

Figure 3-10. Views of crystal packing of **4**: a) Intermolecular π-π stacking and b) π-π interaction between the tpphz ligand and BPh_4^-.

3-2-3. Photo- and electrochemical properties

The electronic spectra of complexes **4**, [**4** + H]$^+$, **5**, and **6** were recorded in MeCN (Figure 3-11) and their absorption maxima are summarized in Table 3-2, together with those of $[Ru^{II}(bpy)_3]^{2+}$ [24a] and $[Ru^{II}(TPA)(bpy)]^{2+}$ for comparison.[26] For all the four complexes, the π– π* transitions of the tpphz moieties were observed as doubly peaked bands at about 350 – 400 nm and the MLCT transitions from the Ru^{II} centers to the tpphz ligands appeared at about 430 nm. The molar coefficients of the MLCT absorption for complex **5** were almost double those for complex **4**, because the MLCT transition from the Ru^{II} center in the $Ru^{II}(bpy)_2$ moiety to the tpphz ligand overlapped that from the Ru^{II} center in the $Ru^{II}(TPA)$ unit. In addition, the MLCT absorption band for complex **6** was slightly weaker than that for complex **4**. The MLCT absorption bands of complexes [**4** + H]$^+$, **5**, and **6** were red-shifted relative to that of **4**, thus indicating a stabilization of the π* orbitals of the tpphz ligands in complexes [**4** + H]$^+$, **5**, and **6** through the ligation of proton or metal ions at the vacant coordination sites of the tpphz ligands in **4**.

Table 3-2. Spectroscopic data in MeCN and CH_2Cl_2.

	Absorption		Emission		
	MeCN	CH_2Cl_2	MeCN	CH_2Cl_2	PrCN[c]
	λ_{max}, nm (ε [× 10^{-3} M^{-1} cm^{-1}])		λ_{max}, nm (λ_{irr}, nm)		
$[Ru(bpy)_3]^{2+}$ [a]	451 (14.1), 386 (4.6)		607 (450)		
$[Ru(bpy)(TPA)]^{2+}$ [b]	453		–	–	
$[Ru(bpm)(TPA)]^{2+}$ [b]	480		–	–	
$[Ru(phen)(TPA)]^{2+}$ [b]	423		–	–	
4	424 (13.4), 381 (34.5), 363 (23.6)	428	514 (424)	467 (424)	595, 550 (400)
[**4** + H]$^+$	428 (10.1), 378 (23.2), 363 (18.0)	430	–	490 (424)	607, 571 (405)
5	442 (24.7), 371 (32.3), 353 (25.3)	442	615 (442)	591 (442)	516 (400)
6	437 (11.5), 378 (34.5), 359 (23.7)	485	–	569 (485)	629 (430)
4'	433 (sh, 6.9)				537 (425)
[**4'** + H]$^+$	408 (sh, 9.5)				532, 516 (420)
5'	437 (21.6)				534 (440)
6'	405 (sh, 6.6)				543 (450)
$[(bpy)_2Ru(\mu\text{-tpphz})Ru(bpy)_2]^{4+}$ [a]	442 (36.1), 370 (34.6), 351 (28.1)		671 (443)		

[a] See ref. [28c]. [b] See ref. [26b]. [c] Phosphorescence spectra were recorded in *n*-butyronitrile (PrCN) at –196 ºC.

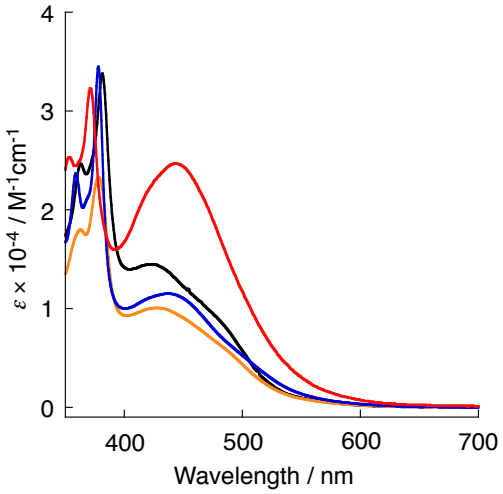

Figure 3-11. Electronic spectra of complexes **4** (black), [**4** + H]$^+$ (orange), **5** (red), and **6** (blue) in MeCN.

In MeCN, complexes **4**, [**4** + H]$^+$, **5**, and **6** exhibited relatively weak phosphorescent emissions, which were derived from the relaxation of the triplet MLCT excited states (Figure 3-12). Other previously reported Ru^{II}(TPA)(diimine) complexes[26] did not display phosphorescence, owing to quenching by the photodissociation reaction of the axial pyridine moiety of the TPA ligand through metal-centered (MC) triplet excited states.[26] The observation of phosphorescence of the Ru^{II}(TPA)(tpphz) complexes indicates that the dissociation pathways of the pyridine moiety through the MC triplet excited states of complexes **4**, [**4** + H]$^+$, **5**, and **6** should not be so thermally accessible and, thus, that the triplet MLCT states could be stabilized and relatively emissive. It should be noted that the emissions that were observed for the four complexes were enhanced in CH_2Cl_2 and similar behavior was also observed for the corresponding compound, $[(bpy)_2Ru^{II}(\mu\text{-tpphz})Ru^{II}(bpy)_2]^{4+}$.[37]

The redox potentials of **4**, [**4** + H]$^+$, **5**, and **6** were determined by cyclic and differential-pulse voltammetries (CV and DPV, respectively) at room temperature in MeCN solution containing tetrabutylammonium hexafluorophosphate ($(n\text{-Bu})_4NPF_6$) as a supporting electrolyte under an Ar atmosphere (Figure 3-13). The electrochemical data are summarized in Table 3-3. The redox potentials that were assigned to the $Ru^{II/III}$ redox couples for the Ru^{II}(TPA) units were almost identical for all the four complexes (+1.07 V vs SCE) and the redox waves were pseudo-reversible. These results indicate that protonation and metal coordination at the vacant diimine site of the tpphz ligand do not perturb the characteristics of the Ru^{II}(TPA) unit on the other rim of the tpphz ligand. Complex **5** showed another oxidation wave at +1.31 V vs SCE, which should be derived from the $Ru^{II/III}$ redox couple for the Ru center in the $Ru^{II}(bpy)_2$ moiety. This conclusion is consistent with the results of the DFT calculations, as described above. On the other hand, the reduction waves of the tpphz ligand ($tpphz^{0/1-}$) were positively shifted by protonation and metal coordination at the vacant diimine site of the tpphz ligand and the redox potentials increased in the order: **4** (–0.97 V) < [**4** + H]$^+$ (–0.95 V) < **6** (–0.93 V) < **5** (–0.87 V). This trend can be accounted by the stabilization of the π^* orbital of the tpphz ligand through protonation and metal coordination (see above).

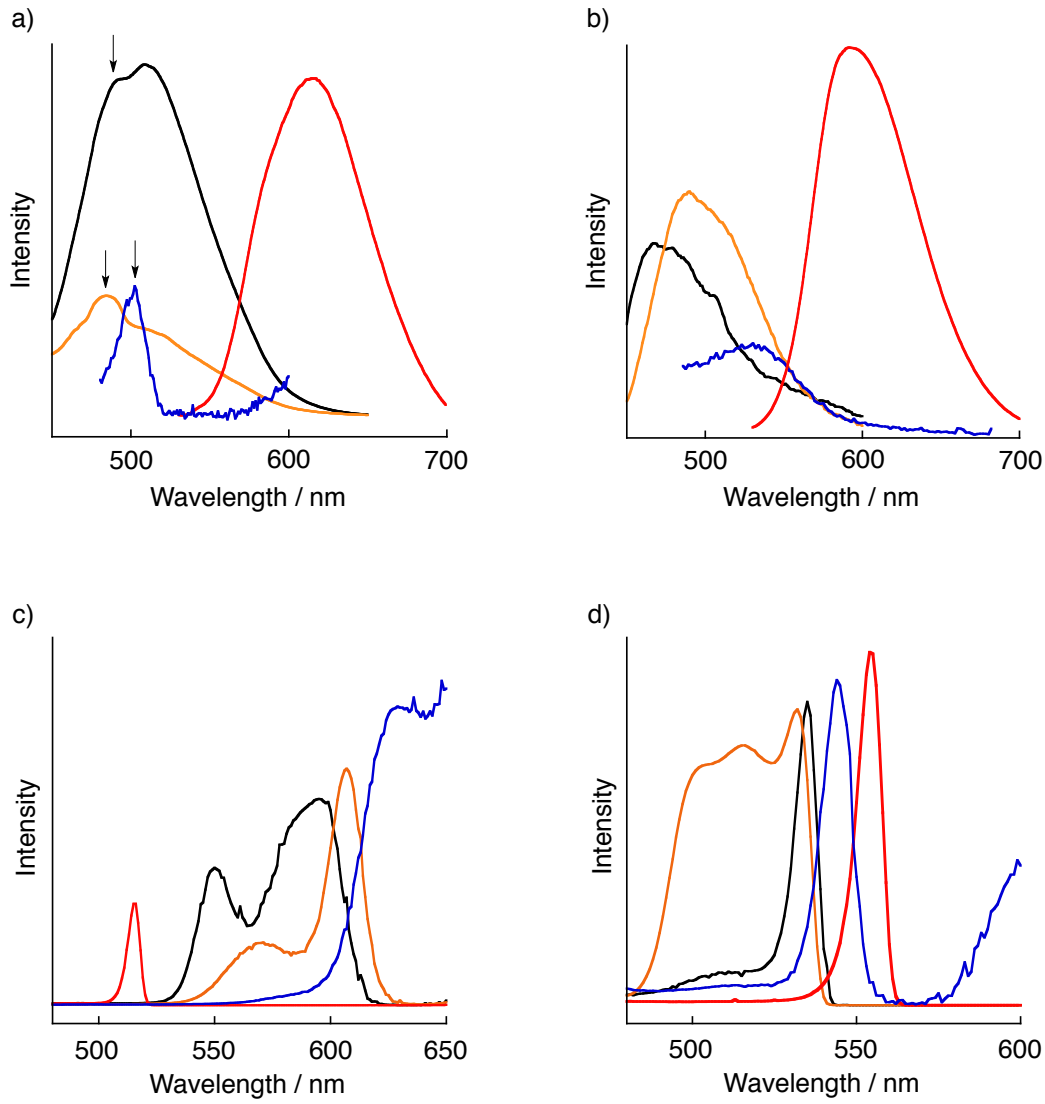

Figure 3-12. Above: Emission spectra of complexes **4** (black), [**4** + H]$^+$ (orange), **5** (red), and **6** (blue) in MeCN (a) and CH_2Cl_2 (b) at room temperature. Below: emission spectra of complexes **4** (black), [**4** + H]$^+$ (orange), **5** (red), and **6** (blue) in PrCN (c) and **4'** (black), [**4'** + H]$^+$ (orange), **5'** (red), and **6'** (blue) in PrCN (d) at –196 ºC. The emissions indicated by arrows were derived from the Raman diffraction of the incident light. The wavelengths of the incident light are λ = 424 nm for complex **4**, 424 nm for complex [**4** + H]$^+$, 442 nm for complex **5**, 485 nm for complex **6**, 425 nm for complex **4'**, 420 nm for complex [**4'** + H]$^+$, 440 nm for complex **5'**, and 450 nm for complex **6'**.

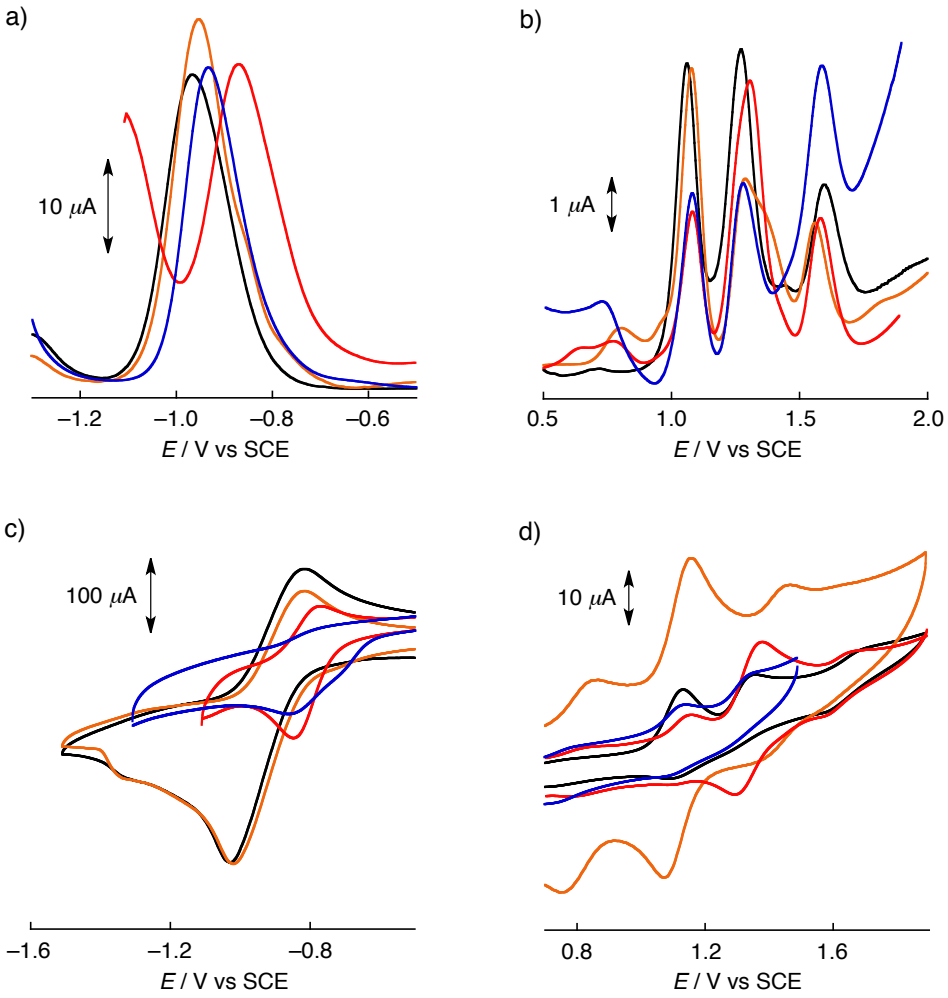

Figure 3-13. a) b) DPV and c) d) CV of complexes **4** (black), [**4** + H]$^+$ (orange), **5** (red) and **6** (blue) in CH_3CN containing $(n\text{-Bu})_4NPF_6$ (0.1 M) at room temperature.

Table 3-3. Redox potentials (V vs SCE) of Ru^{II}(tpphz) complexes **4** – **6**, $[Ru(bpy)_2(tpphz)]^{2+}$ and $[(\mu\text{-tpphz})\{Ru(bpy)_2\}_2]^{4+}$ as references.[28b]

Compound	tpphz$^{0/\bullet-}$	Ru^{II}/Ru^{III}
4	–0.97	+1.06
[**4** + H]$^+$	–0.95	+1.07
5	–0.87	+1.07 / +1.31
6	–0.93	+1.08
$[(bpy)_2Ru(tpphz)]^{2+}$ [a]	–0.87	+1.33
$[(bpy)_2Ru(\mu\text{-tpphz})Ru(bpy)_2]^{4+}$ [a]	–0.71	+1.34

[a] Potentials were determined by differential pulse voltammetry in MeCN in the presence of 0.1 M $(n\text{Bu})_4NPF_6$ as the supporting electrolyte under a N_2 atmosphere at room temperature. [b] See ref. [28b].

3-2-4. Thermal dissociation reactions

The thermal dissociation of the axial pyridylmethyl arms in complexes **4**, [**4** + H]$^+$, **5**, and **6** were

investigated by ^{1}H NMR spectroscopy in MeCN-d_3. When solutions of these complexes were heated at 80 ºC in MeCN-d_3, the intensity of the methylene signals of the TPA ligands gradually decreased and, instead, another set of signals appeared in relatively upfield regions (Figure 3-14) for all of the four complexes. These new signals contained an AB quartet pair (J = 16.2 Hz) and a singlet in the range of δ 3 – 5 ppm, all of which were derived from the methylene protons of the TPA ligand. As described in the previous spectra of the reports,[26] the spectroscopic changes that were observed in the ^{1}H NMR spectra could be ascribed to the thermal dissociation of the axial pyridylmethyl moiety of the TPA ligand to give partially dissociated complexes **4'**, [**4'** + H]$^+$, **5'**, and **6'** (Figure 3-14, open form), accompanied by a structural change to afford a facially tridentate TPA ligand with one uncoordinated pyridylmethyl arm. The upfield-shifted singlet signal was derived from the methylene protons of the dissociated pyridylmethyl moiety.[26] For further confirmation of the formation of the "open-form" complexes with accompanying axial MeCN ligands that were derived from the solvent, MS (ESI-TOF) analyses of the four products, that were obtained from the thermal reactions

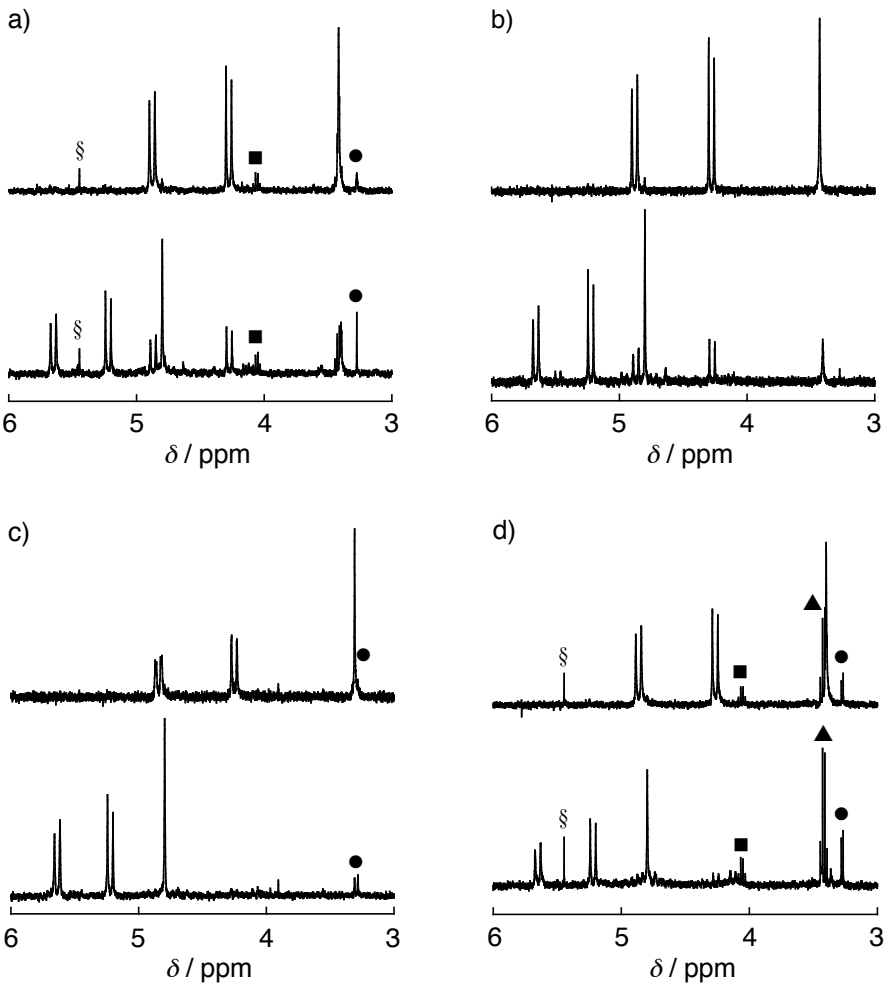

Figure 3-14. ^{1}H NMR spectroscopic changes upon photoirradiation of complexes **4** (a), [**4** + H]$^+$ (b), **5** (c), and **6** in MeCN-d_3 (d). Concentration: 1.7 mM (a), 1.6 mM (b), 1.3 mM (c), 1.7 mM (d). Top: ^{1}H NMR open form; bottom: ^{1}H NMR spectra after photoirradiation at 420 nm for 10 h. §: CH_2Cl_2, ■: EtOAc, ▲: Et_2O, ●: MeOH.

of complexes **4**, [**4** + H]$^+$, **5**, and **6**, were performed by using MeCN as a solvent. The observed peak clusters in the spectra were in good agreement with those expected for the corresponding MeCN-coordinated species in light of the *m*/*z* values and isotopic patterns (Figure 3-15). In addition, the product of the thermal reaction of complex **4** in MeCN gave a ^{1}H NMR signal at δ 2.16 ppm in MeCN-d_3, which was ascribed to the coordinated MeCN ligand (Figure 3-16). The ^{1}H NMR signal showed a slight downfield shift (by $\Delta\delta$ = 0.20 ppm) compared to that of free MeCN, owing to coordination to the Ru^{II} center.

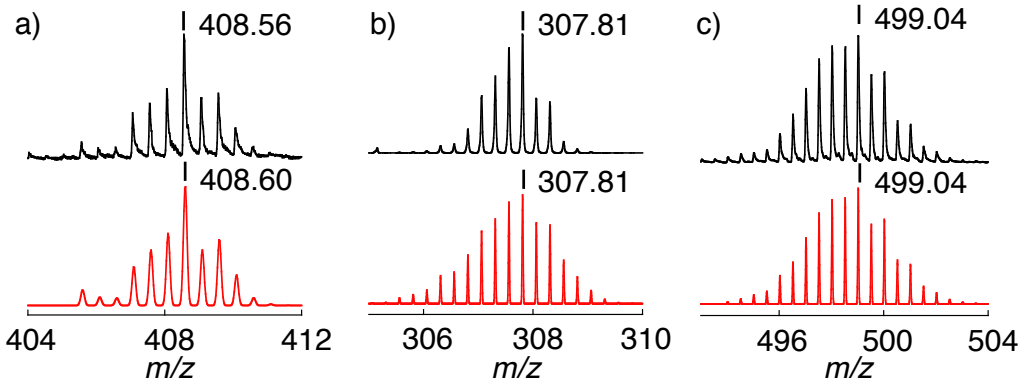

Figure 3-15. MS (ESI-TOF) of complexes **4'** (a), **5'** (b), and **6'** in MeCN (c). Top: experimental results; bottom: simulated spectra.

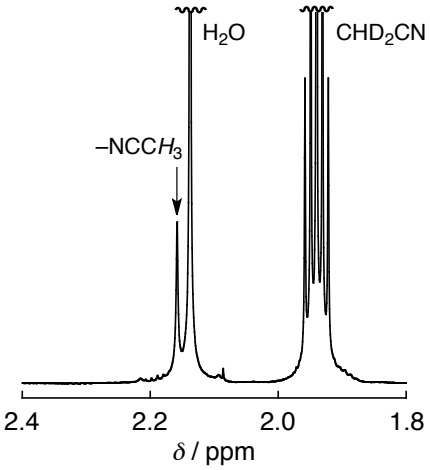

Figure 3-16. ^{1}H NMR spectrum of **6'** in MeCN-d_3 at room temperature.

Kinetic analysis of the thermal dissociation reactions of the axial pyridine moiety was performed to investigate the reaction mechanisms (Table 3-4). The first-order rate constants of the reactions at various temperatures were determined in MeCN by monitoring the absorbance changes at 440 nm for each complex (see the Experimental Section). The obtained rate constants were plotted against the inverse of the temperature to provide an Eyring plot (Figure 3-17).[38] The activation parameters of the reaction, activation enthalpy ($\Delta H^{\ddagger}$), and activation entropy ($\Delta S^{\ddagger}$) were determined by linear analysis. The activation parameters of the four complexes investigated herein were very similar to one another (Table 3-4), thus indicating that their thermal dissociation reactions all proceeded through the same mechanism. The large, negative $\Delta S^{\ddagger}$

values indicate that the transition state involves strong MeCN coordination to the Ru^{II} center (see below) through an interchange-associative (I_a) mechanism (Scheme 3-2).[39] The positive $\Delta H^{\ddagger}$ values also indicate that the seven-coordinate Ru^{II} complex is thermodynamically unstable as a transition state.[33]

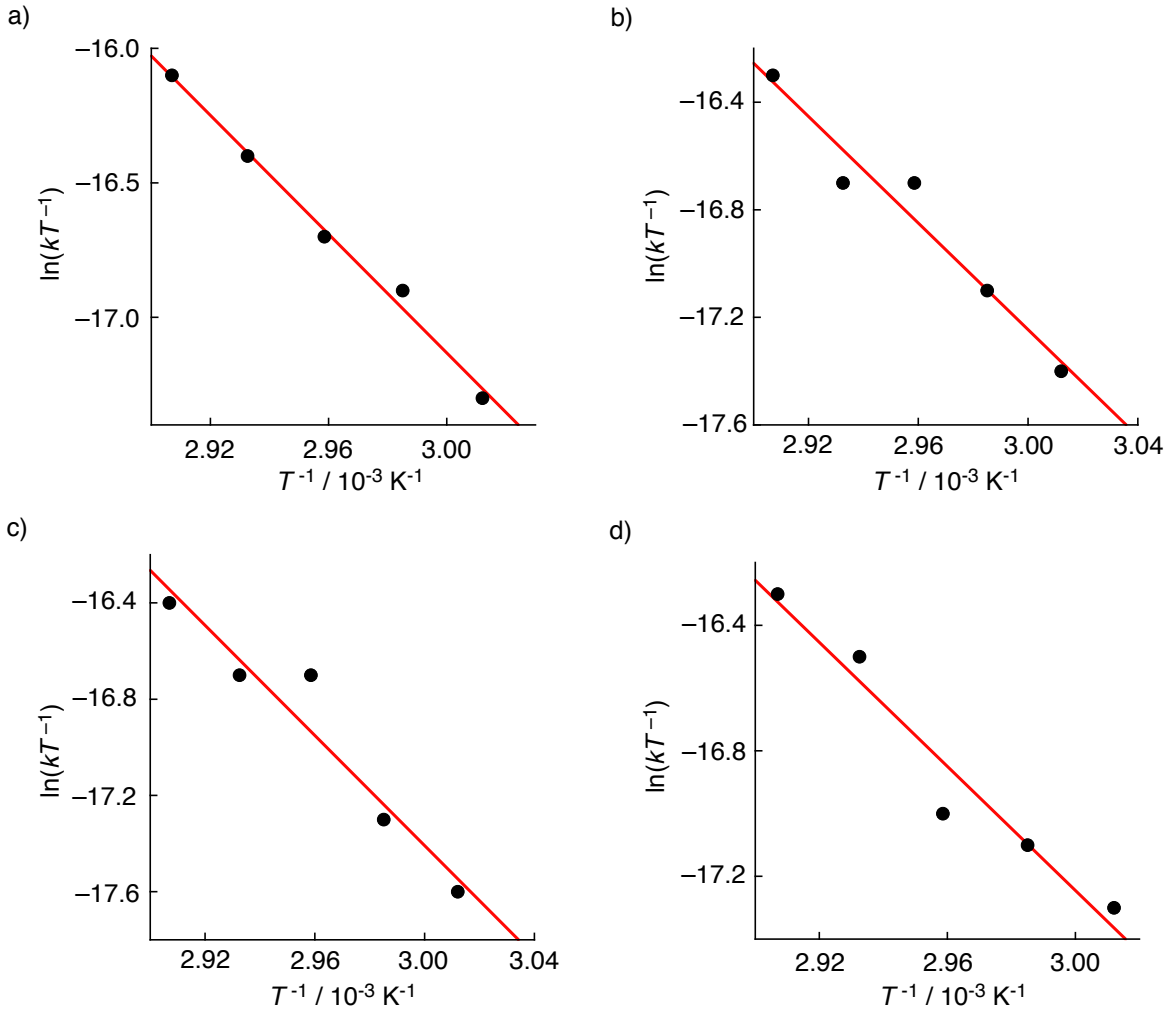

Figure 3-17. Eyring plots for thermal reactions of **4** (a), $[\mathbf{4} + H]^+$ (b), **5** (c) and **6** (d) in MeCN-d_3.

Table 3-4. First-order rate constants (k) [$\times 10^{-5}$ s^{-1}] and activation parameters for the thermal structural changes of complexes **4**, $[\mathbf{4} + H]^+$, **5**, and **6** in MeCN-d_3.

	4	$[\mathbf{4} + H]^+$	**5**	**6**
k (332 K)	1.0	0.90	0.72	0.99
k (335 K)	1.5	1.3	1.0	1.3
k (338 K)	1.8	1.8	1.8	1.4
k (341 K)	2.6	2.0	1.9	2.4
k (344 K)	3.4	2.8	2.6	2.9
$\Delta H^{\ddagger}$ [kJ mol^{-1}]	92	77	95	82
$\Delta S^{\ddagger}$ [J mol^{-1} K^{-1}]	–64	–111	–57	–94

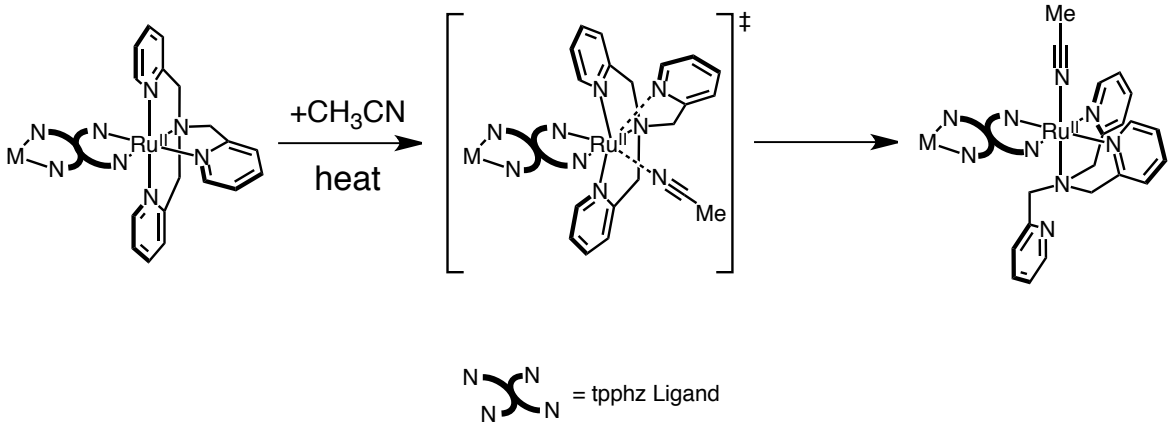

Scheme 3-2. A plausible reaction mechanism of the thermal dissociation reaction. **M** = blank, H^+, $Ru^{II}(bpy)_2$ or $Pd^{II}Cl_2$.

3-2-5. Photoinduced recoordination of the dissociated pyridine

The photoinduced recoordination reactions of the dissociated pyridine moieties in complexes **4'**, [**4'** + H]$^+$, **5'**, and **6'** were investigated by using NMR spectroscopy (Figure 3-14) under photoirradiation at 430 nm. On the photoirradiation of a solution of **4'** in MeCN-d_3, the ^{1}H NMR signals for the methylene TPA protons in the dissociated species gradually diminished, whilst the signals for closed-form complex **4** gradually became more intense. After 4 h, the spectroscopic changes ceased, thus indicating that the reaction mixture had reached a photostationary state, and the integral ratio between complexes **4** and **4'** was 2:1 (Figure 3-14a, bottom), that is, 67% conversion from complex **4'** into complex **4**. The photoirradiation of a solution of protonated complex [**4'** + H]$^+$ also afforded a photostationary state between complexes [**4** + H]$^+$ and [**4'** + H]$^+$. However, in comparison to neutral complex **4**, the conversion from the open form into the closed form was much improved, thus exhibiting an integral ratio of [**4** + H]$^+$/[**4'** + H]$^+$ = 5:1 (Figure 3-14b, bottom), that is, 83% conversion from complex [**4'** + H]$^+$ into [**4** + H]$^+$. In sharp contrast, it should be noted that the photoirradiation of solutions of dinuclear complexes **5'** and **6'** for 10 h led to complete conversion into closed-form species **5** and **6**, without the presence of any remaining complexes **5'** and **6'**, respectively (Figure 3-14c, d, bottom). Similar behaviors were also observed in the photochemical reactions of closed-form complexes **4** and [**4** + H]$^+$ in MeCN-d_3, thus giving rise to a photostationary state that included the corresponding open-form complex (**4'** or [**4'** + H]$^+$). In sharp contrast, no spectroscopic changes were observed during the course of the photoirradiation of solutions of **5** and **6** in MeCN-d_3.

To investigate the mechanism of the complete conversion of the open-form dinuclear complexes into their corresponding closed form, the quantum yields (ϕ, at 430 nm) for the photoinduced recoordination of the pyridine moiety in complexes **4'**, [**4'** + H]$^+$, **5'**, and **6'** (Table 3-5) were determined. Experiments with $[Fe^{III}(oxalato)_3]^{3-}$ as an actinometer, in accordance with previously reported procedure,[40] allowed us to determine the quantum yields in the photoconversion of complexes **4'**, [**4'** + H]$^+$, **5'**, and **6'** to be 0.014, 0.015, 0.024, and 0.013, respectively. Because the quantum yields for the four complexes are not significantly different to one another, the reason for the different conversion efficiencies of these four complexes cannot be the improvement in the quantum yields of the recoordination reactions of the

dissociated pyridine moiety relative to those of the corresponding photodissociation reactions. The detailed reaction mechanisms will be discussed below.

Table 3-5. Quantum yields (ϕ) of the recoordination reactions at λ = 430 nm and the photoconversion efficiencies of open-form complexes **4'** – **6'**.

Compound	Quantum yields (ϕ)	Photoconversion efficiency [%] (λ_{irr} [nm])
4'	0.014	67 (430)
[**4'** + H]$^+$	0.015	83 (430)
5'	0.024	100 (430)
6'	0.013	100 (430)
[Ru(TPA)(bpy)]$^{2+}$ [a]	0.0057	40 (423)
[Ru(TPA)(bpm)]$^{2+}$ [a]	0.028	89 (453)
[Ru(TPA)(phen)]$^{2+}$ [a]	0.011	65 (423)

[a] See ref. [26].

3-2-6. Perturbation of the excited states by metal coordination

As mentioned above, the four Ru^{II}-tpphz complexes **4**, [**4** + H]$^+$, **5**, and **6** showed thermal dissociation reactions in MeCN, concomitant with their structural transformation into open-form complexes **4'**, [**4'** + H]$^+$, **5'**, and **6'**, respectively, in quantitative yields, which contained a free pyridylmethyl moiety on the facial η^3-TPA ligand and an axial MeCN ligand. Thus, in MeCN, the open-form complexes are thermodynamically more stable than the closed-form complexes. This result is consistent with the calculated energy difference between complexes **5** and **5'** as mentioned above.

Under photoirradiation conditions, the open-form complexes turned back to their corresponding closed-form complexes. Complex **4'** afforded a photostationary state with a conversion efficiency of 67% from complex **4'**, protonated complex [**4** + H]$^+$ exhibited improved efficiency (83%) from [**4'** + H]$^+$, and dinuclear complexes **2** and **3** achieved complete conversion to their corresponding closed-form complexes. To elucidate the controlling factor of the photoinduced conversion efficiency, the author focused on the perturbation of the energy level of the triplet MLCT excited states (^{3}MLCT*) by protonation and metal coordination at the vacant diimine site of the tpphz ligand. It has been proposed that the photodissociation of ligands in Ru^{II} complexes occurs through the triplet MC excited states (^{3}MC*) that are formed by the thermal conversion of the ^{3}MLCT* states, which generated through very fast intersystem crossing from the singlet MLCT excited state (^{1}MLCT*).[41] From the resulting ^{3}MC* state, the ligand dissociation proceeds as a thermal process through an unstable coordinated intermediate (Figure 3-18a).[41] The photodissociation and photo-recoordination reactions of Ru^{II}(TPA)(diimine) complexes proceed in the same manner. The axial pyridine moiety in the closed form and the coordinated MeCN molecule in the open form dissociate through their corresponding ^{3}MC* states. Based on the UV/Vis and emission spectra of complexes, **4**, [**4** + H]$^+$, **5**, and **6**, the ^{1}MLCT* and ^{3}MLCT* states are stabilized by protonation or metal coordination at the vacant diimine site of the tpphz ligand that is bound to the Ru^{II}(TPA) unit. The cause of the bathochromic shifts of

the MLCT absorption and the emission maxima is stabilization of the LUMO (π^*) orbital that is localized on the tpphz ligand by protonation or metal coordination.[42]

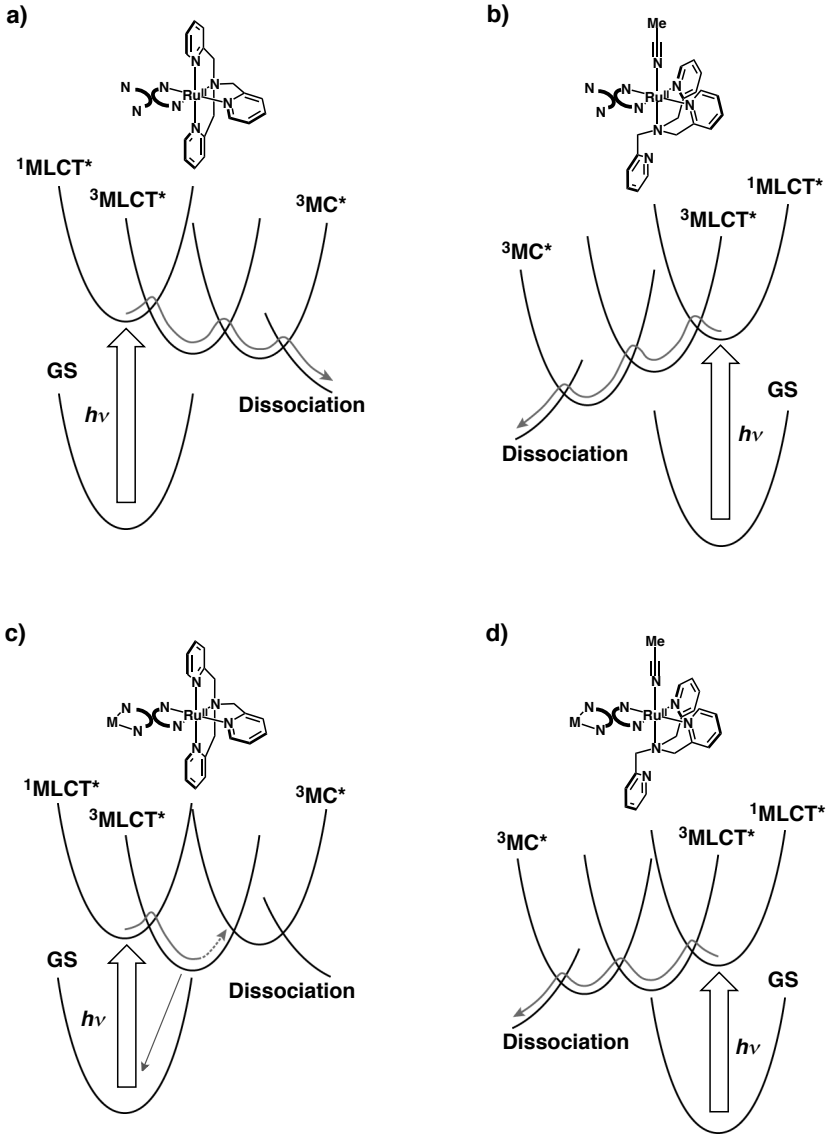

Figure 3-18. Plausible energy diagrams for the photoinduced dissociation and recoordination reactions of Ru^{II}(TPA)(tpphz) complexes **4** (a), **4'** (b), **5** or **6** (c), and **5'** or **6'** (d). GS denotes the ground state.

The stabilization of the π^* orbital of the tpphz ligand was also confirmed by electrochemical studies, in which the reduction potential of the tpphz ligand was positively shifted in the order: **5** > **6** > [**4** + H]$^+$ > **4** (see above). However, protonation and metal coordination at the vacant diimine site of the tpphz ligand probably do not affect the ^{3}MC* state of the Ru^{II} center in the Ru^{II}(TPA) unit, judging from the identical oxidation potentials of the $Ru^{II/III}$ redox couples for the units in all four complexes. Therefore, in the closed forms, which contain the tetradentate TPA ligand, the transition process from the ^{3}MLCT* state into the ^{3}MC* state can be perturbed by protonation and metal coordination at the vacant site of the tpphz ligand, when the ^{3}MLCT* state is well-stabilized relative to the ^{3}MC* state (Figure 3-18c). As a result, the activation barrier

($\Delta G_1^{\ddagger}$) of the thermal transition from the ^{3}MLCT* state into the ^{3}MC state becomes large enough not to be overcome at the reaction temperature (Figure 3-19, lower black line). On the other hand, the ^{3}MC* states of the open-form complexes are highly stabilized in comparison with those in the closed-form complexes, because the Ru^{II} centers are weakly coordinated by an MeCN molecule instead of a strong pyridine ring of the TPA ligand (Figure 3-18b, d).[43] As a consequence, the ^{3}MC* state is at a lower energy than the ^{3}MLCT* state in the MeCN-bound open-form complexes, even after the ^{3}MLCT* state is stabilized by protonation or metal coordination at the vacant site of the tpphz ligand (Figure 3-18d). Therefore, the activation barrier of the thermal transition from the ^{3}MLCT* state into the ^{3}MC state remains low enough to promote the dissociation reaction of the MeCN ligand at the reaction temperature.

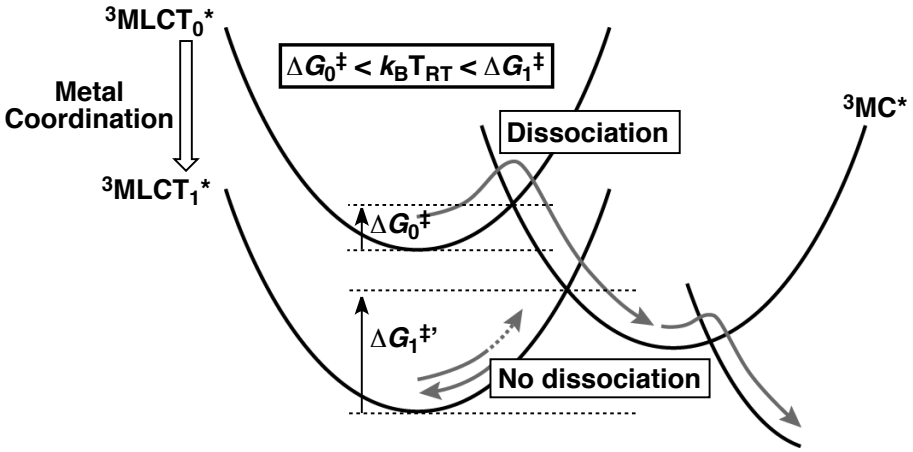

Figure 3-19. Schematic representation of the stabilization of a ^{3}MLCT* state by metal coordination to the ligand and the resulting disturbance of the transition into the MC* state.

3-3. Conclusion

The completely photochromic structural conversion has been achieved between the closed and open forms of dinuclear [{Ru^{II}(TPA)}(μ-tpphz)(ML)] complexes (ML = $Ru^{II}(bpy)_2$, $Pd^{II}Cl_2$), thus demonstrating molecular bistability. Heating a solution of the closed-form complex in MeCN quantitatively afforded the corresponding open-form complex, which contained a coordinated MeCN ligand and a facial η^3-TPA ligand, with an uncoordinated pyridylmethyl arm. On the contrary, illumination of the solution induced the complete conversion of the partially dissociated (open-form) complex that was obtained from the thermal process into the original fully coordinated (closed-form) complex. This reversible structural conversion between two states of a transition-metal complex has been accomplished by a simple perturbation of the electronic structure of the complex, that is, further metal coordination to the other coordination site of the π-conjugated bis-diimine ligand of the complex. Metal coordination to the opposite site of the bis-diimine ligand causes a lowering of the energy level of the LUMO (π^*) orbital of the ligand, which results in the stabilization of the ^{3}MLCT* state of the complex. In the closed form, the stabilization of the ^{3}MLCT* state hinders the transition into the ^{3}MC* state, which is the key excited state in the photoinduced ligand dissociation and recoordination, whereas the ^{3}MC* state in the closed form is originally stabilized by the substitution of one pyridine ligand

for an MeCN solvent molecule, and thus, the transition from the ^{3}MLCT* to ^{3}MC* is still possible even after further metal coordination.

The strategy presented in this chapter is applicable to the development of the complete regulation of molecular functionality by external stimuli on the basis of molecular bistability. This kind of unique molecular machinery, which is completely controlled by thermal and photonic stimuli, is highly promising for future applications in photoresponsive drug-delivery systems[44] or on/off switchable catalysts.[45, 46]

3-4. Experimental section

Materials and synthesis. Phendiamine,[31] $[RuCl(TPA)]_2$ $(ClO_4)_2$,[35] and $[RuCl_2(bpy)_2]\cdot 2H_2O$[32] were prepared according to literature procedures. Phendione was synthesized according to a literature procedure[30] and purified by column chromatography on silica gel (Wakogel C-200, 75 – 150 μm; $CHCl_3$/MeOH, 10:1 v/v).

Methods. NMR measurements were performed on JEOL EX270 and Bruker AVANCE400 spectrometers. UV/Vis absorption spectra were recorded in MeCN on a Shimazu UV-3600 spectrophotometer at room temperature. Emission spectra were recorded on JASCO FP-6500 and HITACHI F-4500 spectrofluorometers at room temperature. MS (ESI-TOF) was performed on Applied Biosystems QSTAR Pulsar i and JEOL JMS-T100CS mass spectrometers. Photoirradiation of the sample was performed by using a Xe light source (300 W) on an ASAHI SPECTRA MAX-301.

$[Ru^{II}(TPA)(phendione)](PF_6)_2$. Orange solid of $[Ru^{II}(TPA)]_2(ClO_4)_2$[35] (0.432 g, 0.41 mmol) was added to a degassed solution of phendione[30] (0.450 g, 2.1 mmol) in MeOH (50 mL) under an Ar atmosphere. The mixture was heated at reflux for overnight and then cooled to room temperature. NH_4PF_6 was added to the solution to give a brown precipitate. The precipitate was filtered, thoroughly washed with Et_2O, and then dried under vacuum. Yield: 0.551 g (0.62 mmol, 75%). ^{1}H NMR (MeCN-d_3): δ 9.86 (dd, J = 5.4, 0.7 Hz, 1H; phen-H2), 9.26 (dd, J = 5.4, 1.3 Hz, 1H; phen-H9), 9.08 (d, J = 5.8 Hz, 1H; pyr-H6(ax)), 8.71 (dd, J = 7.9, 1.2 Hz, 1H; phen-H4), 8.42 (dd, J = 7.9, 1.2 Hz, 1H; phen-H7), 8.18 (dd, J = 6.2, 2.1 Hz, 1H; phen-H3), 7.80 (dd, J = 5.6, 0.7 Hz, 2H; pyr-H6(eq)), 7.74 – 7.70 (m, 3H; pyr-H4(ax) and pyr-H4(eq)), 7.67 (td, J = 7.8, 1.5 Hz, 1H; phen-8 H), 7.41 (d, J = 7.9 Hz, 3H; pyr-H3(ax) and pyr-H3(eq)), 7.34 (td, J = 6.7, 1.4 Hz, 1H; pyr-H5(ax)), 7.05 (t, J = 6.5 Hz, 2H; pyr-H5(eq)), 5.50 and 5.17 (ABq, J = 17.1 Hz, 4H; CH_2(eq)), 4.75 (s, 2H; CH_2(ax)). MS (ESI): calcd for $[M - 2PF_6]^{2+}$: m/z = 301.05, found: m/z = 301.06. Anal: calcd (%) for $C_{30}H_{24}N_6O_2P_2F_{12}Ru$: C 40.41, H 2.71, N 9.43, found: C 40.70, H 2.90, N 9.70.

$[Ru^{II}(TPA)(tpphz)](PF_6)_2$ (**4**): Brown solid of $[Ru^{II}(TPA)(phendione)](PF_6)_2$ (0.199 g, 0.22 mmol) was added to a degassed solution of phendiamine[31] (0.100 g, 0.48 mmol) in MeOH (60 mL) under an Ar atmosphere. The mixture was heated at reflux for 12 h and then cooled to room temperature. The solution was filtered through Celite 535 and thoroughly washed with MeCN. NH_4PF_6 and water were added to the concentrated filtrate to afford a precipitate. The orange product was filtered, thoroughly washed with water, EtOAc, and Et_2O, and dried under vacuum. Yield: 0.172 g (0.16 mmol, 73%). ^{1}H NMR (MeCN-d_3, 1.7 mM): δ 10.14 (d, J = 5.6 Hz, 1H; tpphz(*h*)-H6), 9.75 – 9.70 (m, tpphz(*h*)-H4, 3H; tpphz(*j*)-H6 and pyr-H6(ax)), 9.62 (d, J = 7.8 Hz, 1H; tpphz(*c*)-H6), 9.56 (d, J = 5.6 Hz, 1H; tpphz(*a*)-H4), 9.32 (d, J = 6.1 Hz, 1H;

tpphz(*a*)-H6), 8.98 (dd, *J* = 4.5, 1.7 Hz, 1H; tpphz(*j*)-H4), 8.85 (dd, *J* = 4.5, 1.7 Hz, 1H; pyr-H5(ax)), 8.43 (dd, *J* = 8.1, 2.7 Hz, 1H; tpphz(*h*)-H5), 8.02 (dd, *J* = 8.1, 2.8 Hz, 1H; tpphz(*c*)-H4), 7.96 (d, *J* = 5.0 Hz, 2H; pyr-H6(eq)), 7.92 – 7.85 (m, 2H; pyr-H4(ax) and tpphz(*j*)-H5), 7.78 (t, *J* = 8.4 Hz, 1H; tpphz(*c*)-H5), 7.62 (td, *J* = 7.7, 1.7 Hz, 2H; pyr-H4(eq)), 7.48 – 7.42 (m, 4H; pyr-H3(ax), pyr-H3(eq), and tpphz(*a*)-H5), 6.96 (t, *J* = 6.1 Hz, 2H; pyr-H5(eq)), 5.72 and 5.28 (ABq, *J* = 17.1 Hz, 4H; CH_2(eq)), 4.85 (s, 2H; CH_2(ax)). UV/Vis (MeCN): λ_{max} (log ε) = 363 ($\pi\rightarrow\pi^*$, 4.37), 381 ($\pi\rightarrow\pi^*$, 4.54), 424 nm (MLCT, 4.13); MS (ESI): calcd for $[M - 2PF_6]^{2+}$: *m*/*z* = 388.08, found: *m*/*z* = 388.10. Anal: calcd (%) for $C_{42}H_{30}N_{10}P_2F_{12}Ru{\cdot}0.5H_2O$: C 46.94, H 2.91, N 13.03, found: C 46.97, H 3.19, N 13.12.

[Ru(η^3-TPA)(tpphz)(MeCN)(PF_6)$_2$ (4'). A solution of **4** (10 mg, 9.4 μmol) in MeCN (5 mL) was heated at 60 ºC for 5 days in the dark. EtOAc was added to this solution to afford a precipitate. The orange precipitate was filtered, thoroughly washed with EtOAc and Et_2O, and dried under vacuum. Yield: 8 mg (7 μmol, 70%). ^{1}H NMR (MeCN-d_3, 1.7 mM): δ 9.79 (dd, *J* = 8.1, 1.5 Hz, 2H; tpphz(*h*)-H6 and tpphz(*j*)-H6), 9.71 (d, *J* = 8.3 Hz, 2H; tpphz(*h*)-H4 and tpphz(*j*)-H4), 9.11 (d, *J* = 5.3 Hz, 2H; tpphz(*a*)-H6 and tpphz(*c*)-H6), 9.01(d, *J* = 3.2 Hz, 2H; pyr-H6(eq)), 8.79 (dd, *J* = 5.3, 1.2 Hz, 2H; tpphz(*a*)-H4 and tpphz(*c*)-H4), 8.44 (d, *J* = 4.0 Hz, 1H; pyr-H6(ax)), 8.08 (dd, *J* = 8.2, 5.3 Hz, 2H; tpphz(*h*)-H5 and tpphz(*j*)-H5), 7.96 – 7.90 (m, 4H; pyr-H4(eq), tpphz(*a*)-H5, and tpphz(*c*)-H5), 7.54 – 7.46 (m, 5H; pyr-H4(ax), pyr-H5(eq), and pyr-H3(eq)), 7.18 (dd, *J* = 6.8, 4.9 Hz, 1H; pyr-H5(ax)), 7.02 (d, *J* = 7.8 Hz, 1H; pyr-H3(ax)), 4.88 and 4.28 (ABq, *J* = 17.1 Hz, 2H; CH_2(eq)), 3.42 (s, 1H; CH_2(ax)), 2.16 (s, 3H; MeCN). UV/Vis (MeCN): λ_{max} (log ε) [nm] = 433 (MLCT, 3.84). MS (ESI): calcd for $[M - 2PF_6]^{2+}$: *m*/*z* = 408.60, found: *m*/*z* = 408.56.

[Ru(TPA)(tpphz-H$^+$)](PF_6)$_3$ ([4 + H]$^+$). Trifluoromethanesulfonic acid (8 μL, 0.09 mmol) was added to a solution of complex **4** (0.031 g, 0.029 mmol) in MeCN (20 mL). The solution was filtered through Celite 535 and thoroughly washed with MeCN. NH_4PF_6 and water were added to the concentrated filtrate to afford a precipitate. The orange product was filtered, thoroughly washed with water, and dried under vacuum. Yield: 0.021 g (0.017 mmol, 59%). ^{1}H NMR (MeCN-d_3, 1.6 mM): δ 10.17 – 10.12 (m, 2H; tpphz(*h*)-H6 and pyr-H6(ax)), 10.07 (dd, *J* = 8.2, 1.5 Hz, 1H; tpphz(*h*)-H4), 9.99 (dd, *J* = 8.2, 1.2 Hz, 1H; tpphz(*j*)-H6), 9.78 (dd, *J* = 8.1, 0.8 Hz, 1H; tpphz(*c*)-H6), 9.58 (dd, *J* = 5.4, 1.1 Hz, 1H; tpphz(*a*)-H6), 9.30 – 9.21 (m, 3H; tpphz(*a*)-H4, tpphz(*j*)-H4, and pyr-H5(ax)), 8.51 (dd, *J* = 8.1, 5.5 Hz, 1H; tpphz(*h*)-H5), 8.29 – 8.21 (m, 2H; tpphz(*j*)-H5 and pyr-H4(ax)), 8.07 (dd, *J* = 7.1, 5.4 Hz, 1H; tpphz(*c*)-H4), 7.81 (dd, *J* = 5.8, 0.8 Hz, 2H; pyr-H6(eq)), 7.76 (td, *J* = 7.7, 1.3 Hz, 1H; tpphz(*a*)-H5), 7.61 (td, *J* = 7.7, 1.5 Hz, 2H; pyr-H4(eq)), 7.45 – 7.37 (m, 4H; pyr-H3(ax), pyr-H3(eq), and tpphz(*c*)-H5), 6.92 (t, *J* = 6.1 Hz, 2H; pyr-H5(eq)), 5.65 and 5.23 (ABq, *J* = 17.1 Hz, 4H; CH_2(eq)), 4.80 (s, 2H; CH_2(ax)). UV/Vis (MeCN): λ_{max} (log ε) [nm] = 363 ($\pi\rightarrow\pi^*$, 4.26), 378 ($\pi\rightarrow\pi^*$, 4.37), 428 (MLCT, 4.00). Anal: calcd (%) for $C_{42}H_{31}N_{10}P_3F_{18}Ru{\cdot}H_2O{\cdot}0.5MeCN$: C 41.31, H 2.78, N 11.76, found: C 41.48, H 3.06, N 11.56.

[Ru(η^3-TPA)(tpphz-H$^+$)(MeCN)](PF_6)$_3$ ([4' + H]$^+$). A solution of [**4** + H]$^+$ (12 mg, 0.010 mmol) in MeCN (5 mL) was heated at 60 ºC for 5 days in the dark. EtOAc was added to the solution to afford a precipitate. The orange precipitate was filtered, thoroughly washed with EtOAc and Et_2O, and dried under vacuum. Yield: 9 mg (7 μmol, 70%). ^{1}H NMR (MeCN-d_3, 1.6 mM): δ 9.77 (dd, *J* = 8.1, 1.6 Hz, 2H; tpphz(*h*)-H6 and tpphz(*j*)-H6), 9.66 (d, *J* = 8.0 Hz, 2H; tpphz(*h*)-H4 and tpphz(*j*)-H4), 9.12 (d, *J* = 5.5 Hz, 2H; tpphz(*a*)-H6

and tpphz(*c*)-H6), 8.95 (d, *J* = 3.6 Hz, 2H; pyr-H6(eq)), 8.79 (dd, *J* = 5.3, 1.2 Hz, 2H; tpphz(*a*)-H4 and tpphz(*c*)-H4), 8.44 (d, *J* = 4.8 Hz, 1H; pyr-H6(ax)), 8.07 (dd, *J* = 8.2, 5.3 Hz, 2H; tpphz(*h*)-H5 and tpphz(*j*)-H5), 7.95–7.90 (m, 4H; pyr-H4, tpphz(*a*)-H5, and tpphz(*c*)-H5), 7.52 – 7.46 (m, 5H; pyr-H4(ax), pyr-H5(eq), and pyr-H3(eq)), 7.18 (dd, *J* = 7.6, 4.9 Hz, 1H; pyr-H5(ax)), 7.04 (d, *J* = 7.8 Hz, 1H; pyr-H3(ax)), 4.88 and 4.28 (ABq, *J* = 16.9 Hz, 2H; CH_2(eq)), 3.43 (s, 1H; CH_2(ax)), 2.16 (s, 3H; MeCN). UV/Vis (MeCN): λ_{max} (log ε) [nm] = 408 (MLCT, 3.98).

[(bpy)$_2$Ru(μ-tpphz)Ru(TPA)](PF$_6$)$_4$ (5). A solution of [$RuCl_2(bpy)_2$]·$2H_2O$[32] (96 mg, 0.19 mmol) and silver trifluoromethane-sulfonate (98 mg, 0.38 mmol) in acetone (30 mL) was heated at 40 ºC for 8 h and then cooled to room temperature. After filtration to remove the resulting silver chloride and washing the solid with acetone (10 mL), the solution of complex **4** (82.3 mg, 0.077 mmol) in acetone (20 mL) was added to the collected filtrate. Then, the mixture was degassed and stirred for 3 days under an Ar atmosphere at room temperature. The solution was filtered, NH_4PF_6 and water were added, and the mixture was stored at 4 ºC for 2 h until a red precipitate appeared. The precipitate was filtered off, washed with water, EtOH, and Et_2O, and dried under vacuum. Yield: 110 mg (0.062 mmol, 80%). ^{1}H NMR (MeCN-d_3, 1.3 mM): δ 10.56 (d, *J* = 4.5 Hz, 1H; tpphz(*h*)-H6), 10.34 (d, *J* = 7.2 Hz, 1H; tpphz(*h*)-H4), 10.24 (d, *J* = 7.0 Hz, 1H; tpphz(*j*)-H6), 10.14 – 10.04 (m, 2H; tpphz(*j*)-H4 and pyr-H6(ax)), 9.64 (d, *J* = 7.3 Hz, 1H; tpphz(*c*)-H6), 8.92 – 8.85 (m, 5H; pyr-H5(ax), pyr'-H6(ax), and pyr'-H6(eq)), 8.72 – 8.63 (m, 3H; tpphz(*h*)-H5 and pyr'-H3(eq)), 8.33 – 8.05 (m, 12H; pyr-3H(ax), pyr-4H(ax), pyr-H6(eq), pyr'-H5(ax), pyr'-H3(ax), pyr'-H4(eq), tpphz(*c*)-H4, and tpphz(*j*)-H5), 7.87 (t, *J* = 7.7 Hz, 1H; tpphz(*a*)-H6), 7.77 – 7.60 (m, 8H; pyr-H5(eq), pyr-H3(eq), pyr'-H4(ax), tpphz(*a*)-H5, and tpphz(*a*)-H4), 7.52 (t, *J* = 6.0 Hz, 1H; tpphz(*c*)-H5), 7.42 (t, *J* = 5.9 Hz, 2H; pyr'-H5(eq)), 7.05 (t, *J* = 6.1 Hz, 2H; pyr-H4(eq)), 6.12 and 5.59 (ABq, *J* = 17.5 Hz, 4H; CH_2(eq)), 5.18 (s, 2H; CH_2(ax)). UV/Vis (MeCN): λ_{max} (log ε) [nm] = 353 ($\pi\rightarrow\pi^*$, 4.40), 371 ($\pi\rightarrow\pi^*$, 4.51), 442 (MLCT, 4.39). MS (ESI): calcd for [M – 4PF_6]$^{4+}$: *m*/*z* = 297.55, found: *m*/*z* = 297.59. Anal: calcd (%) for $C_{62}H_{46}N_{14}P_4F_{24}Ru_2$·$2H_2O$: C 41.25, H 2.79, N 10.86, found: C 41.10, H 2.85, N 10.77.

[(bpy)$_2$Ru(μ-tpphz)Ru(η^3-TPA)(MeCN)](PF$_6$)$_4$ (5'). A solution of **5** (20 mg, 0.011 mmol) in MeCN (5 mL) was heated at 60 ºC for 5 days in the dark. EtOAc was added to this solution to form a precipitate. The orange precipitate was filtered, thoroughly washed with EtOAc and Et_2O, and dried under vacuum. Yield: 15 mg (8.3 μmol, 75%). ^{1}H NMR (MeCN-d_3, 1.3 mM): δ 10.03 (d, *J* = 5.3 Hz, 2H; tpphz(*h*)-H6 and tpphz(*j*)-H6), 9.99 (dd, *J* = 8.3, 1.2 Hz, 2H; tpphz(*a*)-H6 and tpphz(*c*)-H6), 9.06 (d, *J* = 5.4 Hz, 2H; pyr-H6(eq)), 8.84 (dd, *J* = 5.4, 1.2 Hz, 2H; pyr'-H6(ax)), 8.58 (d, *J* = 8.1 Hz, 2H; pyr'-H6(eq)), 8.54 (d, *J* = 8.2 Hz, 2H; tpphz(*h*)-H4 and tpphz(*j*)-H4), 8.44 (d, *J* = 4.8 Hz, 1H; pyr-H6(ax)), 8.30 (dd, *J* = 5.3, 1.2 Hz, 2H; tpphz(*a*)-H4 and tpphz(*c*)-H4), 8.18 – 8.12 (m, 4H; tpphz(*h*)-H5 and tpphz(*j*)-H5), 8.05 – 8.00 (m, 4H; pyr'-H4(ax) and pyr'-H4(eq)), 7.93 – 7.87 (m, 4H; pyr-H4(eq), tpphz(*a*)-H5, and tpphz(*c*)-H5), 7.74 (d, *J* = 5.5 Hz, 2H; pyr'-H3(ax) and pyr'-H3(eq)), 7.56 (td, *J* = 7.8, 1.8 Hz, 1H; pyr-H4(ax)), 7.51 – 7.44 (m, 6H; pyr-H5(eq), pyr'-H5(ax) and pyr'-H5(eq)), 7.28 – 7.20 (m, 3H; pyr-H5(ax), pyr-H3(eq)), 6.96 (d, *J* = 7.8 Hz, 1H; pyr-H3(ax)), 4.85 and 4.25 (ABq, *J* = 17.1 Hz, 2H; CH_2(eq)), 3.31 (s, 2H; CH_2(ax)), 2.16 (s, 3H; MeCN). UV/Vis (MeCN): λ_{max} (log ε) [nm] = 437 (MLCT, 4.33). MS (ESI): calcd for [M – 4PF_6]$^{4+}$: *m*/*z* = 307.81; found: *m*/*z* = 307.81.

[$Cl_2Pd(\mu$-tpphz)Ru(TPA)]$(PF_6)_2$ (6). A solution of **4** (42 mg, 0.040 mmol) and $PdCl_2$ (41 mg, 0.29 mmol) in EtOH (25 mL) was degassed and heated at reflux for 24 h under an Ar atmosphere. Then, the solution was cooled to room temperature and the solvent was removed under vacuum. The residual brown solid was dissolved in MeCN and the black precipitate was filtered off. The volatile compounds in the orange filtrate were removed and the residue was dissolved in a small amount of DMSO. The solution was filtered, NH_4PF_6 and water were added, and the mixture was stored at 4 ºC for 2 h until a red precipitate appeared. The precipitate was filtered off, washed with water, EtOH, and Et_2O, and dried under vacuum. Yield: 21 mg (0.017 mmol, 43%). ^{1}H NMR (MeCN-d_3, 1.5 mM): δ 10.32 (d, J = 5.1 Hz, 1H; tpphz(*h*)-H6), 9.98 (d, J = 8.2 Hz, 1H; tpphz(*h*)-H4), 9.70 (d, J = 8.1 Hz, 1H; tpphz(*j*)-H6), 9.64 (d, J = 5.3 Hz, 1H; tpphz(*a*)-H6), 9.59 – 9.56 (m, 2H; tpphz(*c*)-H6 and pyr-H6(ax)), 9.30 (d, J = 5.3 Hz, 1H; tpphz(*a*)-H4), 9.11 – 9.06 (m, 2H; tpphz(*j*)-H4 and pyr-H5(ax)), 7.91 (d, J = 5.0 Hz, 2H; pyr-H6(eq)), 7.76 (t, J = 7.0 Hz, 1H; tpphz(*a*)-H5), 7.58 (td, J = 7.8, 1.5 Hz, 2H; pyr-H4(eq)), 7.46 – 7.38 (m, 4H; tpphz(*c*)-H3, pyr-H3(ax), and pyr-H3(eq)), 6.89 (t, J = 6.3 Hz, 2H; pyr-H5(eq)), 5.66 and 5.22 (ABq, J = 17.0 Hz, 4H; CH_2(eq)), 4.80 (s, 2H; CH_2(ax)). UV/Vis (MeCN): λ_{max} (log ε) [nm] = 359 ($\pi\rightarrow\pi^*$, 4.37), 378 ($\pi\rightarrow\pi^*$, 4.54), 437 (MLCT, 4.06). MS (ESI): calcd for $[M - 2PF_6]^{2+}$: m/z = 476.51, found: m/z = 476.49. Anal: calcd (%) for $C_{42}H_{30}N_{10}P_2F_{12}Cl_2RuPd$: C 38.89, H 2.80, N 10.80, found: C 39.19, H 2.50, N 10.88.

[$Cl_2Pd(\mu$-tpphz)Ru(η^3-TPA)(MeCN)]$(PF_6)_2$ (6'). A solution of **6** (12 mg, 9.7 μmol) in MeCN (5 mL) was heated at 60 ºC for 5 days in the dark. EtOAc was added to this solution to afford a precipitate. The orange precipitate was filtered, thoroughly washed with EtOAc and Et_2O, and dried under vacuum. Yield: 8 mg (6 μmol, 62%). ^{1}H NMR (MeCN-d_3, 1.7 mM): δ 9.99 (dd, J = 4.2, 1.2 Hz, 2H; tpphz(*h*)-H6 and tpphz(*j*)-H6), 9.64 (dd, J = 8.2, 1.3 Hz, 2H; tpphz(*h*)-H4 and tpphz(*j*)-H4), 9.23 (dd, J = 5.4, 1.3 Hz, 2H; tpphz(*a*)-H6 and tpphz(*c*)-H6), 9.10 (d, J = 5.2 Hz, 2H; tpphz(*a*)-H4 and tpphz(*j*)-H4), 8.89 (dd, J = 5.3, 1.3 Hz, 2H; pyr-H6(eq)), 8.47 (dd, J = 4.8, 1.0 Hz, 1H; pyr-H6(ax)), 8.24 – 8.18 (m, 4H; pyr-H4(eq), tpphz(*h*)-H5, and tpphz(*j*)-H5), 7.91 (td, J = 7.9, 1.5 Hz, 2H; tpphz(*a*)-H5 and tpphz(*c*)-H5), 7.56 (td, J = 7.8, 1.8 Hz, 1H; pyr-H4(ax)), 7.52 – 7.54 (m, 4H; pyr-H3(eq) and pyr-H5(eq)), 7.22 (m, 1H; pyr-H5(ax)), 7.04 (d, J = 7.9 Hz, 1H; pyr-H3(eq)), 4.87 and 4.27 (ABq, J = 17.0 Hz, 4H; CH_2(eq)), 3.40 (s, 2H; CH_2(ax)), 2.15 (s, 3H; MeCN). UV/Vis (MeCN): λ_{max} (log ε) [nm] = 405 (MLCT, 3.82). MS (ESI): calcd for $[M - 2PF_6]^{2+}$: m/z = 499.04, found: m/z = 499.04.

Electrochemical measurements. Cyclic and differential-pulse voltammetry were performed in MeCN in the presence of 0.1 M $[(n\text{-Bu})_4N]PF_6$ ($TBAPF_6$) as an electrolyte under an Ar atmosphere at room temperature, with a Pt disk as a working electrode, $Ag/AgNO_3$ as a reference electrode, and Pt wire as an auxiliary electrode.

Photoirradiation. The photoirradiation of **4**, $[\mathbf{4} + H]^+$, **5**, and **6** was performed by using a Xe light source (300 W) on an ASAHI SPECTRA MAX-301 that was equipped with a band-path filter for a bandwidth-at-half-maximum of 20 nm, centered at 430 nm. The complexes were dissolved in freshly distilled MeCN to a concentration of 3.4×10^{-5} M for the UV/Vis measurements and in MeCN-d_3 to a

concentration of 1.6 mM for the ^{1}H NMR experiments. The sample solutions were degassed by bubbling with Ar. The degassed solutions were irradiated at 430 nm for 12 h and the reaction was monitored by monitoring the absorption or ^{1}H NMR spectroscopic changes.

Determination of quantum yields: The quantum yields of the photodissociation reactions of **4**, [**4** + H]$^+$, **5**, and **6** were determined by using standard methods on an actinometer (potassium ferrioxalate) in water with photoirradiation at 430 nm.[40] The reaction was monitored to observe the decrease in absorbance at 430 nm over time. The data for the initial stage, during which a linear change was observed, were used to determine the quantum yield.[47]

Kinetics analysis of the thermal processes. The absorbance change at 440 nm was monitored and fit to Equation (1).

$$\mathrm{Abs} = \mathrm{Abs}_\infty + (\mathrm{Abs}_0 - \mathrm{Abs}_\infty)e^{-kt} \qquad (1)$$

Determination of rate constants by using ^{1}H NMR spectroscopy: The concentration of the starting complex at each time was determined as the integral ratio between the signal of the equatorial methylene moieties of the TPA ligand and that of the methyl groups of tetraethylsilane, which was used as an internal standard. The decrease in concentration of the starting complex was plotted against the time and the plot was fitted to Equation (2).

$$c = c_0 e^{-kt} \qquad (2)$$

Similar experiments were performed at various temperatures and the obtained rate constants were plotted against the reciprocal of the temperature. The resulting plot was fitted to the Eyring equation (Equation (3)) to estimate the activation parameters.

$$\ln(kT^{-1}) = -\Delta H^{\ddagger} R^{-1} T^{-1} + \Delta S^{\ddagger} R^{-1} + \ln(\chi k_B/h) \qquad (3)$$

X-ray crystallography of 4. A single crystal of **4** was obtained by recrystallization through the slow diffusion of benzene into its solution in acetone in the presence of excess sodium tetraphenylborate to exchange the counteranion for improved crystallinity. The diffraction data were measured on a Rigaku Mercury CCD system at the Photon Factory–Advanced Ring for Pulse X-rays (PF-AR NW2A) of the High Energy Accelerator Research Organization (KEK). The data were integrated, scaled, and corrected for absorption by using the HKL2000 program. The structure was solved by using direct methods (SIR-97) and expanded with differential Fourier techniques. All non-hydrogen atoms were refined anisotropically and the refinement was performed by using full-matrix least-squares on F. All calculations were performed by using the Yadokari-XG crystallographic software package.[48]

Crystallographic data: $C_{42}H_{30}N_{10}Ru{\cdot}2B(C_6H_5)_4{\cdot}C_4H_8O_2$; *Mw* = 904.40; red-orange crystals; monoclinic; space

group $P2_1/n$; a = 14.3387(7), b = 17.8504(8), c = 33.121(2) Å; β = 95.39(2)°; V = 8439.9(8) Å^3; Z = 4; ρ_{calcd} = 1.321 g cm^{-3}; F_{000} = 3512; $R1$ = 0.1071 ($I > 2\sigma(I)$), $wR2$ = 0.3066 (all data); GOF = 0.984. CCDC-921694 (**4**) contains the supplementary crystallographic data and these data can be obtained free of charge from The Cambridge Crystallographic Data Centre via www.ccdc.cam.ac.uk/data_request/cif.

Computational methods. The structures of **5** and **5'** were optimized by using the hybrid (Hartree–Fock/DFT) B3LYP functional.[49] The SDD basis set[50] were used for Ru atoms and the D95** basis set[51] for H, C, and N atoms. The program was the Gaussian 09 package.[52] A model structure of **2** was developed on the basis of the crystal structures of [Ru^{II}(TPA)(phen)](PF$_6$)$_2$[26] and *cis*-[Ru^{II}Cl$_2$(bpy)$_2$].[32]

Reference and notes

[1] a) V. Balzani, A. Credi, M. Venturi, *Molecular Devices and Machines*, Wiley-VCH, Weinheim, **2003**; b) V. Balzani, A. Credi, F. M. Raymo, J. F. Stoddart, *Angew. Chem. Int. Ed.* **2000**, *39*, 3348–3391; c) K. Kinbara, T. Aida, *Chem. Rev.* **2005**, *105*, 1377–1400; d) W. R. Browne, B. L. Feringa, *Nat. Nanotechnol.* **2006**, *1*, 25 –35.

[2] a) A. Bissell, E. Córdova, A. E. Kaifer, J. F. Stoddart, *Nature* **1994**, *369*, 133-137; b) J. D. Badjic, V. Balzani, A. Credi, S. Silvi, J. F. Stoddart, *Science* **2004**, *303*, 1845-1849.

[3] a) J.-P. Collin, C. Dietrich-Buchecker, P. Gavina, M. C. Jimenez-Molero, J.-P. Sauvage, *Acc. Chem. Res.* **2001**, *34*, 477-487; b) M. C. Jimenez, C. Dietrich-Buchecker, J.-P. Sauvage, *Angew. Chem. Int. Ed.* **2000**, *39*, 3284-3287; c) M. C. Jimenez-Molero, C. Dietrich-Buchecker, J.-P. Sauvage, *Chem. Eur. J.* **2002**, *8*, 1456-1466; d) M. C. Jimenez-Molero, C. Dietrich-Buchecker, J.-P. Sauvage, *Chem. Commun.* **2003**, 1613-1616.

[4] G. S. Kottas, L. I. Clarke, D. Horinek, J. Michl, *Chem. Rev.* **2005**, *105*, 1281-1376.

[5] a) N. Koumura, R. W. J. Zijlstra, R. A. van Delden, N. Harada, B. L. Feringa, *Nature* **1999**, *401*, 152-154; b) B. L. Feringa, *Acc. Chem. Res.* **2001**, *34*, 504-513; c) J. Wang, B. L. Feringa, *Science* **2011**, *331*, 1429-1432.

[6] a) D. A. Leigh, J. K. Y. Wong, F. Dehez, F. Zerbetto, *Nature* **2003**, *424*, 174-179; b) J. V. Hernandez, E. R. Kay, D. A. Leigh, *Science* **2004**, *306*, 1532-1537; c) E. R. Kay, D. A. Leigh, F. Zerbetto, *Angew. Chem. Int. Ed.* **2007**, *46*, 72-191.

[7] a) T. R. Kelly, M. C. Bowyer, K. V. Bhaskar, D. Bebbington, A. Garcia, F. Lang, M. H. Kim, M. P. Jette, *J. Am. Chem. Soc.* **1994**, *116*, 3657-3658; b) T. R. Kelly, I. Tellitu, J. P. Sestelo, *Angew. Chem. Int. Ed. Engl.* **1997**, *36*, 1866-1868; c) A. P. Davis, *Angew. Chem. Int. Ed.* **1998**, *37*, 909-910; d) T. R. Kelly, H. De Silva, R. A. Silva, *Nature* **1999**, *401*, 150-152; e) T. R. Kelly, R. A. Silva, H. De Silva, S. Jasmin, Y. Zhao, *J. Am. Chem. Soc.* **2000**, *122*, 6935-6949; f) C. Manzano, W.-H. Soe, H. S. Wong, F. Ample, A. Gourdon, N. Chandrasekhar, C. Joachim, *Nat. Mater.* **2009**, *8*, 576-579; g) S. Pekker, E. Kovats, G. Oszlanyi, G. Benyei, G. Klupp, G. Bortel, I. Jalsovszky, E. Jakab, F. Borondics, K. Kamaras, M. Bokor, G. Kriza, K. Tompa, G. Faigel, *Nat. Mater.* **2005**, *4*, 764-767.

[8] a) T. Muraoka, K. Kinbara, Y. Kobayashi, T. Aida, *J. Am. Chem. Soc.* **2003**, *125*, 5612-5613; b) T.

Muraoka, K. Kinbara, T. Aida, *Nature* **2006**, *440*, 512–515.

[9] a) I. Rayment, W. R. Rypniewski, K. Schmidt-Baese, R. Smith, D. R. Tomchick, M. M. Benning, D. A. Winkelmann, G. Wesenberg, H. M. Holden, *Science* **1993**, *261*, 50-58; b) I. Rayment, H. M. Holden, M. Whittaker, C. B. Yohn, M. Lorenz, K. C. Holmese, R. A. Milligan, *Science* **1993**, *261*, 58-65.

[10] a) D. Stock, A. G. W. Leslie, J. E. Walker, *Science* **1999**, *286*, 1700-1705; b) R. I. Menz, J. E. Walker, A. G. W. Leslie, *Cell* **2001**, *106*, 331-341.

[11] a) P. Bodis, M. R. Panman, B. H. Bakker, A. Mateo-Alonso, M. Prato, W. J. Buma, A. M. Brouwer, E. R. Kay, D. A. Leigh, S. Woutersen, *Acc. Chem. Res.* **2009**, *42*, 1462-1469; b) S. Bonnet, J.-P. Collin, *Chem. Soc. Rev.* **2008**, 37, 1207-1217; c) S. Saha, J. F. Stoddart, *Chem. Soc. Rev.* **2007**, *36*, 77-92.

[12] a) K.-W. Cheng, C.-C. Lai, P.-T. Chiang, S.-H. Chiu, *Chem. Commun.* **2006**, 2854-2856; b) T. Ooya, D. Inoue, H. S. Choi, Y. Kobayashi, S. Loethen, D. H. Thompson, Y. H. Ko, K. Kim, N. Yui, *Org. Lett.* **2006**, *8*, 3159-3162; c) C.-K. Koo, B. Lam, S.-K. Leung, M. H.-W. Lam, W.-Y. Wong, *J. Am. Chem. Soc.* **2006**, *128*, 16434-16435.

[13] S. Saha, A. H. Flood, J. F. Stoddart, S. Impellizzeri, S. Silvi, M. Venturi, A. Credi, *J. Am. Chem. Soc.* **2007**, *129*, 12159-12171.

[14] a) C. P. Collier, G. Mattersteig, E. W. Wong, Y. Luo, K. Beverly, J. Sampaio, F. M. Raymo, J. F. Stoddart, J. R. Heath, *Science* **2000**, *289*, 1172-1175; b) C. P. Collier, J. O. Jeppesen, Y. Luo, J. Perkins, E. W. Wong, J. R. Heath, J. F. Stoddart, *J. Am. Chem. Soc.* **2001**, *123*, 12632-12641; c) V. Balzani, M. Clemente-León, A. Credi, B. Ferrer, M. Venturi, A. H. Flood, J. F. Stoddart, *Proc. Natl. Acad. Sci. U.S.A.* **2006**, *103*, 1178-1183.

[15] a) S. Silvi, A. Arduini, A. Pochini, A. Secchi, M. Tomasulo, F. M. Raymo, M. Baroncini, A. Credi, *J. Am. Chem. Soc.* **2007**, *129*, 13378–13379; b) H. Wu, D. Zhang, L. Su, K. Ohkubo, C. Zhang, S. Yin, L. Mao, Z. Shuai, S. Fukuzumi, D. Zhu, *J. Am. Chem. Soc.* **2007**, *129*, 6839-6846; c) V. Serreli, C.-F. Lee, E. R. Kay, D. A. Leigh, *Nature* **2007**, *445*, 523-527.

[16] a) P. Thordarson, E. J. A. Bijsterveld, A. E. Rowan, R. J. M. Nolte, *Nature* **2003**, *424*, 915-918; b) C. Monnereau, P. Hidalgo Ramos, A. B. C. Deutman, J. A. A. W. Elemans, R. J. M. Nolte, A. E. Rowan, *J. Am. Chem. Soc.* **2010**, *132*, 1529–1531; c) M. von Delius, E. M. Geertsema, D. A. Leigh, D.-T. D. Tang, *J. Am. Chem. Soc.* **2010**, *132*, 16134–16145.

[17] a) S. Shinkai, T. Nakaji, Y. Nishida, T. Ogawa, O. Manabe, *J. Am. Chem. Soc.* **1980**, *102*, 5860-5865; b) S. Shinkai, T. Nakaji, T. Ogawa, K. Shigematsu, O. Manabe, *J. Am. Chem. Soc.* **1981**, *103*, 111-115.

[18] a) K. Ichimura, S.-K. Oh, M. Nakagawa, *Science* **2000**, *288*, 1624-1626; b) Y. Yu, M. Nakano, T. Ikeda, *Nature* **2003**, *425*, 145.

[19] a) M. V. Peters, R. Goddard, S. Hecht, *J. Org. Chem.* **2006**, *71*, 7846–7849; b) M. V. Peters, R. S. Stoll, A. Kühn, S. Hecht, *Angew. Chem. Int. Ed.* **2008**, *47,* 5968–5972; c) R. S. Stoll, M. V. Peters, A. Kuhn, S. Heiles, R. Goddard, M. Bühl, C. M. Thiele, S. Hecht, *J. Am. Chem. Soc.* **2009**, *131*, 357-367.

[20] a) D. Ishii, K. Kinbara, Y. Ishida, N. Ishii, M. Okochi, M. Yohda, T. Aida, *Nature* **2003**, *423*, 628–632; b) A. Bernardos, E. Aznar, M. D. Marcos, R. Martínez-Máñez, F. Sancenón, J. Soto, J. M. Barat, P. Amorós, *Angew. Chem. Int. Ed.* **2009**, *48*, 5884-5887.

[21] L. Fabbrizzi, M. Licchelli, P. Pallavicini, L. Parodi, *Angew. Chem. Int. Ed.* **1998**, *37*, 800-802.

[22] a) C. Lodeiro, A. J. Parola, F. Pina, C. Bazzicalupi, A. Bencini, A. Bianchi, C. Giorgi, A. Masotti, B. Valtancoli, *Inorg. Chem.* **2001**, *40*, 2968-2975; b) P. Pallavicini, G. Dacarro, C. Mangano, S. Patroni, A. Taglietti, R. Zanoni, *Eur. J. Inorg. Chem.* **2006**, 4649–4657.

[23] a) L. Zelikovich, J. Libman, A. Shanzer, *Nature* **1995**, *374*, 790-792; b) L. Fabbrizzi, F. Gatti, P. Pallavicini, E. Zambarbieri, *Chem. Eur. J.* **1999**, *5*, 682-690.

[24] a) B. Durham, V. J. Caspar, J. K. Nagle, T. J. Meyer, *J. Am. Chem. Soc.* **1982**, *104*, 4803-4810; b) B. Durham, S. R. Wilson, D. J. Hodgson, T. J. Meyer, *J. Am. Chem. Soc.* **1980**, *102*, 600-607; c) S. Bonnet, J.-P. Collin, J.-P. Sauvage, E. Schofield, *Inorg. Chem.* **2004**, *43*, 8346**-**8354.

[25] S. Venkataramani, U. Jana, M. Dommaschk, F. D. Sönnichsen, F. Tuczek, R. Herges, *Science* **2011**, *331*, 445-448.

[26] a) T. Kojima, T. Sakamoto, Y. Matsuda, *Inorg. Chem.* **2004**, *43*, 2243-2245; b) T. Kojima, T. Morimoto, T. Sakamoto, S. Miyazaki, S. Fukuzumi, *Chem. Eur. J.* **2008**, *14*, 8904-8915.

[27] S. Miyazaki, T. Kojima, S. Fukuzumi, *J. Am. Chem. Soc.* **2008**, *130*, 1556-1557.

[28] a) R. Knapp, A. Schott, M. Rehahn, *Macromolecules* **1996**, *29*, 478-480; b) J. Bolger, A. Gourdon, E. Ishow, J.-P. Launay, *Inorg. Chem.* **1996**, *35*, 2937-2944; c) G. Pourtois, D. Beljonne, C. Moucheron, S. Schumm, A. Kirsch-De Mesmaeker, R. Lazzaroni, J.-L. Bredas, *J. Am. Chem. Soc.* **2004**, *126*, 683-692.

[29] S. Rau, B. Schäfer, D. Gleich, E. Anders, M. Rudolph, M. Friedrich, H. Görls, W. Henry, J. G. Vos, *Angew. Chem. Int. Ed.* **2006**, *45*, 6215-6218.

[30] M. Yamada, Y. Tanaka, Y. Yoshimoto, S. Kuroda, I. Shimao, *Bull. Chem. Soc. Jpn.* **1992**, *65*, 1006-1011.

[31] S. Bodige, F. M. MacDonnell, *Tetrahedron Lett.* **1997**, *38*, 8159-8160.

[32] B. P. Sullivan, D. J. Salmon, T. J. Meyer, *Inorg. Chem.* **1978**, *17*, 3334-3341.

[33] T. Ishizuka, T. Sawaki, S. Miyazaki, M. Kawano, Y. Shiota, K. Yoshizawa, S. Fukuzumi, T. Kojima, *Chem. Eur. J.* **2011**, *17*, 6652-6662.

[34] a) S. Tschierlei, M. Presselt, C. Kuhnt, A. Yartsev, T. Pascher, V. Sundstroem, M. Karnahl, M. Schwalbe, B. Schaefer, S. Rau, M. Schmitt, B. Dietzek, J. Popp *Chem. Eur. J.* **2009**, *15*, 7678-7688; b) S. Tschierlei, M. Karnahl, M. Presselt, B. Dietzek, J. Guthmuller, L. Gonzalez, M. Schmitt, S. Rau, J. Popp, *Angew. Chem. Int. Ed.* **2010**, *49*, 3981-3984.

[35] T. Kojima, T. Amano, Y. Ishii, M. Ohba, Y. Okaue, Y. Matsuda, *Inorg. Chem.* **1998**, *37*, 4076-4085.

[36] a) S. Miyazaki, K. Ohkubo, T. Kojima, S. Fukuzumi, *Angew. Chem. Int. Ed.* **2007**, *46*, 905-908; b) T. Kojima, T. Sakamoto, Y. Matsuda, K. Ohkubo, S. Fukuzumi, *Angew. Chem. Int. Ed.* **2003**, *42*, 4951-4954; c) S. Miyazaki, T. Kojima, T. Sakamoto, T. Matsumoto, K. Ohkubo, S. Fukuzumi, *Inorg. Chem.* **2008**, *47*, 333-343.

[37] C. Chiorboli, M. A. J. Rodgers, F. Scandola, *J. Am. Chem. Soc.* **2003**, *125*, 483-491.

[38] H. Eyring, *J. Chem. Phys.* **1935**, *3*, 107-115.

[39] a) T. Kojima, S. Miyazaki, K. Hayashi, Y. Shimazaki, F. Tani, Y. Naruta, Y. Matsuda, *Chem. Eur. J.* **2004**, *10*, 6402-6410; b) O. Johansson, L. O. Johannissen, R. Lomoth, *Chem. Eur. J.* **2009**, *15*,

1195-1204.

[40] a) L. J. Heidt, G. W. Tregay, F. A. Middleton, Jr. *J. Phys. Chem.* **1970**, *74*, 1876-1882; b) C. H. Langford, C. A. Houlubor, *Inorg. Chim. Acta* **1981**, *53*, L59-L60.

[41] A. Juris, V. Balzani, F. Barigelletti, S. Campagna, P. Beler, A. von Zelewsky, *Coord. Chem. Rev.* **1988**, *84*, 85-277.

[42] a) F. D'Souza, M. E. Zandler, G. R. Deviprasad, W. Kutner, *J. Phys. Chem. A* **2000**, *104*, 6887-6893; b) Q.-Y. Zhu, Y. Liu, W. Lu, Y. Zhang, G.-Q. Bian, G.-Y. Niu, J. Dai, *Inorg. Chem.* **2007**, *46*, 10065-10070.

[43] In general, CH_3CN is a weaker ligand than pyridine in the spectrochemical series to afford a smaller ligand field splitting, and thus a more stable $^3MC^*$ state can be formed for the CH_3CN complex. See: P. Atkins, T. Overton, J. Rourke, M. Weller, F. Armstrong, *Inorganic Chemistry,* 5th ed., Oxford University Press, Oxford, **2010**, pp. 475.

[44] a) A. Jana, K. S. P. Devi, T. K. Maiti, N. D. P. Singh, *J. Am. Chem. Soc.* **2012**, *134*, 7656–7659; b) J. L. Vivero-Escoto, I. I. Slowing, C.-W. Wu, V. S.-Y. Lin, *J. Am. Chem. Soc.* **2009**, *131*, 3462-3463.

[45] T. Kojima, K. Nakayama, K. Ikemura, T. Ogura, S. Fukuzumi, *J. Am. Chem. Soc.* **2011**, *133*, 11692–11700.

[46] a) H. Sugimoto, T. Kimura, S. Inoue, *J. Am. Chem. Soc.* **1999**, *121*, 2325–2326; b) R. Cacciapaglia, S. Di Stefano, L. Mandolini, *J. Am. Chem. Soc.* **2003**, *125*, 2224–2227; c) D. Sud, T. B. Norsten, N. R. Branda, *Angew. Chem. Int. Ed.* **2005**, *44*, 2019-2021.

[47] G. Gauglitz, In *Photochromism Molecule and Systems* Revised Edition (Eds.: H. Dürr, H. Bouas-Laurent), Elsevier, Amsterdam, **2003**, pp. 30.

[48] a) K. Wakita, Yadokari-XG, Software for Crystal Structure Analyses, **2001**; b) C. Kabuto, S. Akine, T. Nemoto, E. Kwon, Release of Software (Yadokari-XG 2009) for Crystal Structure Analyses. *J. Cryst. Soc. Jpn.* **2009**, *51*, 218.

[49] a) A. D. Becke, *Phys. Rev. A* **1988**, *38*, 3098-3100; b) C. Lee, W. Yang, R. G. Parr, *Phys. Rev. B* **1988**, *37*, 785-789; c) A. D. Becke, *J. Chem. Phys.* **1993**, *98*, 5648-5652.

[50] D. Andrae, U. Haeussermann, M. Dolg, H. Stoll, H. Preuss, *Theor. Chem. Acc.*, **1990**, *77* 123-141.

[51] T. H. Dunning, P. J. Hay, In *Modern Theoretical Chemistry*, Vol. 3, (Ed.: H. F. Schaefer III, Plenum, New York, **1976**, pp 1-27.

[52] Gaussian 09, Revision B.01, M. J. Frisch, G. W. Trucks, H. B. Schlegel, G. E. Scuseria, M. A. Robb, J. R. Cheeseman, G. Scalmani, V. Barone, B. Mennucci, G. A. Petersson, H. Nakatsuji, M. Caricato, X. Li, H. P. Hratchian, A. F. Izmaylov, J. Bloino, G. Zheng, J. L. Sonnenberg, M. Hada, M. Ehara, K. Toyota, R. Fukuda, J. Hasegawa, M. Ishida, T. Nakajima, Y. Honda, O. Kitao, H. Nakai, T. Vreven, J. A. Montgomery, Jr., J. E. Peralta, F. Ogliaro, M. Bearpark, J. J. Heyd, E. Brothers, K. N. Kudin, V. N. Staroverov, R. Kobayashi, J. Normand, K. Raghavachari, A. Rendell, J. C. Burant, S. S. Iyengar, J. Tomasi, M. Cossi, N. Rega, J. M. Millam, M. Klene, J. E. Knox, J. B. Cross, V. Bakken, C. Adamo, J. Jaramillo, R. Gomperts, R. E. Stratmann, O. Yazyev, A. J. Austin, R. Cammi, C. Pomelli, J. W. Ochterski, R. L. Martin, K. Morokuma, V. G. Zakrzewski, G. A. Voth, P. Salvador, J. J. Dannenberg, S.

Dapprich, A. D. Daniels, Ö. Farkas, J. B. Foresman, J. V. Ortiz, J. Cioslowski, D. J. Fox, Gaussian, Inc., Wallingford CT, **2009**.

Chapter 4
Photocatalytic and photoelectrocatalytic hydrogen evolution using a ruthenium(II)-tpphz complex

4-1. Introduction

Dihydrogen is one of plausible candidates of clean energy sources to replace fossil fuels;[1, 2] however, present productions of dihydrogen mainly require a great amount of thermal energy. In the case of steam-methane reforming, which is the most general method to produce dihydrogen at present, the process proceeds at 700 – 800 ºC in the presence of a Ni or Ru catalyst and releases a large amount of carbon dioxide.[2e] Thus, production of dihydrogen from abundant sources such as water with use of clean and sustainable energy including sunlight is inevitably required for future sustainable society.[3-8]

Along this line, photocatalytic water splitting has been intensively investigated with use of heterogeneous catalysts such as semiconducting materials;[9] for example, Fujishima and Honda have reported electrochemical photolysis of water, so-called 'Honda-Fujishima effect', in which a semiconductor electrode (TiO_2) loaded with a continuous voltage is photoirradiated to evolve dioxygen and dihydrogen molecules from the surface as a result of water-splitting.[9a] When a noble metal such as Pt, Pd, or Rh is deposited on semiconductor particles consisting of TiO_2, white light irradiation to the semiconducting particles allows us to observe photocatalytic hydrogen evolution based on water-splitting, in which the semiconductor particles and the metal loaded on their surface play roles of a photocatalyst and a promoter, respectively.[9b]

For the first example of homogeneous photocatalytic hydrogen-evolution systems, Sutin and coworkers have employed a Co^{II} complex having a macrocyclic ligand as a catalyst and $[Ru(bpy)_3]^{2+}$ ion as a photosensitizer to reduce protons of water molecules in the presence of ascorbate ion.[6a] Later, Castellano and coworkers have improved the turnover number (TON) of the catalysis up to 35 with use of a Co^{II}-dimethylglyoximate complex as a catalyst in the presence of Cu^{I} complex as a photosensitizer and dimethyl-*p*-toluidine as an electron donor.[6e] Additionally, a molecular catalyst for hydrogen evolution, in which a Pd^{II} complex moiety as a catalyst and a Ru^{II} complex moiety as a photosensitizer are covalently linked, has been also reported to show a relatively high TON, 150 (Figure 4-1).[8a] Including these examples

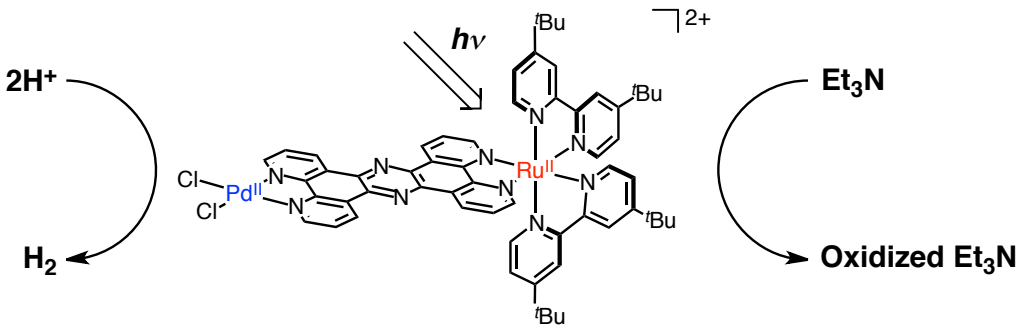

Figure 4-1. Photocatalytic hydrogen evolution using Ru^{II}–Pd^{II} dyad complex.

Fe^{II} complex in THF has been recently reported, in which the 1,2-phenylenediamine ligands of the complex mentioned above, molecular catalysts for hydrogen evolution reported so far include a metal center as an active site of the hydrogen evolution. On the other hand, photochemical hydrogen production with use of an has been reported to act as a hydrogen evolution site.[10]

Herein, the author describes photocatalytic hydrogen evolution catalyzed by a Ru^{II}-complex (**7** or **8**) having a π-expanded heteroaromatic diimine ligand with use of a sacrificial reductant such as triethylamine. Scrutiny into the hydrogen production process revealed that the reaction involves an intermediate having a 2H-reduced π-expanded heteroaromatic diimine ligand, and thus, the Ru moiety is not the catalytic site but just a photosensitizer and the π-expanded heteroaromatic diimine ligand plays a principal role in the hydrogen evolution as the active site.

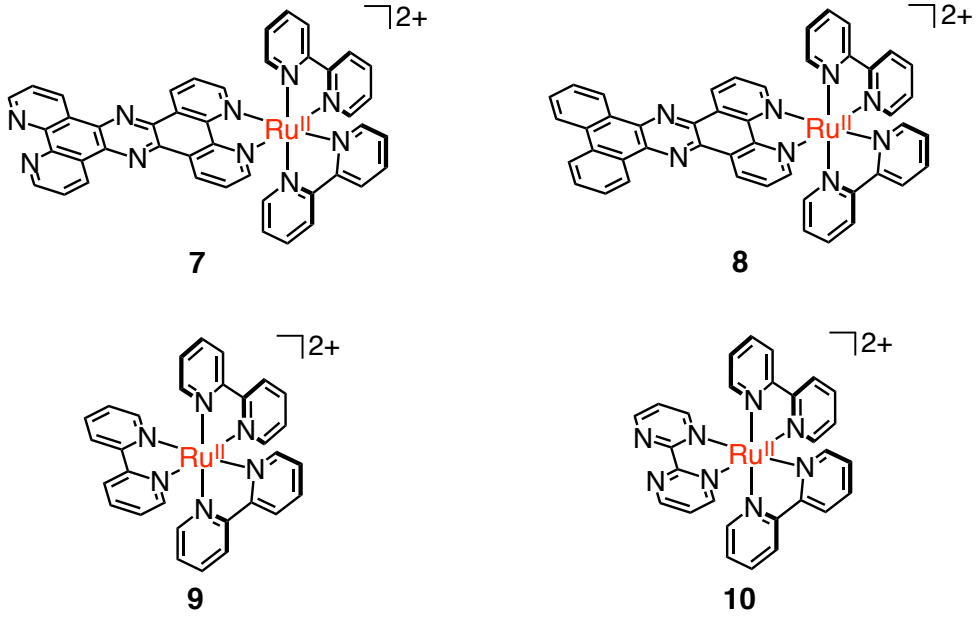

Chart 4-1. Molecular structures of ruthenium(II)-polypyridine complexes **7**, **8**, **9** and **10**.

4-2. Results and discussion

4-2-1. Electrochemical measurements and phosphorescence quenching of 7

The Ru^{II} complex, **7**,[11] employed as a catalyst in this work, has two 2,2'-bipyridine (bpy) molecules and one tetrapyridophenazine (tpphz) molecule as ligands (Chart 4-1). As a counter anion of the complex, perchlorate was chosen due to the reasonable solubility into aqueous media. In the cyclic and differential-pulse voltammograms (CV and DPV, respectively) of **7**·$(ClO_4)_2$ in CH_3CN including 0.1 M tetrabutylammonium hexafluorophosphate ($(n\text{-}Bu)_4NPF_6$) as an electrolyte, reduction waves were observed at –0.98 and –1.12 V vs SCE (Figure 4-2), the former of which was assigned to the reduction of the tpphz ligand and the latter was to that of a bpy ligand.[11]

To explore the photochemical properties of **7**, the reductive quenching behaviors of the triplet excited state of **7** (^{3}**7***)[12] were investigated with use of various chemical reductants. The emission spectrum of **7**·$(ClO_4)_2$ with the excitation wavelength at 424 nm in a water : CH_3OH = 1 : 1 mixed solvent, in the

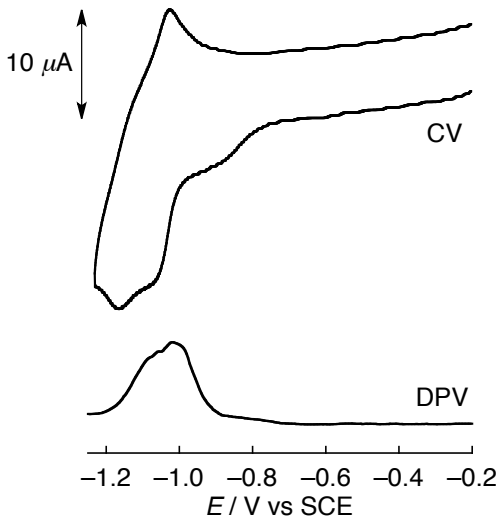

Figure 4-2. CV and DPV of **7**·$(ClO_4)_2$ (1 mM) in MeCN including $(n\text{-Bu})_4NPF_6$ (0.1 M) at room temperature.

of reductants, exhibited phosphorescence centered at 634 nm at room temperature (Figure 4-3; black line). Upon addition of Et_3N (1.8 M) as a chemical reductant, the phosphorescence was quenched by 76% (Figure 4-3; red line); hence, ^{3}**7*** can be efficiently quenched by Et_3N. For seeking a better sacrificial reductant, phosphorescence quenching efficiencies were determined with use of other reductants (Table 4-1). Among the reductants examined in this work, L-ascorbic acid (As) and oxalic acid (Ox) exhibited comparable quenching efficiencies to that with Et_3N; 89% for As and 61% for Ox, and *N*-ethylmorpholine (EtMor) performed quenching with lower efficiency of 12%. Ferrocene (Fc) as a reductant also showed degradation of the phosphorescence of **7**. However, interference on light absorption of **7** by the absorption of Fc was very severe in the visible region (ε = 82 for Fc at λ_{max} = 440 nm), because a large excess amount of Fc, 1000 equiv against **7**·$(ClO_4)_2$, was used in the experiment, and thus, the incident light should be exclusively absorbed

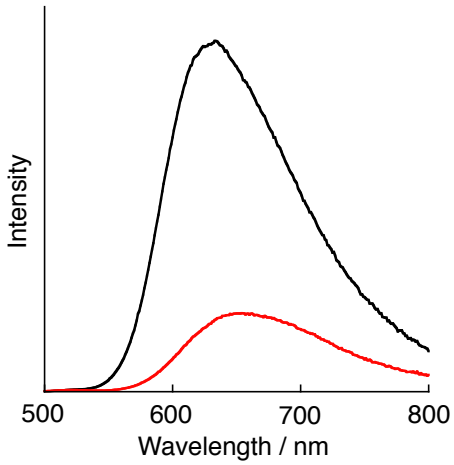

Figure 4-3. Phosphorescence spectra of **7**·$(ClO_4)_2$ (25 mM, λ_{ex} = 424 nm) in water : MeOH = 1 : 1 (black line) and in water : MeOH : Et_3N = 3 : 3 : 2 mixed solvents (red line).

with Fc. Therefore, the quenching efficiencies could not be estimated correctly. The quenching efficiencies of Et_3N, As, Ox and EtMor can be accounted by relation between the oxidation potentials (E_{ox}) of the reductants and the reduction potential (E_{red}) of ^{3}**7***; the calculated E_{red} of ^{3}**7*** is +1.06 V vs SCE, and thus, ^{3}**7*** can be quenched by Et_3N (E_{ox} = +0.80 V vs SCE), As (+0.15), Ox (+0.98) and EtM (> +1.0), judging from the E_{ox} values obtained from DPV measurements (Figure 4-4). Additionally, as E_{ox} of the reductant lowers, the quenching efficiency becomes higher, due to the increase of driving force of electron transfer from the reductants to ^{3}**7***.

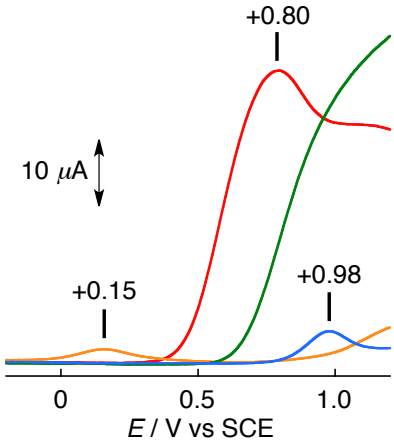

Figure 4-4. DPVs of triethylamine (11 mM, red), L-ascorbic acid (1 mM, orange), oxalic acid (1 mM, blue line) and *N*-ethylmorpholine (11 mM, green line) in MeOH : phosphate buffer (pH 7.0) = 1 : 1 mixed solvent.

Table 4-1. Summary of the properties of the electron donors employed in this work: the first oxidation potentials (E_{ox}) of electron donors, quenching efficiencies (*Eff*) for phosphorescence of **7**·$(ClO_4)_2$, the amount of hydrogen evolution catalyzed by **7**·$(ClO_4)_2$ with an electron donor under photoirradiation (380 – 670 nm), and the initial rates (v_{H2}) of the photocatalytic hydrogen evolution under photoirradiation (380 – 670 nm)[a]

Entry	Electron Donor	E_{ox} [V vs SCE]	*Eff*	H_2 evolution [μmol][b]	v_{H2} [nmol h^{-1}]
1	Et_3N	+0.80[c]	76%[e]	0.083	8.2[e]
2	*N*-ethylmorpholine	> 1[c]	12%[e]	0.015	1.5[e]
3	Oxalic Acid	+0.98[c]	61%[f]	0.015	1.5[f]
4	L-Ascorbic Acid	+0.15[c]	89%[g]	0.003	0.25[g]
5	Ferrocene	+0.05[d]	——	0.029	0.3[h]

[a] [**7**·$(ClO_4)_2$] = 25 μM for all measurements. [b] The amount of H_2 evolved for initial 10 h. [c] In CH_3OH/phosphate buffer (1 : 1 v/v, pH 7.0). [d] In CH_3OH/water (4 : 1 v/v) with 0.1 M tetramethylammonium chloride as an electrolyte. [e] In CH_3OH/H_2O/electron donor (3 : 3 : 2 v/v, 4 mL): the concentration of the electron donor in the solution is 1.8 M. [f] In CH_3OH/phosphate buffer (1 : 1 v/v, 4 mL, pH 6.0) with an electron donor (1.1 M). [g] In CH_3OH/phosphate buffer (1 : 1 v/v, 4 mL, pH 7.0) with an electron donor (0.025 M). [h] In CH_3OH/water (4 : 1 v/v, 4 mL) with an electron donor (0.025 M).

4-2-2. Photocatalytic hydrogen evolution with **7**·$(ClO_4)_2$ as a catalyst

Photoirradiation of white light (380 – 670 nm) to the solution of **7**·$(ClO_4)_2$ (25 μM) in a mixed solvent of water : CH_3OH = 1 : 1 (3 mL), including Et_3N (1.8 M) as a sacrificial reductant, was performed for 6 h at room temperature. As a result, evolution of 0.08 μmol of dihydrogen was observed with gas chromatography (GC) and the TON based on the catalyst was determined to be 1. Similar photocatalystic hydrogen evolution was also performed with the other reductants employed for the reductive quenching experiments in Section 4-2-1; however, the amount of hydrogen evolution was not related to the quenching efficiencies and using Et_3N as the reductant afforded the highest rate of hydrogen evolution among them (Table 4-1). The low efficiency for As as a reductant is probably due to the back electron transfer, because the redox process of As is exceptionally reversible among the reductants used in this study.[13]

Dilution of the catalyst to 2.5 μM and further elongation of the reaction time to 380 h, 1.6 μmol of dihydrogen evolved was detected and then the TON was improved to 160. The highest TON was obtained with use of triethanolamine as a reductant, and the TON of the hydrogen evolution was determined to be 620 for 380 h.

4-2-3. Photoelectrocatalytic hydrogen evolutions with **7**·$(ClO_4)_2$

To improve an efficiency of the hydrogen evolution, a photoelectrocatalytic reaction[14] was performed, using electrolysis as electron sources for the reduction of the tpphz ligand. At first, a change of the electric current by irradiation of white light (380 – 670 nm) was observed in CH_3OH : borate buffer (pH 9.5) = 1 : 1 with a continuous voltage at –1.4 V vs Ag/AgCl loaded on the working electrode (Figure 4-5). The current clearly increased upon photoirradiation, which indicates that a catalytic reaction can proceed in the presence of **7**·$(ClO_4)_2$ under photoirradiation accompanying with electrolysis. When photoirradiation of a white light (380 – 670 nm) was performed for 3 h on the glassy-carbon working electrode surface, on which a

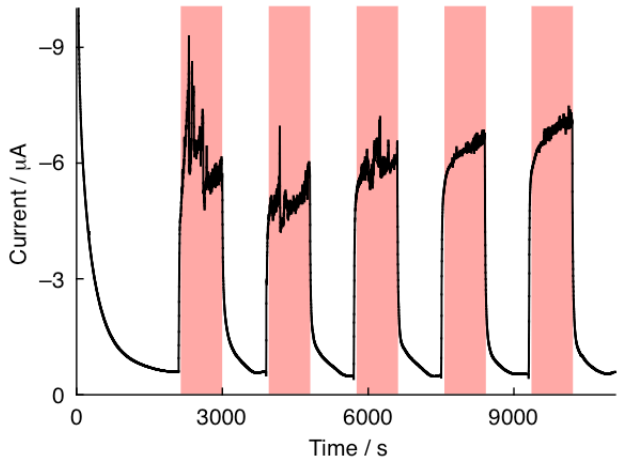

Figure 4-5. Electric currents with (white) and without (red) photoirradiation of white light (380 – 670 nm) to the solution of **7**·$(ClO_4)_2$ (300 μM) in CH_3OH : borate buffer (pH 9.5) = 1 : 1, applying a continuous voltage at –1.4 V vs Ag/AgCl on the working electrode. Working electrode: glassy carbon, counter electrode: Pt wire, reference electrode: Ag/AgCl.

continuous voltage was loaded at –1.40 V vs Ag/AgCl in the solution of **7**·$(ClO_4)_2$ (300 μM) in CH_3OH : borate buffer (pH 9.5) = 1 : 1 mixed solvent (5 mL) containing no chemical electron donors, 76 μmol of hydrogen was evolved and the TON based on the catalyst was determined to be 51. In contrast, only the electrolysis at the same applied voltage in the dark did not exhibit any hydrogen evolution. Additionally, only the photoirradiation without electrolysis did not afford any signs of hydrogen evolution. Therefore, both light irradiation and electrolysis are necessary for the hydrogen evolution by **7**·$(ClO_4)_2$.

4-2-4. Catalytically active site in 7 for the hydrogen evolution

The coordination sites of the Ru^{II} center in **7** are fully occupied with substitution-inert diimine ligands, and thus, the Ru^{II} center cannot be the active site for the hydrogen production. Therefore, to investigate the active site in **7**, the catalytic activity of four Ru^{II} complexes was explored, having similar structures to that of **7**; complex **8**[15] with a π-expanded diimine ligand, in which the two nitrogen atoms at the *h*- and *j*-pyridine rings of the tpphz ligand are replaced by C-Hs (Chart 4-1), $[Ru^{II}(bpy)_3]^{2+}$ (**9**), and $[Ru^{II}(bpy)_2(bpm)]^{2+}$ (**10**, bpm = 2,2'-bipyrimidyl) were also examined as catalysts for hydrogen evolution under the same conditions. In consequence, complex **8**·$(ClO_4)_2$ performed catalytic hydrogen evolution with showing a comparable or slightly better efficiency to that of **7**·$(ClO_4)_2$, whereas with use of complexes **9**·$(ClO_4)_2$ and **10**·$(ClO_4)_2$, no hydrogen evolution was observed (Figure 4-6). Therefore, the active site of the catalytic hydrogen evolution for **7** is presumed to be not the Ru^{II} center, not the terminal vacant diimine moiety, but the pyrazine moiety at the center of the tppz ligand in **7**.

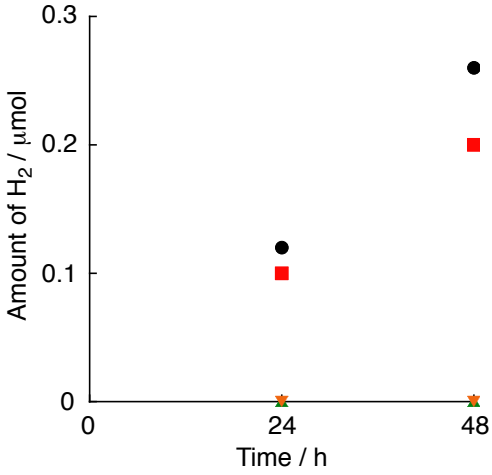

Figure 4-6. Amount of dihydrogen evolved by photocatalytic reaction (λ_{irr} = 380 – 670 nm) using **7**·$(ClO_4)_2$ (red filled square), **8**·$(ClO_4)_2$ (black filled circle), **9**·$(ClO_4)_2$ (orange triangle) and **10**·$(ClO_4)_2$ (green inverted-triangle). The concentration of the catalyst in the solution was set as 25 μM in water : MeOH : Et_3N = 1 : 1 : 1 mixed solvent.

4-2-5. Characterization of the reaction intermediate for the hydrogen evolution with 7

To explore the reaction mechanism of the catalytic hydrogen evolution, UV-Vis and ^1H NMR spectroscopies were applied to monitor the reaction of **7** under photoirradiation of white light (380 – 670 nm)

in the presence of Et_3N. Complex **7**·$(ClO_4)_2$ exhibits an MLCT absorption band at 450 nm and a π-π* transition band of the tpphz moiety around 380 nm in the water : CH_3OH = 1 : 1 mixed solvent (the light blue trace in Figure 4-7). Under photoirradiation with the white light to the solution of **7**·$(ClO_4)_2$ in the

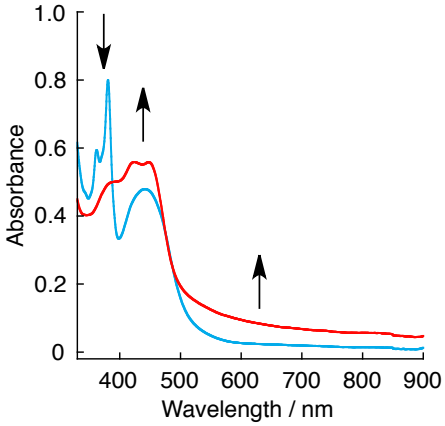

Figure 4-7. UV-Vis spectral change under photoirradiation (380 – 670 nm) to the solution of **7**·$(ClO_4)_2$ in water : CH_3OH : Et_3N = 1 : 1 : 1 mixed solvent at room temperature: before photoirradiation (light blue trace) and after 10 min irradiation (red trace).

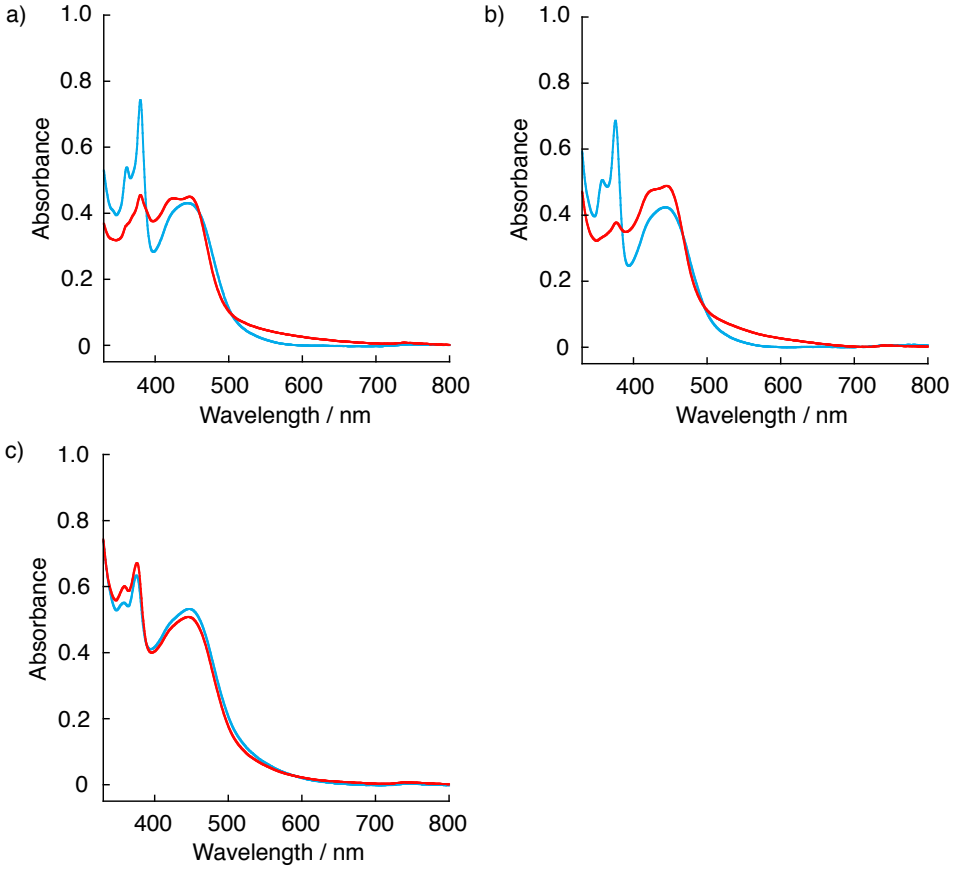

Figure 4-8. UV-vis spectral changes at room temperature upon photoirradiation (380 – 670 nm) for 30 min to the solution of **7**·$(ClO_4)_2$ (25 μM) in water : MeOH = 1 : 1 mixed solvent, containing a reductant: (a) *N*-ethylmorpholine (1.8 M), (b) oxalic acid (1.1 M), and (c) L-ascorbic acid (0.025 M).

presence of Et_3N (1.8 M), the π-π* transition band, observed around 380 nm gradually decreased and the MLCT band gradually increased, concomitant with the appearance of a broad absorption band in the range of 500 – 800 nm (the red trace in Figure 4-7), which could be assigned to that due to decomposed products derived from $1e^-$-oxidized Et_3N.[16] The change was completed within 10 min, and the quantum yield of the change was determined to be 30% by a typical actinometer method.[17] Similar spectral changes were observed with use of other reductants (Figure 4-8). In addition, a similar spectral change was observed in the case of the electrolytic reduction at –1.4 V vs SCE in the presence of tetramethylammonium chloride (Me_4NCl) as an electrolyte in a CH_3OH : borate buffer (pH 9.5) = 1 : 1 mixed solvent (Figure 4-9). The disappearance of the π-π* transition band of the tpphz moiety indicates decrease of the π-conjugation circuit expanding to the whole tpphz moiety.

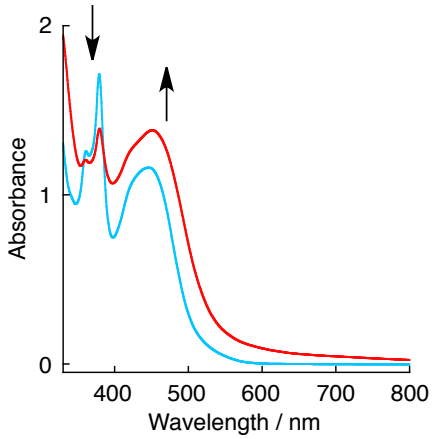

Figure 4-9. UV-Vis spectral change of **7**·$(ClO_4)_2$ (300 μM) in the presence of Me_4NCl (0.1 M) as an electrolyte in CH_3OH : borate buffer (pH 9.5) = 1 : 1 mixed solvent, applying a continuous voltage at –1.4 V vs Ag/AgCl at room temperature under dark and Ar atmosphere: before electrolysis (light blue trace) and after 6 h electrolysis (red trace). The UV-vis measurements were preformed in a quartz cell with 2 mm path length. Working electrode: glassy carbon, counter electrode: Pt wire, reference electrode: Ag/AgCl.

When photoirradiation with white light (380 – 670 nm) was performed to the solution of **7**·$(ClO_4)_2$ (0.3 mM) and Et_3N (71 mM) in D_2O : CD_3OD = 1 : 1 mixed solvent, the ^1H NMR signals of the tpphz ligand in **7** showed downfield shifts, whereas those of the bpy ligands were almost intact (Figure 4-10). The ^1H NMR spectral change suggests that the photoproduct (**11**) derived from **7** should have a 2H-reduced tpphz ligand at the central pyrazine moiety (Scheme 4-1) to cause the decrease of the *π*-conjugation circuit. In addition, complex **8** also afforded a reduced intermediate (**12**), similar to **11**, under photoirradiation in the presence of Et_3N (Figure 4-11).

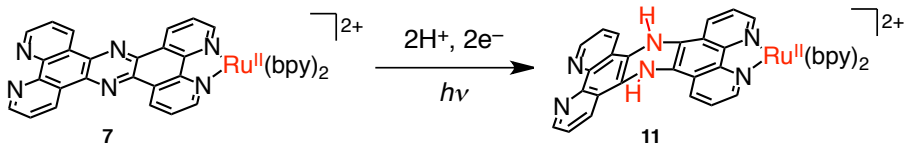

Scheme 4-1. Photochemical reduction of **7** to form **11**.

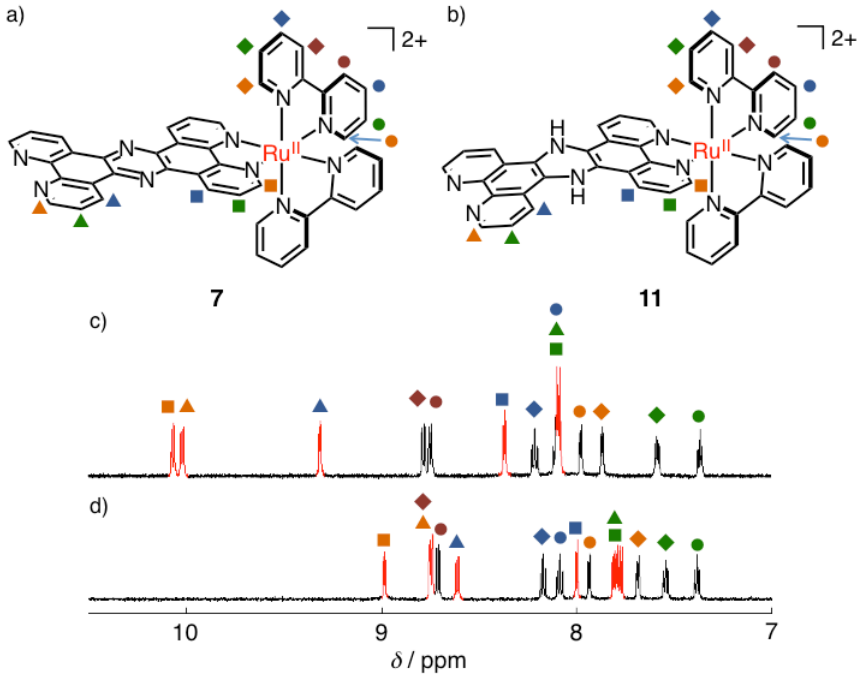

Figure 4-10. Molecular structures of (a) **7** and (b) **11**. ^{1}H NMR spectra of **7**·$(ClO_4)_2$ in D_2O : CD_3OD = 1 : 1 mixed solvent in the presence of Et_3N (71 mM) (c) and after photoirradiation with white light (380 – 670 nm) for 30 min at room temperature (d). The red signals indicate those derived from the hydrogen atoms of the tpphz moiety, and the symbols indicate the positions of protons in the structures of **7** and **11** shown above.

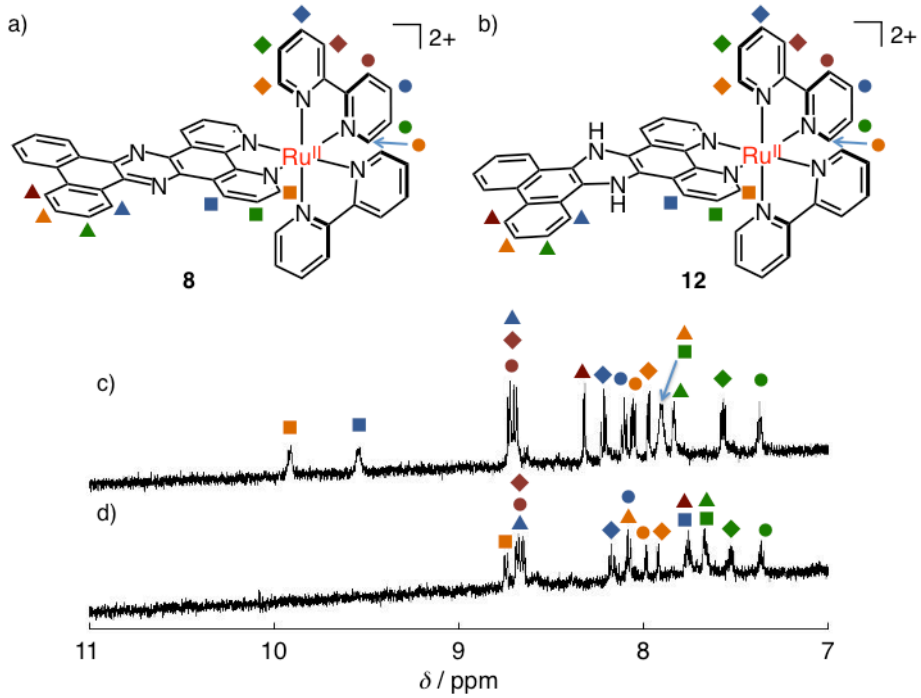

Figure 4-11. ^{1}H NMR spectral change of **8**·$(ClO_4)_2$ (0.20 mM) with Et_3N (1.0 mM) in CD_3OD : D_2O = 1 : 1 mixed solvent: (a) before and (b) after photoirradiation (380 – 670 nm).

The N*H* atoms of the reduced pyrazine moiety in **11** cannot be observed with ^{1}H NMR spectroscopy in deuterated protic solvents due to the exchange with protic deuterated solvents. Therefore, the ^{1}H NMR spectrum of **11**·$(ClO_4)_2$, which was generated from **7**·$(ClO_4)_2$ by photoirradiation at 450 nm for 2 h in a sealed NMR tube, was measured at 223 K in non-deuterated solvents under Ar with use of a "water-gate" method.[18] The method successfully suppressed the OH signal at 5.6 ppm, derived from CH_3OH and water. The CH_3 signal of CH_3OH was also presaturated with irradiation to observe the exchangeable NH proton signal without disturbance with the non-deuterated solvent signals (Figure 4-12a). Furthermore, for a reference, the OH signal was presaturated with the conventional irradiation and the CH_3 signal of CH_3OH was suppressed with the "water-gate" method (Figure 4-12b), and the differential spectrum of them was obtained (Figure 4-12c). As a result, a broad signal derived from the NHs was observed at 8.1 ppm in the non-deuterated solvent (Figure 4-12c, d).

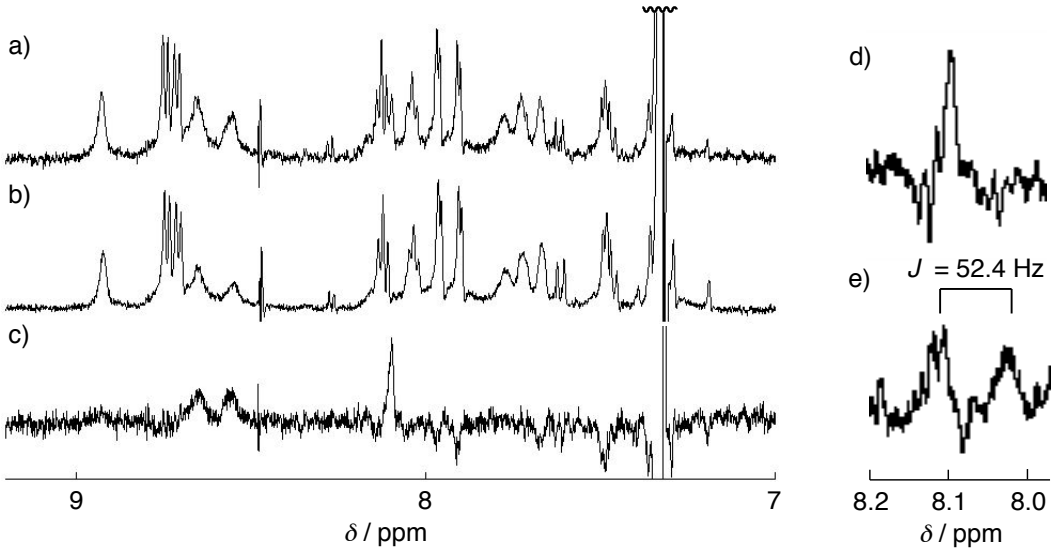

Figure 4-12. ^{1}H NMR spectra of **7**·$(ClO_4)_2$ in CH_3OH : benzene-d_6 = 9 : 1 mixed solvent with solvent suppression by a "water-gate" method for the signal of the hydroxyl group (CH_3OH and H_2O) and presaturation for the signal of the methyl group (CH_3OH) (a), and by the "water-gate" method for the signal of CH_3OH and presaturation for the signal of CH_3OH and H_2O (b), and the differential spectrum between a and b (c and d). The differential ^{1}H NMR spectrum in (e) was obtained with similar procedure for that of (d) with (**7**-^{15}N)·$(ClO_4)_2$, and the coupling constant, $J(^{15}N\text{-}^1H)$ is determined to be 52.4 Hz. All measurements were done at 223 K.

In addition, complex (**7**-^{15}N)·$(ClO_4)_2$, whose two nitrogen atoms in the pyrazine moiety of the tpphz ligand were labeled with ^{15}N (98%), was photoirradiated to generate (**11**-^{15}N)·$(ClO_4)_2$ with the same procedure for **11**·$(ClO_4)_2$. The ^{1}H NMR signal at 8.1 ppm for the N-H proton of (**11**-^{15}N)·$(ClO_4)_2$ was observed as a doublet ($^1J(^{15}N\text{-}^1H)$ = 52.4 Hz) (Figure 4-12e). The coupling constant between the ^{15}N and ^{1}H atoms is in the typical range of those reported in literatures.[19] To directly observe the reduction of the pyrazine moiety of the tpphz ligand, ^{15}N NMR spectra of ^{15}N-labeled complexes were also measured under high concentration conditions.

To improve the solubility of **7**-^{15}N in CH_3OH, the counter ions were changed from ClO_4^- to Cl^-, using the ion-exchange resin DOWEX MATATHON A2 (Cl^- form). In the ^{15}N NMR spectrum of (**7**-^{15}N)·Cl_2, a singlet signal was observed at δ 308.22 ppm, calibrated with an external reference of $(NH_4)_2SO_4$ (20.55 ppm), at room temperature (Figure 4-13a). On the other hand, after photoirradiation to the solution of (**7**-^{15}N)·Cl_2 for 4 h in the presence of Et_3N (71 mM) in CH_3OH, the ^{15}N signal was shifted to 68.86 ppm at room temperature (Figure 4-13b). Theses results indicated that the hybridization of the N atoms of the pyrazine moiety is changed from sp^2 hybridization to sp^3 one in the course of the photochemical reduction. Upon lowering the temperature to 195 K, the ^{15}N NMR signal of (**11**-^{15}N)·Cl_2 was shifted to73.43 ppm and the signal was split into a doublet due to coupling with a ^{1}H atom (J = 81.6 Hz), indicating that the ^{15}N atoms at the pyrazine moiety in the photochemical product (**11**-^{15}N)·Cl_2 are bound to an H atom (Figure 4-13c, d). These observations strongly support the hydrogenation of the pyrazine nitrogen atoms of the tpphz ligand as the results of photoinduced proton-coupled electron transfer (PCET), in which protons are derived from the solvent (MeOH) and electrons are from Et_3N.

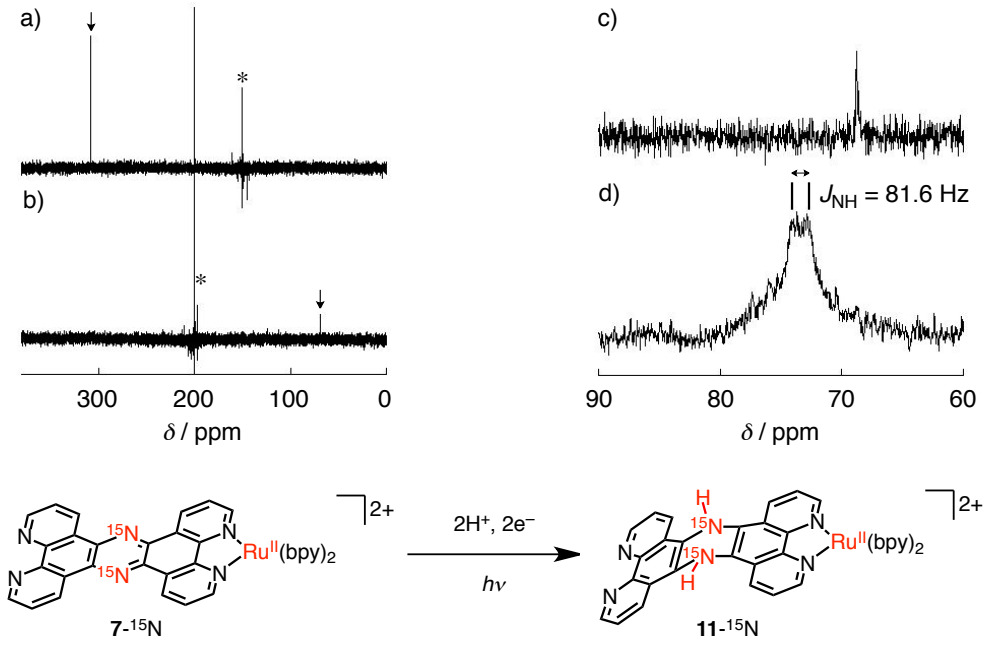

Figure 4-13. ^{15}N NMR spectra in CH_3OH : benzene-d_6 = 9 : 1 mixed solvent of (**7**-^{15}N)·Cl_2 (a) and after photoirradiation (380 – 670 nm) in the presence of Et_3N at room temperature (b and c) and at 195 K (d). Arrows in (a) and (b) indicates the signals assigned to the ^{15}N atoms of the pyradine moiety of **7**-^{15}N and the corresponding ^{15}N atom of the photochemical product, **11**-^{15}N, respectively. * = artifact at frequency center.

In addition, complex **11**·$(ClO_4)_2$ is highly air-sensitive; once it was exposed to air, it immediately turned back to **7**, exemplifying the high reactivity of **11** as a reductant (Figure 4-14). After quenching **11**·$(ClO_4)_2$ with air, the solution was analyzed with iodometry. When a NaI solution was added to the reaction mixture after the exposure to dioxygen, the absorbance around 350 nm did not increase (Figure 4-15). If the solution contains H_2O_2, absorption around 350 nm should appear due to I_3^- formed by oxidation of I^- with H_2O_2. The

lack of the absorption around 350 nm due to I_3^- after the treatment of the solution with KI indicates that the product from the reaction of O_2 with **11** is not H_2O_2.

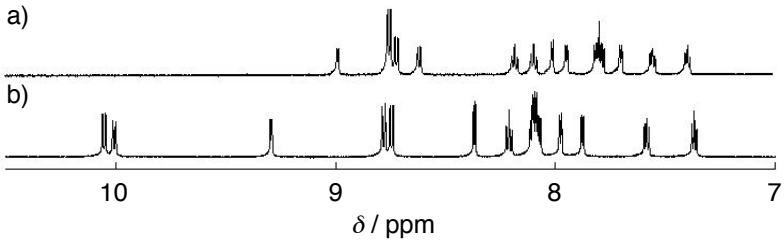

Figure 4-14. ^{1}H NMR spectrum of **11**·$(ClO_4)_2$ generated by photoirradiation to **7**·$(ClO_4)_2$ (300 μM) with white light (380 – 670 nm) for 4 h in the presence of 5 equiv of Et_3N in CD_3OD (a), and that after exposure to dioxygen (10 μL) to the solution of **11**·$(ClO_4)_2$ (b).

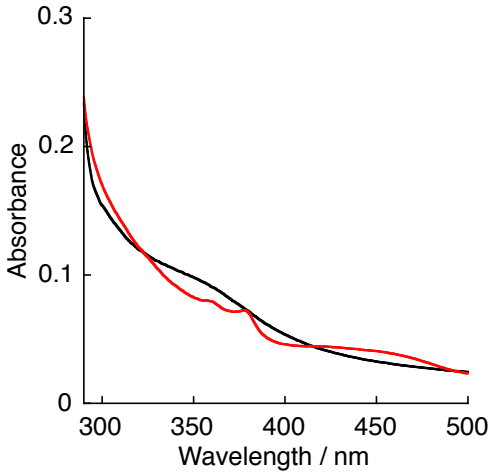

Figure 4-15. UV-vis spectra of 1 M NaI in acetonitrile (2 mL, black line) and after addition of a photochemical reaction solution (100 μL) of **7**·$(ClO_4)_2$ (red line). The reaction solution was prepared as follows: a solution of **7**·$(ClO_4)_2$ (25 μM) in a CH_3OH/H_2O (1 : 1 v/v) mixed solvent in the presence of Et_3N (1 mL) was irradiated with 380 – 670 nm for 8 h under Ar, and then O_2 was added to the cell with continuous flow for 10 min. After stirring the mixture for 5 min, the UV-vis spectrum was measured to obtain the red trace.

DFT optimization on **11** was performed at the B3LYP/SDD level of theory (Figure 4-16). The reduced tpphz ligand is very slightly distorted and the N*H* atoms are slightly deviated from the tpphz plane to the same direction. Additionally, the LUMO is located on the two bpy ligands and the Ru-side phenanthlorine moiety of the reduced tpphz ligand, and the π-conjugation on the whole tpphz moiety, observed in **7**,[11c] disappears after the reduction (Figure 4-16). This is consistent with the fact that the π-π* transition band around 380 nm, derived from the tpphz ligand, weakened in the course of the photochemical reduction (Figure 4-7).

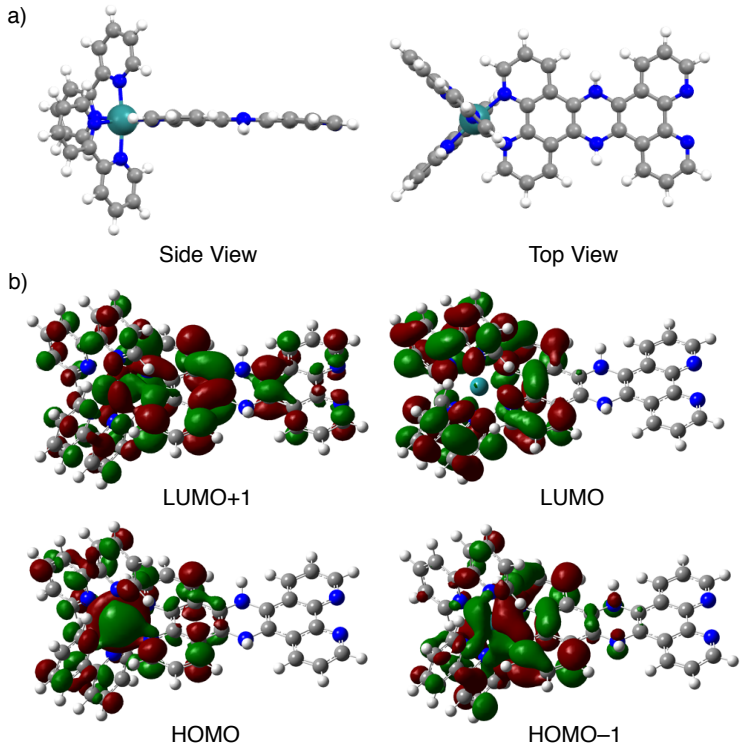

Figure 4-16. DFT calculations on **11** at the B3LYP/SDD level of theory: (a) the optimized structure of **11** and (b) frontier MOs of **11**.

4-2-6. Kinetic studies on the photochemical formation of 11

To confirm the formation mechanism of **11**, dependence of the rate of the photochemical process on the concentration of **7** and on the irradiation power were explored. The formation rate of **11**·$(ClO_4)_2$ increased in response to increase of the concentration of **7**·$(ClO_4)_2$ in the concentration range of 0 – 40 μM and showed a saturation behavior around 60 μM (Figure 4-17a). Also, the irradiation power affected the formation rate of **11**·$(ClO_4)_2$, which increased depending on the irradiation power of white light controlled by ND-filter (Figure 4-17b). The dependence indicates that the photochemical process includes an intermolecular reaction, such as disproportionation.

To investigate kinetic isotope effect (KIE) on the formation of **11**·$(ClO_4)_2$, photoirradiation was performed to the solutions of **7**·$(ClO_4)_2$ in H_2O/CH_3OH and D_2O/CD_3OD mixed solvents and the progress of the reaction was monitored with the absorption spectral change at 380 nm, which derives from the π-π* transition band of **7** (Figure 4-18). As a result, the reaction in the deuterated solvent was faster than that in the non-deuterated solvent; the initial rate in the non-deuterated solvent (v_H) was determined to be 0.88×10^{-6} M s^{-1} and that in the deuterated solvent (v_D) was 1.4×10^{-6} M s^{-1}. Thus, the KIE value (v_H/v_D) was determined to be 0.63 for the formation of **11**·$(ClO_4)_2$. Additionally, the quantum yield in the deuterated solvent (Φ_D) was higher than that in the non-deuterated solvent (Φ_H): $\Phi_H = 0.30$ and $\Phi_D = 0.48$. The reverse KIE indicates that the bond formation including H atoms is involved in the rate-determining step (RDS).[20] Therefore, the RDS of the photochemical process is probably the N-H bond formation to form **11**.

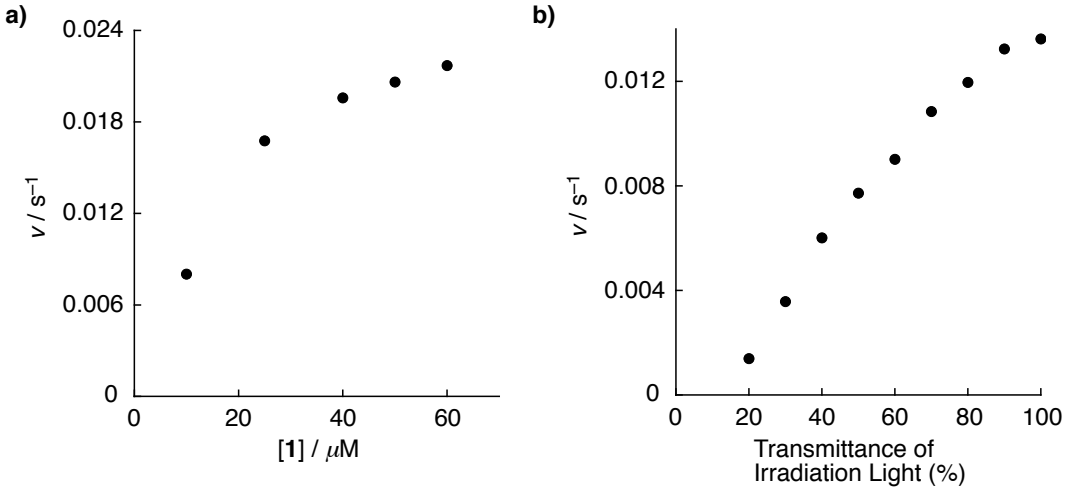

Figure 4-17. a) A plot of the initial rates (v) of the formation of **11**·$(ClO_4)_2$ from **7**·$(ClO_4)_2$ through a photochemical process against the initial concentration of **7**. The reactions were done in a mixed solvent (3 mL) of CH_3OH : H_2O = 1 : 1 in the presence of Et_3N (1 mL) under irradiation of white light (380 – 670 nm). The initial rates were obtained from the linear analysis with use of the absorbance changes at 380 nm. b) A plot of the initial rates of the formation of **11**·$(ClO_4)_2$ from **7**·$(ClO_4)_2$ through a photochemical process against the irradiation power. The reactions were done in a mixed solvent (3 mL) of CH_3OH : H_2O = 1 : 1 in the presence of Et_3N (1 mL) under irradiation of white light (380 – 670 nm). The initial rates were obtained from the linear analysis with use of the absorbance changes at 380 nm. The irradiation power was controlled by a ND-filter equipped to the light source unit.

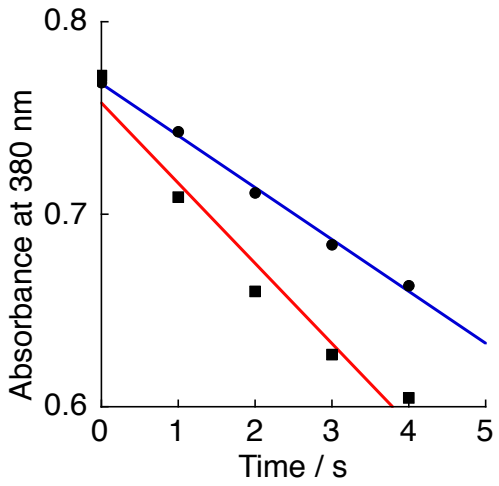

Figure 4-18. Absorbance change at 380 nm in the initial step of the photochemical reduction of **7**·$(ClO_4)_2$ (25 μM) in H_2O : CH_3OH : Et_3N = 3 : 3 : 2 mixed solvents (filled circles, blue line) and D_2O : CD_3OD : Et_3N = 3 : 3 : 2 mixed solvents (filled squares, red line) under photoirradiation (λ = 420 nm) at 297 K.

When the solution of **11**·$(ClO_4)_2$ was kept under dark, the UV-Vis and ^1H NMR spectra indicated the recovery of **7**·$(ClO_4)_2$ from **11**·$(ClO_4)_2$. In the UV-vis spectral changes, the absorption from 400 nm to 900 nm initially increased (Figure 4-19a), which was assigned to that due to decomposed products derived from $1e^-$-oxidized Et_3N. Subsequently, the absorption assigned to the π-π* transition of the tpphz ligand recovered

(Figure 4-19b). In the ^{1}H NMR spectral changes, the signals assigned to **11**·$(ClO_4)_2$ initially became broad, and subsequently, the signals assigned to **7**·$(ClO_4)_2$ recovered (Figure 4-20). The spectrum was completely changed into the same as the spectrum of **7**·$(ClO_4)_2$ after 86 h. During the dark reaction, however, hydrogen evolution was not observed at all, and the reaction rate of the dark reaction was very slow in comparison with those of the catalytic hydrogen evolution. Therefore, in the dark reaction, the recovery from **11** to **7** probably occurs through the reaction of **11** with decomposed products derived from $1e^-$-oxidized Et_3N formed in photoinduced electron transfer from Et_3N to ^{3}**7***.[21] Thus, the hydrogen evolution process from the intermediate **11** requires further photoirradiation, which matches to the fact that hydrogen evolution required both photoirradiation and electrolysis in the photoelectrocatalytic reaction, while the reaction did not occur only by the electrochemical reduction at the same potential (See section 4-2-3).

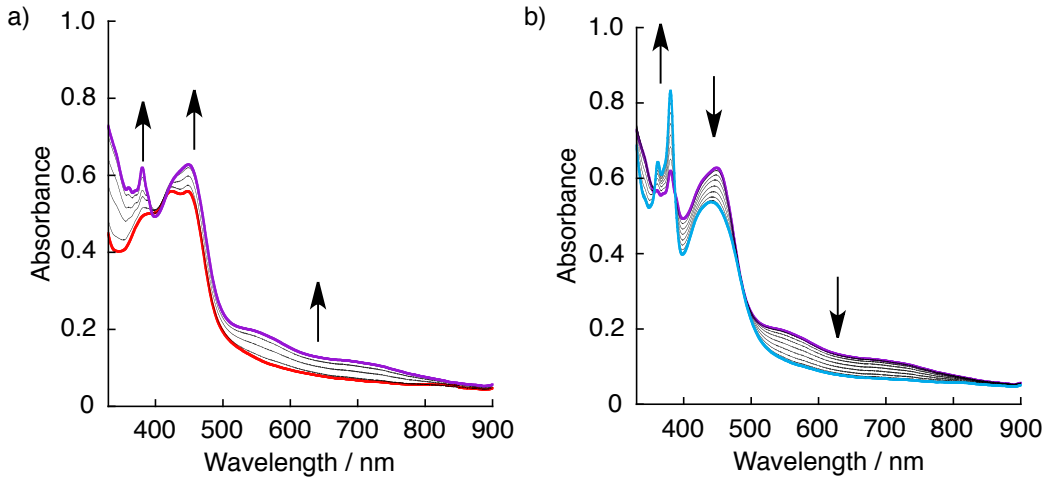

Figure 4-19. UV-vis spectral changes of **11**·$(ClO_4)_2$ in water : MeOH = 1 : 1 mixed solvent in the dark at room temperature: (a) 0 – 10 h (every 2 h) and (b) 10 – 26 h (every 2 h).

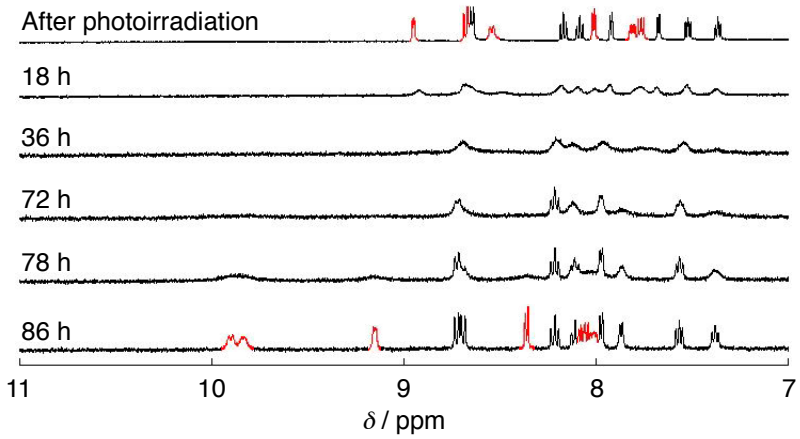

Figure 4-20. ^{1}H NMR spectral change of **11**·$(ClO_4)_2$ in CD_3OD at room temperature in the dark. Complex **11**·$(ClO_4)_2$ was generated by photoirradiation (380 – 670 nm, for 4 h) to **7**·$(ClO_4)_2$ (300 μM) in the presence of 5 equiv Et_3N in CD_3OD. The red signals in the spectra at 0 and 86 h are derived from the hydrogens assigned to the reduced tpphz ligand in **11** and the tpphz ligand in **7**, respectively.

4-2-7. Kinetic studies on the catalytic hydrogen evolution process

The amounts of hydrogen evolved from the catalytic reaction were monitored with GC both in H_2O/CH_3OH and D_2O/CD_3OD mixed solvents (Figure 4-21) under photoirradiation. In sharp contrast to the result of the photochemical process to form the intermediate **11**·$(ClO_4)_2$ (See Section 4-2-6), the hydrogen evolution in the non-deuterated solvent was faster than that in the deuterated solvent. The initial rates were determined to be 7.8 nmol h^{-1} in the non-deuterated solvent and 1.5 nmol h^{-1} in the deuterated solvent, respectively, which indicates the KIE value to be 5.2 for the final hydrogen evolution process from **11**·$(ClO_4)_2$. The rate constants of the H_2 evolution were much slower than those of the formation of **11**·$(ClO_4)_2$. Therefore, the RDS of the whole catalytic hydrogen evolution by **7**·$(ClO_4)_2$ is not the photochemical process to afford the intermediate **11**·$(ClO_4)_2$ but the hydrogen evolution process from **11**·$(ClO_4)_2$. The normal KIE observed in the hydrogen

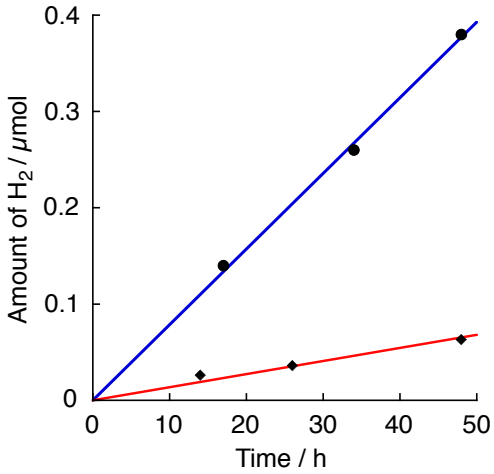

Figure 4-21. The amount of dihydrogen evolved in photocatalytic reaction in H_2O : CH_3OH = 1 : 1 (filled circles, blue line) and D_2O : CD_3OD = 1 : 1 (filled diamonds, red line), containing **7**·$(ClO_4)_2$ (25 μM) under photoirradiation of a white light (380 – 670 nm) at 297 K.

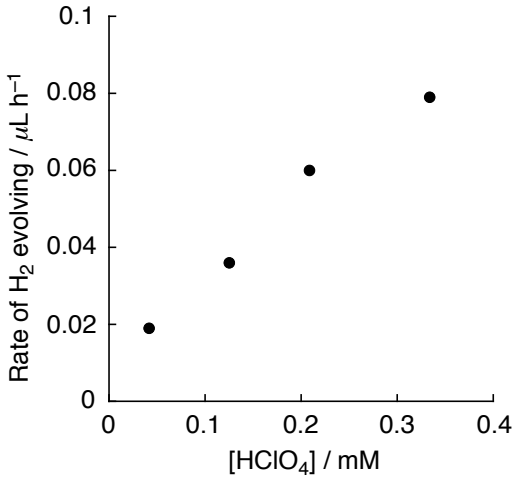

Figure 4-22. The rate of H_2 evolution catalyzed by **7**·$(ClO_4)_2$ (25 μM) in a mixed solvent (3 mL) of CH_3OH : H_2O = 1 : 1 in the presence of Et_3N (1 mL) and 70% $HClO_4$ (10 μL, 30 μL, 50 μL and 80 μL) under photoirradiation (380 – 670 nm).

evolution process clearly indicates that the RDS in the process should be cleavage of a bond involving a hydrogen atom.

Dependence of the hydrogen evolution rates on proton concentration was also investigated. With increasing the amount of $HClO_4$ added to the sample solution, the hydrogen evolution rates increased almost proportionally (Figure 4-22). Thus, protons are involved in the hydrogen evolution process. Based on the observations, the author proposes that the hydrogen evolution occurs through an intermolecular coupling between a proton and one of NH of **11** as a hydride donor, followed by aromatization to recover the pyrazine moiety and simultaneous deprotonation of the remaining N-H proton to recover **7** (See below).

4-2-8. Reaction mechanism of photochemical hydrogen evolution catalyzed by 7

Based on the results described above, complex **11** is confirmed to be an intermediate of the catalytic hydrogen evolution by **7**. In a plausible catalytic cycle (Scheme 4-2), the photoexcitation of **7** forms the ^{3}**7*** state as the first step, which is reductively quenched with Et_3N to afford $[Ru^{II}(bpy)_2(tpphz^{\bullet-})]^+$. The reduced tpphz ligand in $[Ru^{II}(bpy)_2(tpphz^{\bullet-})]^+$ catches a proton to generate the intermediate **11** probably through a disproportionation reaction.[22] The disproportionation reaction is supported by dependence of the rate of the photochemical process on the concentration of **7** and on the irradiation power. Subsequently, dihydrogen molecule was formed by reaction of the intermediate **11** with protons present in the solvent under photoirradiation, as evidenced by the dependence of the hydrogen evolution efficiency on the proton concentration. In addition, KIE for the rate of the hydrogen evolution catalyzed by **7** indicates that the RDS throughout all the process is the H-H bond formation between the intermediate and a proton.

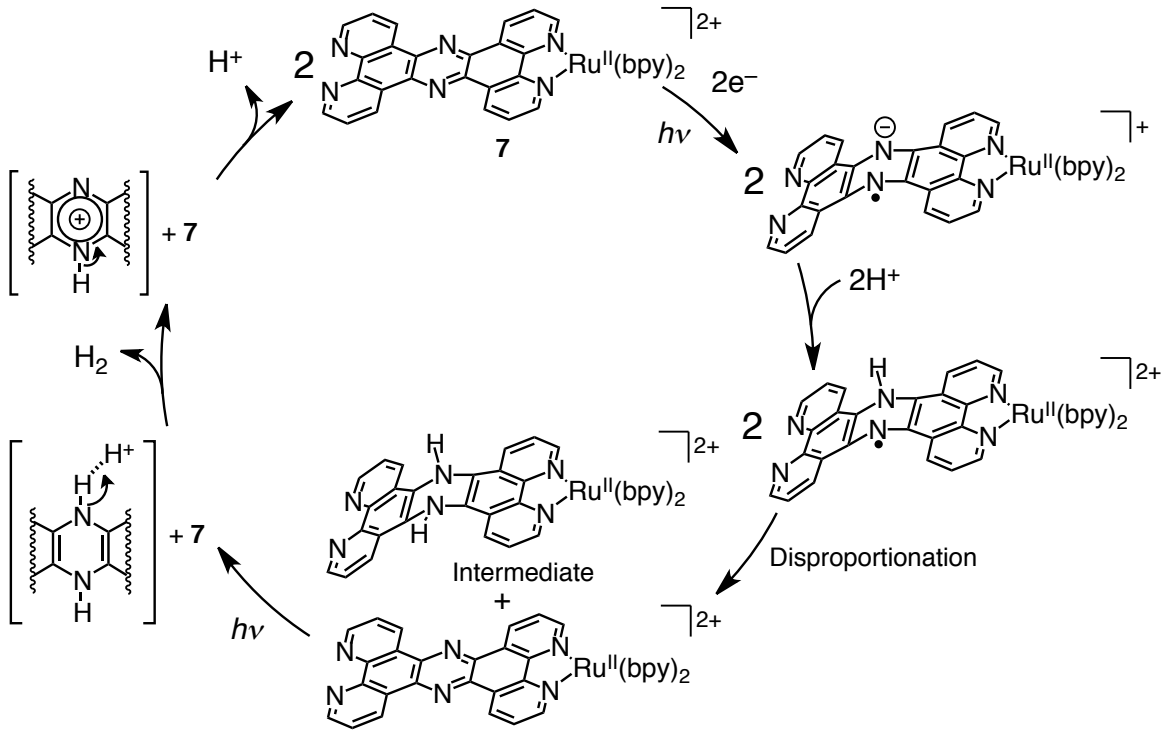

Scheme 4-2. A plausible reaction mechanism of the photocatalytic hydrogen evolution with **7**.

4-3. Summary

A photocatalytic hydrogen evolution has been demonstrated in an aqueous media with use of an electron donor and a Ru^{II} complex as a catalyst, which has tpphz as a π-expanded diimine ligand. It should be noted that the intermediate of the hydrogen evolution has been detected and characterized by spectroscopic methods. The active site of the hydrogen evolution has been verified to be the π-expanded diimine ligand, in which uncoordinated and potentially basic pyrazine nitrogen atoms are responsible for the formation of an intermediate having the 2H-reduced π-expanded ligand. The 2H-reduced intermediate (**11**) is formed *via* intermolecular disproportionation of one-electron-reduced and protonated species of **7** as a product of photoinduced PCET. Furthermore, the plausible mechanism of hydrogen evolution has been revealed to involve a photoinduced reaction of **11** with proton as the final step to form H_2. As for catalytic hydrogen evolution reactions, it is very rare that the catalytic center is not the metal center but an organic ligand.[10] The fact that the organic ligand can act as the active site for the hydrogen evolution reaction suggest that facile adjustability of the properties of organic ligands should be effective to develop more efficient catalytic systems based on ruthenium(II)-polypyridine complexes. In addition, the high reducing activity of the 2H-reduced intermediate **11** can be utilized to reductions of organic substrates.

4-4. Experimental section

General.

All reactions and measurements were carried out under argon. $[Ru^{II}(bpy)_2(tpphz)](ClO_4)_2$ (**7**·$(ClO_4)_2$),[11a] $[Ru^{II}(bpy)_2(taptp)](ClO_4)_2$ (**8**·$(ClO_4)_2$),[14] $[Ru^{II}(bpy)_3](ClO_4)_2$ (**9**·$(ClO_4)_2$)[23] and $[Ru^{II}(bpy)_2(bpm)](ClO_4)_2$ (**10**·$(ClO_4)_2$)[24] were synthesized according to the literature methods. NMR measurements were performed on a Bruker AVANCE-600 spectrometer. ^{15}N NMR spectrum was calibrated with an external reference of $(^{15}NH_4)_2SO_4$ (δ 20.55 ppm) in H_2O. UV-vis absorption spectra were recorded with use of Shimadzu UV-3600 and UV-2450 spectrometers. Emission spectra were recorded on a HORIBA FluoroMax-4 spectrometer. Electrochemical measurements were performed using a BAS ALS-710D electrochemical analyzer. Gas chromatography was performed using a Shimadzu GC-2014 equipped with a thermal conductivity detector (TCD) and a capillary column packed with molecular sieves 5A. Photoirradiation of the sample was performed by using a Xe light source (300 W) on an ASAHI SPECTRA MAX-301.

Synthesis.

^{15}N-Labeled 1,10-phenanthroline-5,6-dioxime. The labeled compound was synthesized according to the literature method for the non-labeled analog.[25] ^{15}N-enriched hydroxylamine hydrochloride (supplied by CIL) was used to form the ^{15}N-labeled oxime groups.

^{15}N-Labeled 5,6-diamino-1,10-phenanthroline. The labeled compound was synthesized according to the literature method for the non-labeled analog.[25] ^{15}N-Labeled 1,10-phenanthroline-5,6-dioxime was used as the starting compound to form the ^{15}N-labeled amino groups. ^1H NMR (DMSO-d_6): δ 8.77 (dd, J = 4.1, 1.3 Hz, 2H; phen-H2 and phen-H9), 8.48 (dd, J = 8.4, 1.3 Hz, H2; phen-H4 and phen-H7), 7.60 (dd, J = 8.4, 4.2 Hz, H2; phen-H3 and phen-H8), 5.31 (s, 1H; NH), 5.11 (s, 1H; NH).

^{15}N-Labeled $[Ru^{II}(bpy)_2(tpphz)](ClO_4)_2$ ($(7\text{-}^{15}N)\cdot(ClO_4)_2$). The labeled compound was synthesized according to the literature method for the non-labeled analog.[11a] ^{15}N-Labeled 5,6-diamino-1,10-phenanthroline was used to form the ^{15}N-labeled tpphz ligand with $[Ru^{II}(bpy)_2$(1,10-phenanthroline-5,6-dione)$](PF_6)_2$.[11a] ^{1}H NMR (MeCN-d_3): δ 9.42 (dd, J = 8.2, 1.8 Hz, 2H; tpphz-Ha), 9.19 (dd, J = 8.2, 0.9 Hz, 2H; tpphz-Ha'), 8.62 (d, J = 8.0 Hz, 2H; bpy-H3), 8.58 (d, J = 8.0 Hz, 2H; bpy-H3'), 8.29 (dd, J = 5.0, 1.1 Hz, 2H; tpphz-Hc'), 8.24 (t, J = 5.2 Hz, 4H; tpphz-Hc and bpy-H6), 8.18 (td, J = 8.0, 1.4 Hz, 2H; bpy-H4), 8.05 (td, J = 8.0, 1.4 Hz, 2H; bpy-H4'), 7.94 (dd, J = 5.5, 0.9 Hz, 2H; bpy-H6'), 7.83 (dd, J = 8.2, 5.0 Hz, 2H; tpphz-Hb), 7.69 (dd, J = 7.9, 4.3 Hz, 2H; tpphz-Hb'), 7.54 (ddd, J = 5.5, 1.4, 0.9 Hz, 2H; bpy-H5), 7.39 (ddd, J = 5.5, 1.4, 0.9 Hz, 2H; bpy-H5'). ^{15}N NMR (MeCN-d_3): δ 244.71 (s). MS (ESI): calcd for $[M - 2ClO_4]^{2+}$: m/z = 400.07, found: m/z = 400.07.

Formation of $\mathbf{11}\cdot(ClO_4)_2$. The reaction to form **11** and its NMR measurements were performed in a sealed NMR tube under Ar. A white light (380 – 670 nm) was irradiated to the solution containing $\mathbf{7}\cdot(ClO_4)_2$ (0.3 mM) and Et_3N (71 mM) in CD_3OD : D_2O = 1 : 1 mixed solvent (0.7 mL) for 30 min under Ar. After photoirradiation, the ^{1}H NMR spectrum of the sample was directly measured at room temperature without isolation of **11**. ^{1}H NMR (CD_3OD : D_2O = 1 : 1): δ 8.98 (d, J = 5.0 Hz, 2H; tpphz-Ha), 8.75 (d, J = 8.2 Hz, 4H; tpphz-Ha' and bpy-H3), 8.72 (d, J = 8.0 Hz, 2H; bpy-H3'), 8.62 (dd, J = 5.0, 1.2 Hz, 2H; tpphz-Hc'), 8.18 (td, J = 8.0, 1.4 Hz, 2H; bpy-H4), 8.10 (td, J = 8.0, 1.2 Hz, 2H; bpy-H4'), 8.01 (t, J = 5.3 Hz, 2H; tpphz-Hc), 7.96 (dd, J = 5.5, 1.0 Hz, 2H; bpy-H6'), 7.83-7.77 (m, 4H; tpphz-Hb and tpphz-Hb'), 7.70 (dd, J = 8.0, 1.5 Hz, 2H; bpy-H6), 7.55 (td, J = 7.9, 1.4 Hz, 2H; bpy-H5), 7.39 (td, J = 8.0, 1.4 Hz, 2H; bpy-H5').

Formation of $(\mathbf{11}\text{-}^{15}N)\cdot Cl_2$. The reaction to form $(\mathbf{11}\text{-}^{15}N)\cdot Cl_2$ and its NMR measurements were performed in a sealed NMR tube under Ar. For the ^{1}H NMR measurements, white light (380 – 670 nm) was irradiated to the solution containing $(\mathbf{7}\text{-}^{15}N)\cdot Cl_2$ (0.7 mM) and Et_3N (71 mM) in CH_3OH : benzene-d_6 = 9 : 1 mixed solvent (0.7 mL) for 4 h under Ar. After photoirradiation, the ^{1}H NMR spectrum of the sample was directly measured at room temperature without isolation of $(\mathbf{11}\text{-}^{15}N)\cdot Cl_2$. ^{1}H NMR ($CH_3OH$: benzene-d_6 = 9 : 1): δ 7.95 (d, J = 19.0 Hz, N*H*). For the ^{15}N NMR measurements, white light (380 – 670 nm) was irradiated to the solution containing $(\mathbf{7}\text{-}^{15}N)\cdot Cl_2$ (1 mM) and Et_3N (0.2 M) in CH_3OH : benzene-d_6 = 9 : 1 mixed solvent (0.7 mL) for 4 h under Ar. After photoirradiation, the ^{15}N NMR spectrum of the sample was directly measured at room temperature without isolation of $(\mathbf{11}\text{-}^{15}N)\cdot Cl_2$. ^{15}N NMR ($CH_3OH$: benzene-d_6 = 9 : 1, at 195 K): δ 73.43 (d, J = 81.6 Hz).

Ion-exchange from $(\mathbf{7}\text{-}^{15}N)\cdot(ClO_4)_2$ to $(\mathbf{7}\text{-}^{15}N)\cdot Cl_2$.

$(\mathbf{7}\text{-}^{15}N)\cdot(ClO_4)_2$ was dispersed in H_2O using a ultrasonic bath sonicator and ion-exchange resin DOWEX MATATHON A2 (Cl^- form) was added to the suspension. The mixture was stirred to solve the dispersed solid for 5 min, and the resin was removed by filtration. $(\mathbf{7}\text{-}^{15}N)\cdot Cl_2$ was obtained by removal of the solvent under vacuum.

Hydrogen evolution catalyzed by $\mathbf{7}\cdot(ClO_4)_2$.

Photocatalytic hydrogen evolution was carried out in a quartz cuvette with five transparent faces (cell volume: 5.34 mL), which was capped by a rubber septum and whose inside was filled with Ar gas. Before photoirradiation, the solution (total volume: 4 mL) was degassed by bubbling with Ar gas for 30 min. A white light of 380 – 670 nm, which was generated from a Xe lamp equipped with a mirror module to remove the UV light, was irradiated to the cuvette from the underneath with a path length of 4 cm. After photoirradiation, 0.1 mL of the gas phase in the cell was taken with a gas-tight syringe and analyzed by GC.

Electrochemical measurements of $\mathbf{7}\cdot(ClO_4)_2$.

Cyclic and differential-pulse voltammetry (CV and DPV) were performed in MeCN in the presence of $[(n\text{-butyl})_4N]PF_6$ ($(n\text{-Bu})_4PF_6$, 0.1 M) as an electrolyte under an Ar atmosphere at room temperature in the dark, with a glassy-carbon disk as a working electrode, $Ag/AgNO_3$ as a reference electrode, and Pt wire as an auxiliary electrode.

Determination of quantum yields of photochemical reactions.

The quantum yield of the photochemical reduction of $\mathbf{7}\cdot(ClO_4)_2$ was determined by using a standard method[16] with an actinometer (potassium ferrioxalate) in water under photoirradiation at 440 nm. The reaction was monitored to observe the decrease in absorbance at 380 nm and the data at the initial stage, during which a linear change was observed, were used to determine the quantum yield.

DFT calculations.

Theoretical calculations of **7** and **11** were performed by using the Gaussian 09 program package.[26] In the ground state **7** and **11** is the singlet state. Restricted density functional theory (RDFT) calculations were carried out at the B3LYP functional.[27, 28] SDD basis[29] for Ru atoms and 6-311+G** basis[30] for H, C, and N atoms are used.

Reference and notes

[1] a) A. Zuttel, A. Borgschulte, L. Schlapbach, *Hydrogen as a Future Energy Carrier*, Wiley-VCH, Weinheim, **2008**; b) N. Armaroli, V. Balzani, *Energy for a Sustainable World: From the Oil Age to a Sun-Powered Future*, Wiley-VCH, Weinheim, **2011**.

[2] a) B. C. H. Steele, A. Heinzel, *Nature* **2001**, *414*, 345-352; b) A. J. Esswein, D. G. Nocera, *Chem. Rev.* **2007**, *107*, 4022-4047; c) V. Artero, M. Chavarot-Kerlidou, M. Fontecave, *Angew. Chem. Int. Ed.* **2011**, *50*, 7238-7266; d) A. Boddien, C. Federsel, P. Sponholz, D. Mellmann, R. Jackstell, H. Junge, G. Laurenczy, M. Beller, *Energy Environ. Sci.* **2012**, *5*, 8907-8911; e) J. A. Turner, *Science* **2004**, *305*, 972-974.

[3] a) E. Borgarello, J. Kiwi, E. Pelizzetti, M. Visca, M. Grätzel, *J. Am. Chem. Soc.* **1981**, *103*, 6324-6329; b) J. I. Goldsmith, W. R. Hudson, M. S. Lowry, T. H. Anderson, S. Bernhard, *J. Am. Chem. Soc.* **2005**, *127*, 7502-7510.

[4] H. I. Karunadasa, E. Montalvo, Y. Sun, M. Majda, J. R. Long, C. J. Chang, *Science* **2012**, *335*,

698-702.

[5] a) M. L. Helm, M. P. Stewart, R. M. Bullock, M. R. DuBois, D. L. DuBois, *Science* **2011**, *333*, 863-866; b) S. J. Hwang, D. C. Powers, A. G. Maher, D. G. Nocera, *Chem. Sci.* **2015**, *6*, 917-922.

[6] a) G. M. Brown, B. S. Brunschwig, C. Creutz, J. F. Endicott, N. Sutin, *J. Am. Chem. Soc.* **1979**, *101*, 1298-1300; b) C. V. Krishnan, N. Sutin, *J. Am. Chem. Soc.* **1981**, *103*, 2141- 2142; c) X. Hu, B. S. Brunschwig, J. C. Peters, *J. Am. Chem. Soc.* **2007**, *129*, 8988-8998; d) T. Lazarides, T. McCormick, P. Du, G. Luo, B. Lindly, R. Eisenberg, *J. Am. Chem. Soc.* **2009**, *131*, 9192-9194; e) R. S. Khnayzer, C. E. McCusker, B. S. Olaiya, F. N. Castellano, *J. Am. Chem. Soc.* **2013**, *135*, 14068-14070; f) K. Kawano, K. Yamauchi, K. Sakai, *Chem. Commun.* **2014**, *50*, 9872-9875.

[7] a) L. Tong, R. Zong, R. P. Thummel, *J. Am. Chem. Soc.* **2014**, *136*, 4881-4884; b) S. Mandal, S. Shikano, Y. Yamada, Y.-M. Lee, W. Nam, A. Llobet, S. Fukuzumi, *J. Am. Chem. Soc.* **2013**, *135*, 15294-15297.

[8] a) G. S. Bindra, M. Schulz, A. Paul, R. Groarke, S. Soman, J. L. Inglis, W. R. Browne, M. G. Pfeffer, S. Rau, B. J. MacLean, M. T. Pryce, J. G. Vos, *Dalton Trans.* **2012**, *41*, 13050- 13059; b) M. G. Pfeffer, T. Kowacs, M. Wächtler, J. Guthmuller, B. Dietzek, J. G. Vos, S. Rau, *Angew. Chem. Int. Ed.* **2015**, *54*, 6627-6631.

[9] a) A. Fujishima, K. Honda, *Nature* **1972**, *238*, 37-38; b) S. Nakabayashi, A. Fujishima, K. Honda, *Chem. Phys. Lett.* **1983**, *102*, 464-465; c) T. Kawai, T. Sakata, *Nature* **1980**, *286*, 474-476; d) K. Kalyanasudaram, E. Borgarello, M. Grätzel, *Helv. Chim. Acta* **1981**, *64*, 362-366.

[10] T. Matsumoto, H.-C. Chang, M. Wakizaka, S. Ueno, A. Kobayashi, A. Nakayama, T. Taketsugu, M. Kato, *J. Am. Chem. Soc.* **2013**, *135*, 8646-8654.

[11] a) J. Bolger, A. Gourdon, E. Ishow, J.-P. Launay, *Inorg. Chem.* **1996**, *35*, 2937-2944; b) J. Bolger, A. Gourdon, E. Ishow, J.-P. Launay, *J. Chem. Soc., Chem. Commun.* **1995**, 1799-1800; c) Y. Sun, D. A. Lutterman, C. Turro, *Inorg. Chem.* **2008**, *47*, 6427-6434.

[12] The triplet excited state of **7** has the lifetime of 1.1 μs in CH_3CN at room temperature. See: C. Chiorboli, C. A. Bignozzi, F. Scandola, E. Ishow, A. Gourdon, J.-P. Launay, *Inorg. Chem.* **1999**, *38*, 2402-2410.

[13] B. S. Winkler, S. M. Orselli, T. S. Rex, *Free Radic. Biol. Med.* **1994**, *17*, 333-349.

[14] a) C. G. Morales-Guio, L. Liardet, M. T. Mayer, S. D. Tilley, M. Grätzel, X. Hu, *Angew. Chem. Int. Ed.* **2014**, *53*, 1-5; b) C. L. Pitman, A. J. M. Miller, *ACS Catal.* **2014**, *4*, 2727-2733.

[15] Y. Liu, A. Chouai, N. N. Degtyareva, D. A. Lutterman, K. R. Dunbar, C. Turro, *J. Am. Chem. Soc.* **2005**, *127*, 10796-10797.

[16] M. Kirch, J.-M. Lehn, J.-P. Sauvage, *Helv. Chim. Acta* **1979**, *62*, 1345-1384.

[17] G. Gauglitz, in *Photochromism Molecule and Systems, Revised Edition* (Eds.: H. Dürr, H. Bouas-Laurent), Elsevier, Amsterdam, **2003**, p30.

[18] M. Piotto, V. Saudek, V. Sklenár, *J. Biomol. NMR* **1992**, *2*, 661-665.

[19] M. Piertzak, A. C. Try, B. Andrioletti, J. L. Sessler, P. Anzenbacher, Jr., H.-H. Limbach, *Angew. Chem. Int. Ed.* **2008**, *47*, 1123-1126.

[20] a) J. M. Camara, T. B. Rauchfuss, *J. Am. Chem. Soc.* **2011**, *133*, 8098-8101; b) H. Kotani, R. Hanazaki, K. Ohkubo, Y. Yamada, S. Fukuzumi, *Chem. Eur. J.* **2011**, *17*, 2777-2785.

[21] Hydrogen evolution from π-conjugated organic compounds, which involves aromatization or extension of π-conjugation, frequently requires photoexcitation. See ref. 9 and K. Ujike, S. Kudoh, M. Nakata, *Chem. Phys. Lett.* **2004**, *396*, 288-292.

[22] S. Kumar Padhi, R. Fukuda, M. Ehara, K. Tanaka, *Inorg. Chem.* **2012**, *51*, 8091-8102.

[23] J. A. Broomhead, C. G. Young, P. Hood, *Inorg. Synth.* **1990**, *28*, 338-340.

[24] O. Hamelin, M. Rimboud, J. Pécaut, M. Fontecave, *Inorg. Chem.* **2007**, *46*, 5354-5360.

[25] S. Bodige, F. M. MacDonnell, *Tetrahedron Lett.* **1997**, *38*, 8159-8160.

[26] Gaussian 09, Revision D.01, M. J. Frisch, G. W. Trucks, H. B. Schlegel, G. E. Scuseria, M. A. Robb, J. R. Cheeseman, G. Scalmani, V. Barone, B. Mennucci, G. A. Petersson, H. Nakatsuji, M. Caricato, X. Li, H. P. Hratchian, A. F. Izmaylov, J. Bloino, G. Zheng, J. L. Sonnenberg, M. Hada, M. Ehara, K. Toyota, R. Fukuda, J. Hasegawa, M. Ishida, T. Nakajima, Y. Honda, O. Kitao, H. Nakai, T. Vreven, J. A. Montgomery, Jr., J. E. Peralta, F. Ogliaro, M. Bearpark, J. J. Heyd, E. Brothers, K. N. Kudin, V. N. Staroverov, R. Kobayashi, J. Normand, K. Raghavachari, A. Rendell, J. C. Burant, S. S. Iyengar, J. Tomasi, M. Cossi, N. Rega, J. M. Millam, M. Klene, J. E. Knox, J. B. Cross, V. Bakken, C. Adamo, J. Jaramillo, R. Gomperts, R. E. Stratmann, O. Yazyev, A. J. Austin, R. Cammi, C. Pomelli, J. W. Ochterski, R. L. Martin, K. Morokuma, V. G. Zakrzewski, G. A. Voth, P. Salvador, J. J. Dannenberg, S. Dapprich, A. D. Daniels, Ö. Farkas, J. B. Foresman, J. V. Ortiz, J. Cioslowski, and D. J. Fox, Gaussian, Inc., Wallingford CT, 2009.

[27] A. D. Becke, *J. Chem. Phys.* **1993**, *98*, 1372-1377.

[28] C. Lee, W. Yang, R. G. Parr, *Phys. Rev. B* **1988**, *37*, 785-789.

[29] D. Andrae, U. Haeussermann, M. Dolg, H. Stoll, H. Preuss, *Theor. Chem. Acc.* **1990**, *77* 123-141.

[30] K. Raghavachari, J. S. Binkley, R. Seeger, J. A. Pople, *J. Chem. Phys.* **1980**, *72*, 650-654.

Chapter 5
Concluding Remarks

In this thesis, toward the efficient utilization of light energy as a clean energy source for chemical reactions, the author has described photochromic complete conversion and photocatalytic hydrogen evolution, both of which proceed through the triplet excited states of ruthenium(II)-polypyridine complexes.

The photochromic complete conversions of ruthenium(II)-polypyridine complexes have been achieved based on dissociations and recoordinations of ligands in ruthenium(II)-polypyridine complexes by photoirradiation and heating; particularly, partial dissociations and recoordinations of axial pyridines of TPA ligands have been discussed in detail. The ruthenium(II)-TPA-pterin complex **1** has been demonstrated to perform the photoisomerization involving a 180°-pseudorotation of the pterin ligand by photoirradiation and heating with complete conversion efficiency. In this isomerization, both forward and backward reactions occur through the partial dissociation of the axial pyridine moiety of the TPA ligand by photoexcitation or heating; the relative position of the energy levels between **1**, **I**, **2** and transition states of the thermal steps is controlled by the steric hindrance between the TPA ligand, the pterin ligand and the coordinated solvent molecules. Also, the dinuclear ruthenium(II)-ruthenium(II) complex **5** and ruthenium(II)-palladium(II) complex **6** exhibit a complete conversion efficiency in the photoinduced structural interconversion between completely coordinated complexes (**5** and **6**) and partially dissociated complexes having an acetonitrile ligand (**5'** and **6'**); however, the strategies to accomplish the complete conversion are different from the cases of the ruthenium(II)-pterin complexes. In the photochromic interconversion of the dinuclear complexes **5** and **6**, to inhibit the partial dissociation of the axial pyridine moiety of the η^4-TPA ligand by photoirradiation, the energy levels of the MLCT triplet excited states can be shifted lower than those of the MC triplet excited states by addition of the cationic metal ions, such as ruthenium(II) and palladium(II), to the π-expanded heteroaromatic ligands. As a result, the ruthenium(II)-η^4-TPA complexes were converted to the partially dissociated ruthenium(II)-η^3-TPA complexes with the acetonitrile ligand by heating in acetonitrile, and subsequently, the partially dissociated complexes were converted to the ruthenium(II)-η^4-TPA complexes by photoirradiation without further dissociation. The complete interconversion in the ruthenium(II) complexes verified in this study should have a great potential in the development of metal-based photoswitchable devices.

The photocatalytic hydrogen evolution was performed using a ruthenium(II) complex, **7**, as a catalyst in an aqueous solvent. In this catalytic system, the π-expanded heteroaromatic ligand (tpphz) of **7** plays a role as the active site for the catalysis, while the ruthenium(II) moiety of **7** plays a role as a photosensitizer in the presence of an electron donor. Under photoirradiation, the pyradine moiety of the tpphz ligand is reduced by the photoinduced electron transfer from the ruthenium(II) center followed by electron transfer from a reductant such as Et_3N to the oxidized ruthenium(III) center; subsequently, a proton in the solvent is attached to one of the pyrazine N atoms of the reduced tpphz ligand. The photochemical product **11**, which is formed *via* disproportionation of the aforementioned one-electron reduced species as an intermediate in the

hydrogen evolution, is thermodynamically stable enough to be characterized by spectroscopic measurements under inert atmosphere. Since the intermediate exhibit high reactivity, the intermediate can reduce a proton in the solvent to generate a dihydrogen molecule under photoirradiation. Since the organic ligand acts as the active site for the catalytic hydrogen evolution, control of the reactivity through the chemical modification around the active site should be facile and make it possible to develop more efficient photocatalytic hydrogen evolving systems.

Throughout this research, the author has achieved utilization of light energy for chemical reactions performed by the ruthenium(II)-polypyridine complexes. In this thesis, the photochemical products (or intermediates) were fully characterized by various spectroscopies, for both the photochromic structural changes and the photocatalytic hydrogen evolution. Characterization of photochemical products is rare, because generally, a photochemical product is thermodynamically unstable. The results are quite significant for deeper understanding of photoinduced structural changes of ruthenium(II)-polypyridine complexes than ever toward construction of well-controlled molecular devices driven by light energy and useful for developing efficient photocatalytic hydrogen evolution as a strategy to fertilize future society in a sustainable way.

List of publications

1) Mechanistic Insights into Photochromic Behavior of a Ruthenium(II)-Pterin Complex
T. Ishizuka, T. Sawaki, S. Miyazaki, M. Kawano, Y. Shiota, K. Yoshizawa, S. Fukuzumi, T. Kojima
Chemistry – A European Journal **2011**, *17*, 6652-6662.

2) Complete Photochromic Structural Changes in Ruthenium(II)-Diimine Complexes, Based on Control of the Excited States by Metalation
T. Sawaki, T. Ishizuka, M. Kawano, Y. Shiota, K. Yoshizawa, T. Kojima
Chemistry – A European Journal **2013**, *19*, 8978-8990.

Acknowledgments

The author would like to give special thanks to Professor Takahiko Kojima for his continuous support, encouragement, patience, immerse knowledge and insightful comments throughout his PhD studies. The author would also appreciate very much Prof. Kojima's valuable suggestions about not only chemistry but also desirable attitudes in one's life. The author's sincere gratitude also goes to Dr. Tomoya Ishizuka for his guidance throughout this research by providing constructive and fruitful advises with great patience and great effort to edit this thesis. The author's thanks also go to Dr. Hiroaki Kotani for his helpful suggestions in chemistry.

The author would like to express his sincere gratitude to Prof. Kazunari Yoshizawa and Prof. Yoshihito Shiota in Institute for Materials Chemistry and Engineering, Kyushu University, for their kind collaboration in DFT calculations. The author would like to appreciate Prof. Masaki Kawano in Tokyo Institute of Technology for his kind collaboration in X-ray diffraction measurements at High Energy Accelerator Research Organization (KEK). Prof. Yasuhiko Yamamoto and Dr. Tomokazu Shibata in University of Tsukuba are gratefully appreciated for their helpful guidance in NMR measurements. The author would like to thank Prof. Takashi Ogura and Ms. Kaoru Mieda in University of Hyogo for their kind collaboration in resonance Raman spectroscopic measurements. The author would like to thank Prof. James M. Mayer, who now belongs to Yale University, for hosting the author during a short stay in his laboratory in University of Washington. The author also expresses his sincere thanks to the member of the Mayer's laboratory and Dr. Hiroaki Hagiwara, who now is an assistant professor in Gifu University, for their valuable guidance in various experimental techniques including analysis of proton-coupled electron transfer.

The author would like to thank all the labmates in the Kojima laboratory, Department of Chemistry, University of Tsukuba, who have experienced a lot of joys together as well as a few of difficulties. The author owes them so much for all the fun we have had in the last seven years. Also, Ms. Miyuki Nakahara should be appreciated for her solicitudes and kind supports in administrative processes.

Last but not the least, the author sincerely appreciates his family for their spiritual support and pecuniary assistance throughout his life.

February 2016

Takuya Sawaki

Kojima laboratory
Department of Chemistry